Diode pumped liquid organic lasers : Toward quasi-continuous wave operation

Md Amir Hamja

UNIVERSITE PARIS XIII –SORBONNE PARIS NORD

École doctorale Sciences, Technologies, Santé Galilée

Laser organique liquide pompé par diode : vers un fonctionnement quasi-continu

Diode pumped liquid organic lasers: toward quasi-continuous wave operation

---

THÈSE DE DOCTORAT

présentée par

Md Amir HAMJA

Laboratoire de physique des lasers

pour l'obtention du grade de

DOCTEUR EN PHYSIQUE

Soutenue le 25.03.2022 devant le jury d'examen constitué de :

KREHER David, Université Versailles St Quentin, Président du jury

CAMY Patrice, Université Caen, Rapporteur

MAGER Loïc, Université Strasbourg 1, Rapporteur

LUCAS-LECLIN Gaelle, Université Paris Saclay, Examinatrice

FORGET Sébastien, Université Sorbonne Paris Nord, Directeur de thèse

CHENAIS Sébastien, Université Sorbonne Paris Nord, Co-directeur de thèse

Résumé

Les lasers à colorant ont été les toutes premières sources cohérentes accordables dans l'histoire des lasers. Ces lasers, basés sur la circulation d'une solution de colorant, sont maintenant considérés comme trop encombrants et pénibles à utiliser, ce qui pousse la recherche vers l'exploration de diverses alternatives à l'état solide. Mais ces alternatives à l'état solide souffrent d'une faible puissance, d'une mauvaise photo stabilité et ne peuvent pas être utilisées en onde continue (CW)/quasi-continue (q-CW). Par conséquent, pour trouver une solution possible, ce travail explore pour la première fois la performance de la stabilité photo- stabilité obtenue avec une conception dans laquelle une cuvette spectroscopique remplie d'une solution de colorant sans aucune circulation est utilisée comme milieu de gain sous pompage par diode, ce qui permet d'obtenir un laser peu coûteux, compact et convivial qui peut être comparé aux lasers à colorant à l'état solide mais avec la stabilité des lasers à colorant liquide d'ancienne génération. Le laser présenté, en plus d'être efficace (efficacité optique ~ 18%) est photos table jusqu'à environ un milliard d'impulsions à une fréquence de répétition de 1 kHz, ce qui est 5 ordres de grandeur plus élevé que la photo stabilité d'un laser à colorant à l'état solide dans les mêmes conditions. Cette photo stabilité exceptionnellement élevée peut être attribuée à la diffusion moléculaire ou à un lent flux convectif de molécules dû à un chauffage localisé dans le milieu, ce qui pourrait être suffisant pour permettre un renouvellement du milieu de gain entre des impulsions consécutives. Cependant, malgré sa grande photo stabilité, le laser n'a pas pu fonctionner au-delà de 2,4 kHz et n'a pas pu produire des durées d'impulsion supérieures à quelques µs. Nous montrons ici que leur limite opérationnelle en termes de taux de répétition n'est pas due à une limite fondamentale imposée par l'accumulation d'états triplets dans le composé organique, ce qui est souvent supposé être le cas dans les lasers organiques à l'état solide. Au contraire, nous démontrons que cette limite est due à la lentille thermique. Nous avons mesuré la composante sans aberration de la lentille thermique par une expérience pompe-sonde et démontré une prolongation possible de l'effet laser jusqu'à 14 kHz avec une correction intracavité appropriée de la lentille thermique. Pour vérifier l'universalité de notre affirmation, nous avons également testé un second colorant et avons obtenu des résultats similaires. En revanche, les lasers à colorant à l'état solide ont besoin d'un milieu de gain mobile afin de fonctionner à des taux de répétition élevés et de surmonter une photo dégradation abrupte. Enfin, nous montrons que ces lasers peuvent également produire un effet laser allant jusqu'à 80 µs lorsqu'ils sont fortement multimodes. Bien que nous ayons démontré expérimentalement le fonctionnement de ces longues impulsions, des recherches théoriques et expérimentales supplémentaires sont nécessaires pour comprendre leur comportement multimode, ce qui peut être une perspective future de ce travail. Une autre perspective de ce travail serait d'étudier le verrouillage de mode dans un laser organique, ce qui nécessite que le laser soit idéalement CW ou q-CW. Nous pensons que notre laser peut être un bon candidat pour l'étude de telles applications laser et donc, à la fin de cette thèse, nous donnons également quelques directions et voies utiles pour

développer un laser organique à verrouillage de mode à faible coût, compact, convivial et accordable dans le futur.

Abstract

Dye lasers have been the very first coherent tunable sources in the history of lasers. These lasers, based on dye solution circulation, are now considered too bulky and painful to operate, pushing research towards the exploration of various solid-state alternatives. But these solid-state alternatives suffer from low power, poor photo-stability and cannot be operated in Continuous wave (CW)/quasi-Continuous wave (q-CW). Therefore, to find a possible solution this work explores for the first time the photo-

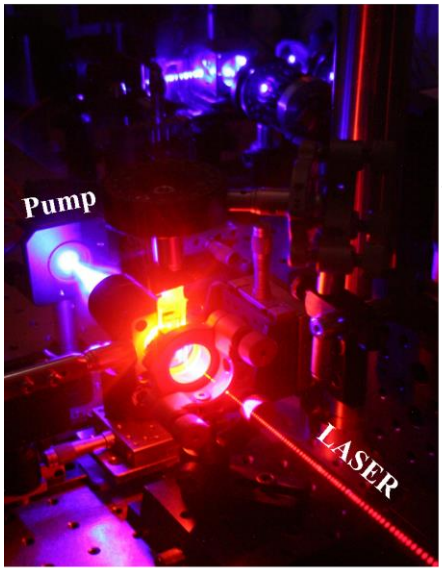

Diode pumped circulation-free liquid dye (DCM) laser

Highly photostable compared to solid-state dye laser

High repetition rate operation

Longer pulse lasing compared to solid-state dye laser

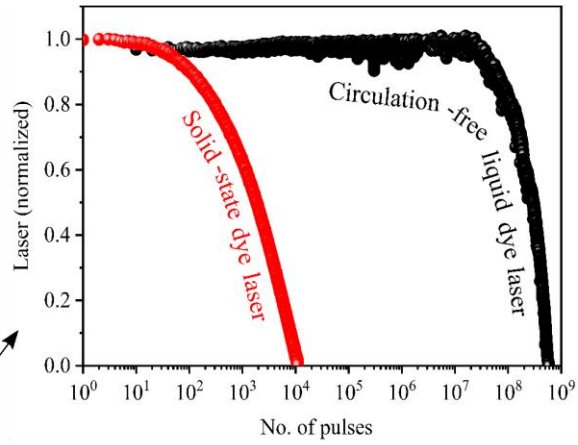

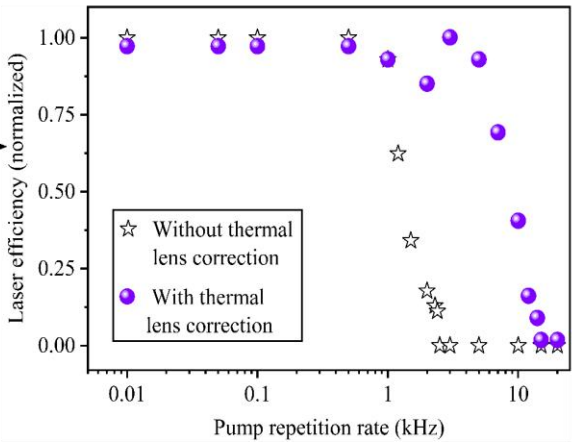

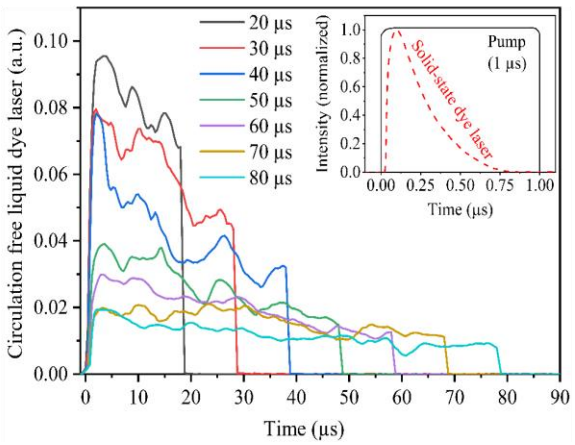

stability performance obtained with a design in which a spectroscopic cuvette filled with dye solution without any circulation is used as a gain medium under diode-pumping, making a low-cost, compact and user-friendly laser which can be compared to solid-state dye lasers but with the stability of older generation liquid dye lasers. The reported laser, in addition of being efficient (optical efficiency ~ 18%) is photo-stable up to roughly a billion of pulses at 1 kHz repetition rate, which is 5 orders of magnitude higher than the photo-stability of a solid-state dye laser in the same conditions. This unusually high photo-stability maybe attributed to molecular diffusion or slow convective flow of molecules due to localized heating in the medium, which might be sufficient to allow a replenishment of the gain medium between consecutive pulses. However, despite being highly photostable, the laser could not be operated beyond 2.4 kHz and could not produce pulse duration longer than few µs. We show here that their operational limit in repetition rates is not due to a fundamental limit imposed by triplet state accumulation in the organic compound which is often assumed to be the case in solid-state organic lasers. Instead, we demonstrate that this limit is due to thermal lensing. We measured the aberration-free component of the thermal lens by a pump-probe experiment and demonstrated a possible prolongation of lasing up to 14 kHz with a proper thermal lens intracavity correction. To check the universality of our claim, we also tested a second dye and found similar results. In contrast, solid-state dye lasers need a moving gain medium in order to be operated at high repetition rates and overcome abrupt photodegradation. Finally, we show that these lasers can also produce up to 80 µs lasing when they are highly multimode. Though we demonstrated such long pulse operation experimentally, more theoretical, and experimental investigation is required to understand their multimode lasing behavior which can be a future perspective of this work. Another perspective of this work would be to investigate mode-locking in organic laser which requires that the laser should be ideally CW or q-CW. We believe that our laser can be a good candidate for investigating such laser applications and hence, at the end of this thesis, we also give some useful direction and pathways to develop a low cost, compact, user friendly and tunable mode-locked organic in laser in future.

Table of contents

1. Motivation of this thesis

It has been more than sixty years since the invention of laser by T. Maiman [1]. Now a days lasers are significantly contributing to widespread real-life applications like DVD players, optical scanners, printers and so on. However, those lasers are mostly based on inorganic materials which are found in few specific wavelengths. Hence, despite being compact and efficient they might not be very suitable in application like spectroscopy. Wavelength tunable sources like OPO or OPA [2] has been developed to address this issue, but those sources are very expensive which restricts their affordability for mass applications. On contrary, another class of tunable sources based on organic fluorescent dyes has long been present in the realm almost from the birth of Maiman's laser. Large fluorescence bandwidth of organic dyes has made their tunability range over the whole visible spectrum. Interestingly, the material choice for organic lasers is almost infinity unlike the case of inorganic ones. Therefore, one can build an organic laser in any unusual wavelength of visible spectrum for very specific application. Organic lasers were first introduced in liquid phase with expensive and complex operating system in a sense that one has to deal with toxic dye solution. This solution needs to be replaced on a regular basis to avoid fast photodegradation of dye molecules. Solid-state organic lasers then appeared as a possible solution soon after the demonstration of liquid organic lasers. The nature of solid-state organic lasers avoided the issues of toxicity and inflammability. Moreover, the preparation of gain medium is low cost via spin coating or thermal evaporation techniques. Therefore, intense research attention was given to establish solid-state organic lasers in applications like spectroscopy[3], bio/chemo sensing[4]. But their expensive pump sources like the ones used by their ancestors – 'liquid dye lasers' was considered as their drawback to enter in application. Soon after the demonstration of thin film based Organic Light Emitting Diodes (OLED)[5] proving the semiconductor properties of organic molecules, researchers dreamed to realize organic lasers under electrical pumping which could solve the issues related to their pump sources. Despite numerous efforts until now, tremendous challenges are still needed to be solved related to several loss mechanisms in those devices which leads to very high lasing threshold. This led researchers to explore existing compact inorganic light emitters e.g., light Emitting Diodes (LED) or Laser Diodes (LD) as the pump source for organic solid-state lasers. As a consequence, successful demonstrations are found in the support of realizing solid-state organic lasers under low-cost LED[6] or laser diode pumping [7]. Thus, the design of optically pumped organic solid-state lasers could be made truly low cost, compact and user friendly but still their performance is not totally satisfactory. One of the alarming issues of those lasers is their poor photostability. Due to this photostability issue, they are also operated at low repetition rates to maintain lasing at least for few seconds. Second issue is that they cannot produce CW/q-CW lasing due to their intrinsic photo-physics (will be described later) while their CW/q-CW lasing might direct towards investigating laser application e.g., mode-locking.

If we closely look at the evolution of organic lasers, we can see an abrupt shift of research interest from liquid to solid-state organic laser in search of a user friendly, compact device. Surprisingly, no efforts

are found in between to investigate a compact, user-friendly circulation-free liquid dye laser's performance in terms of photostability, lasing duration etc. One reason behind that is probably due to unavailability of high-power laser diodes at low price until very recently. Therefore, by combining the advantage of low-cost high-power diode pumping, we propose to investigate circulation-free liquid dye lasers to find solution of above mentioned problems in solid-state dye laser. The liquid gain medium will be filled in mm sized spectroscopic cuvette and will be inserted in a two-mirror laser cavity. Such simple laser setup with no circulation tubing makes it comparable to a low cost, user friendly and compact solid state organic lasers. The motivation of this thesis centers on following aspects-

- ✓ To present, for the first time, a complete photostability study of such circulation free liquid dye laser to compare with the stability of solid-state organic laser using same material, cavity configuration and pump power.

- ✓ To investigate the maximum repetition rate of circulation-free liquid dye lasers which is also a key issue in most organic solid-state lasers. Briefly saying, organic solid-state lasers are intentionally operated at low repetition rates (~ 10 Hz) to avoid fast photo-degradation. While applications might be interested in their high repetition rate operation.

- ✓ To investigate their lasing under long pulse pumping in order to achieve maximum pulse duration from those lasers. It is relevant to mention here that organic lasers cannot produce more than few hundreds of nanosecond (ns) lasing. By achieving long pulse or CW operation would not only solve a scientific challenge but also may break one of the major bottlenecks to realize a compact, tunable, low-cost mode-locked organic lasers. Therefore, this thesis will call the end by discussing some future perspectives of this work especially toward the realization of first mode-locked organic lasers.

The discussion of photo-physics of organic materials is intentionally kept short in this thesis since they can be found in many excellent books e.g. [8–10] on internet. Similarly, general discussion about laser physics is also skipped due to available materials e.g. [11] to understand them.

1.1. Photo-physics of organic materials

Here we will discuss the limitations of organic lasers to produce CW lasing based on the creation of excited triplet states upon absorbing optical excitation. In this regard, we will use following energy level diagram (Figure 1.1) of organic molecules which is well known as Perrin-Jablonski diagram.

1.1.1. Excited states of organic molecules

Figure 1.1 shows that there are two types of energy levels in organic molecules – singlets (S_0, S_1, S_2,….S_n) and triplets (T_1, T_2,….T_n). Each of those states contain vibrational energy states (dotted lines). At thermal equilibrium, all molecules are assumed to be in ground state. Upon optical excitation, excited states are created in organic molecules. A singlet and triplet state are distinguished by their spin statistics. In quantum mechanics, the momentum of a rotating electron is called spin. For an electron, the spin value can be either + $\frac{1}{2}$ or - $\frac{1}{2}$. For simplicity, let's consider a system of two electrons one in ground state and another one is in excited state. If the total spin of the system is zero ($\frac{1}{2} - \frac{1}{2} = 0$) [12], the

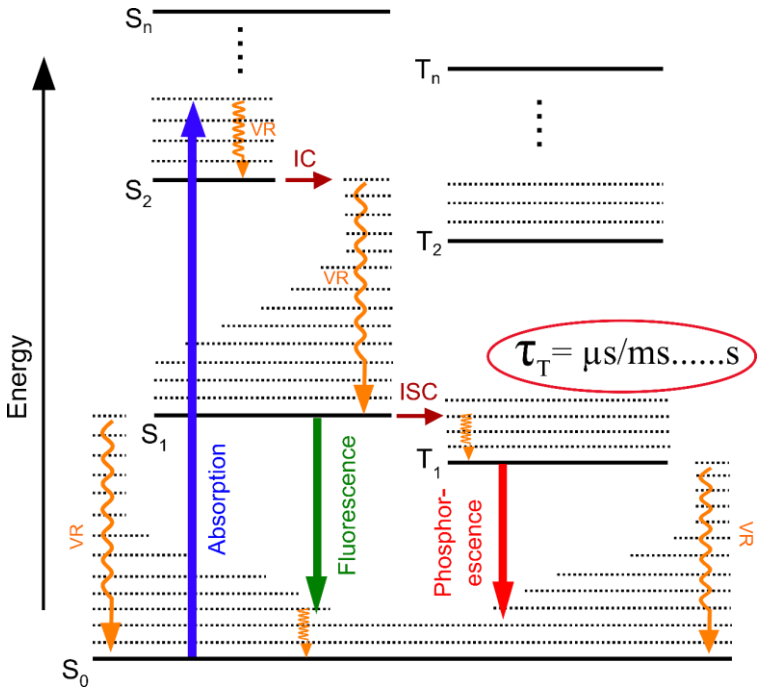

Figure 1.1 : Schematic of Perrin-Jablonski diagram to explain excited state photo-physics of organic molecules.

corresponding electronic state is called singlet states which is represented by an electron pair with opposite spins ↑↓. On the contrary, if spin orientation of the electrons is such that the total spin of the system is non-zero (e.g., $\frac{1}{2} + \frac{1}{2} = 1$ ***or*** $-\frac{1}{2} - \frac{1}{2} = -1$), then the electronic state is called triplet state which can be represented as ↑↑ or ↓↓ . According to quantum mechanics, during each electronic transition the spin of the total system must be conserved which allows electronic transition between singlet-singlet and triplet-triplet only. Therefore, transitions between singlet-triplet or triplet-singlet states are spin forbidden and thus highly improbable, unless there is a strong spin orbit coupling [13] which is simply the overlap of spin wave function and orbital wave function occupying the electron. Under

such condition, the transition from triplet excited state to singlet ground becomes spin allowed giving rise to a radiative emission called phosphorescence.

1.1.2. Radiative and non-radiative pathways from excited states

Once the molecules are promoted to excited singlet states via absorption of photons, they can undergo several decaying mechanisms to find themselves again in ground state, S_0. These decaying mechanisms are of two types: radiative and nonradiative which are briefly discussed below.

- **Radiative decays**

Generally radiative transition takes place between the lowest vibrational level of S_1 or T_1 and one of the sub levels between the ground state according to Kasha's rule[13]. If this happens from singlet states, the process is called fluorescence. On the other hand, radiative transition from triplet state is only possible when the spin-orbit coupling is very large which happens only in phosphorescent materials. Since the transition from first excited triplet state T_1 to ground state S_0 is spin forbidden, the lifetime of triplet state (10^{-6} -1 s)[13] is much longer compared to the first singlet excited state life-time (10^{-10} - 10^{-7} s)[13].

- **Non-radiative decays**

Non-radiative decay pathways can be divided as vibrational relaxation, internal conversion or inter system crossing as schematized in Figure 1.1. Here we will briefly discuss those processes.

(a) *Vibrational relaxation (VR):* Molecules can decay from vibrational energy levels (Figure 1.2) to the main electronic state which occupies those vibrational levels via VR. Similarly, a molecule can also return ground state from an excited singlet state via VR. This process

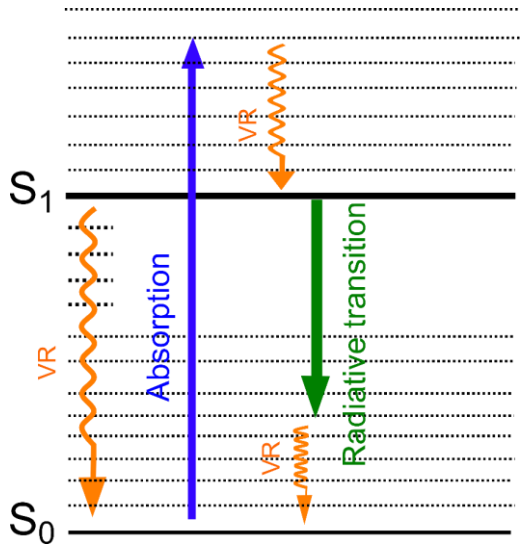

Figure 1.2 : Schematic to explain vibrational relaxation from vibrational energy levels of each electronic state.

is purely non radiative and vibrational energy is dissipated in the form of heat. Typical time scale of VR process is in the order of 10^{-12} s[14].

(b) *Internal conversion (IC):* IC is also a non-radiative electronic transition which occurs between the lowest vibrational level of upper excited energy states and one of the vibrational energy levels of underlying excited state as shown in Figure 1.3. Typical timescale of such transition is around (10^{-14} – 10^{-12} s)[14] making other radiative and non-radiative process unsuccessful to compete with it. However, IC from first excited singlet state to ground state is much slower (10^{-9} – 10^{-7} s)[9] than previous case because the energy gap between first excited singlet state and ground state is much higher compared to the energy gap between any two upper excited singlet state.

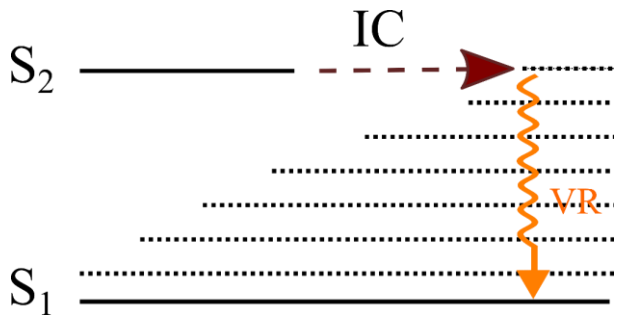

Figure 1.3 : Schematic to demonstrate internal conversion (IC) between two electronic state with same spin multiplicity.

(c) *Intersystem crossing (ISC):* ISC is a radiation less molecular transition between two isoenergic vibrational levels which belong to two excited electronic state of different spin multiplicity as shown in Figure 1.4. Usually, such transition between two electronic states

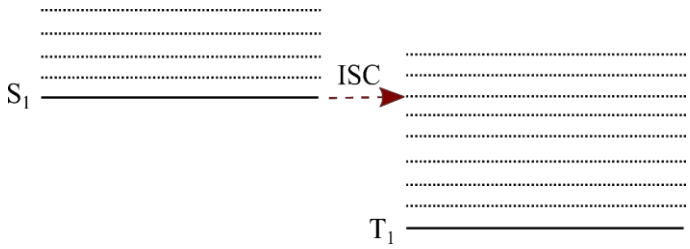

Figure 1.4: Schematic to demonstrate inter system crossing (ISC) between two electronic state with different spin multiplicity.

of different spin multiplicity is forbidden. But, as mentioned before, a strong spin orbit coupling can make such transition possible. In this process, the presence of heavy atoms (Ir, Pt) in the molecular structure can significantly increase the probability of spin-orbit coupling. Indeed, spin orbit coupling efficiency is proportional to Z^4 (Z = atomic number). ISC occurs within typical time scale around 10^{-10} to 10^{-8} s[13].

1.1.3. Detrimental role of triplet states in lasing dynamics of organic molecules

As discussed earlier, when molecules are in excited singlet states upon photon excitation, there are several radiative and non-radiative pathways they can undergo to return back to ground state. Among them, non-radiative decay mechanism via ISC is the most detrimental for their CW operation. During ISC, there is a flip of electronic spin and molecules find them in triplet states. As mentioned earlier, the lifetime of triplet states is quite longer other non-radiative or radiative decay processes. Several things can happen in practical organic laser when the molecules start to fill in triplet states.

i)

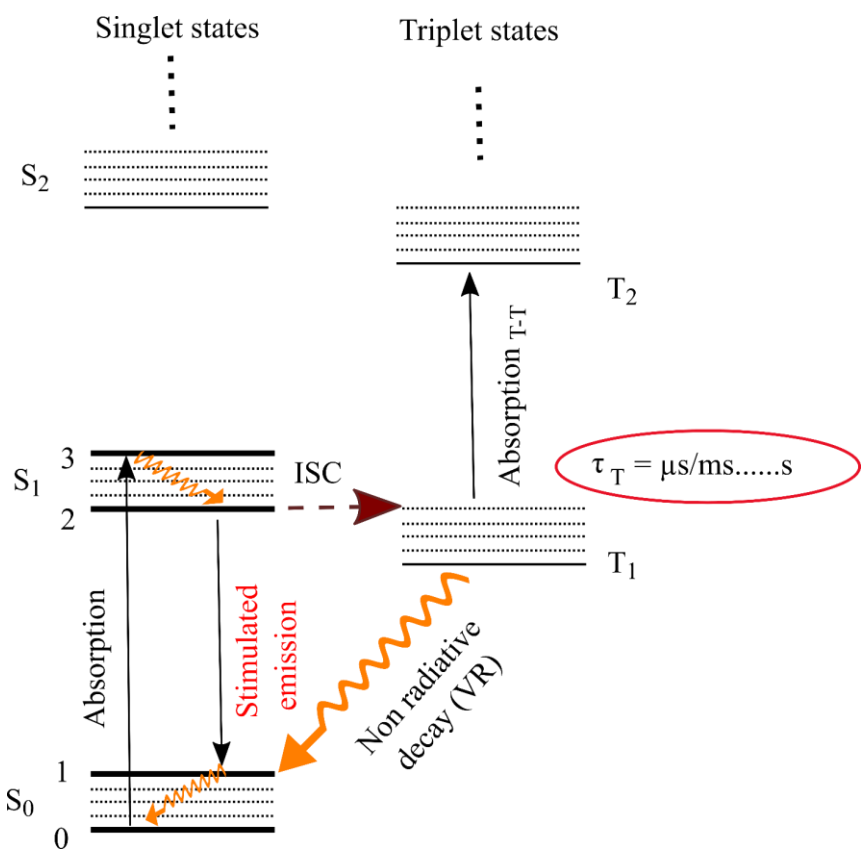

Figure 1.5 : Concept of lasing in organic molecules assuming their energy level as a 4-level system.

One of the most important conditions to obtain lasing in a gain medium is population inversion, which simply means that the higher lying excited state should have more population (electrons) than ground state. So that, there creates a high probability to force the electrons to decay from excited state before they naturally return to ground state after passing their lifetime in that state, which is well known as stimulated emission. In real life, it is impossible to obtain lasing in a two-level system with just ground state and excited state because ground state is always filled with electrons, and it is impossible to promote majority of electrons to excited state to fulfill the condition of population inversion. Fortunately, organic gain medium is approximated as a four-level system as shown in Figure 1.5 where lasing does not occur between excited state and ground state but one of the vibrational levels of ground state. This makes lasing easier in organic materials. However, when molecules start to transfer from singlet state to triplet state through ISC (Figure 1.5), the population inversion is disturbed, which can make it difficult to achieve lasing or can increase lasing threshold significantly.

ii) when molecules find their fate in triplet states, they can absorb laser photons since T-T absorption band overlaps with the lasing emission band[15]. By absorbing laser photons, they can be promoted to higher order triplet states. This is the reason why organic molecules produce lasing up to several hundreds of ns even if they are pumped with CW lasers.

1.2. Brief overview and key issues of state-of-art organic lasers need to be addressed

Organic lasers are the pioneers of coherent tunable sources. The very first organic laser was demonstrated by Sorokin and Lankard in 1966 by pumping a dye solution of pthalocyanine using a Q-switched ruby laser [16]. Four years later in 1970, first continuous wave CW organic laser came into reality by making a flow of Rhodamine 6G solution under continuous pumping from an Ar ion laser[17]. Such solution flow was proven to be useful to relax pump induced temperature gradient, slow down the irreversible photo-degradation[18] of organic molecules and so on. Therefore, solution flow became the state-of-art for liquid dye lasers. Moreover, CW liquid dye lasers were routinely used as a source to generate femtosecond pulses[19] due to their broad emission band before the invention of Titanium-Sapphire (Ti:S) lasers. However, those liquid dye lasers with complex and painful solution flow, as well as with expensive pump sources like frequency doubled or tripled solid-state lasers or another dye laser started to be questioned for lacking user friendliness, compactness and economy. Moreover, dye solution is toxic, carcinogenic, and flammable. Indeed, these issues restricted their steps outside research

laboratories and industries shadowing their real-life applications. This switched the interest towards organic solid-state lasers (OSSLs) to establish compact, user-friendly tunable organic lasers.

OSSL was first introduced in 1967 by Soffer and McFarland[20]. The gain medium was rhodamine 6G dye doped polymethaylmethacrylate (PMMA) and the pump source was the second harmonic of Neodymium doped Yttrium Aluminum Garnet (Nd: YAG) laser. Soon after this demonstration, Peterson and Snavely demonstrated lasing from rhodamine doped PMMA rods pumped by flashlamp excited laser [21]. Indeed, solid-state dye lasers are attractive over liquid dye lasers due to being compact, non-toxic, non-volatile, mechanically stable and user friendly. But the utility of solution flow system in primitive liquid dye lasers started to be clearly visible in the performance of solid-state dye lasers by highlighting their poor photostability and thermal resistance under intense optical pumping. To address this issue, researchers focused on making rigid host medium based on copolymer (polymer made from two or more monomer unites) [22–27] or Sol-gel technique (a method to obtain glass like, simple oxide or mixed oxide matrices are obtained through low temperature solution processing[28,29]. This effort increased their thermal durability under intense optical pumping[30] ~ MW/cm^2 and also improved their photostability though not comparable with the stability of liquid dye lasers with solution flow. However, long fabrication process of the gain media through radical polymerization, sol-gel or copolymerization was considered to be a major drawback of those laser devices. Moreover, post processing of gain medium, before using them in laser cavity, through mechanical processing (cutting, grinding, polishing to obtain optical grade quality) was also tedious.

The discovery of electroluminescence property of organic semiconducting materials and considerable interest to develop Organic Light Emitting Diodes (OLED) based on those materials led towards the realization of the first optically pumped (third harmonic of a femtosecond Nd: YAG laser) microcavity by Tessler et.al. in 1996[30]. In that work, 100 nm thick film of p-phenylene vinylene (PPV) was sandwiched between two highly reflective mirrors to make a high-Q cavity. A number of reports appeared following this work where the gain medium was thin film of organic semiconductor [31–36]. Since those thin film-based devices offer cheap and comparatively quick fabrication of gain medium without the need of further post processing to fit it inside laser cavity, this technology became the state-of-art for making organic lasers.

Thin film based organic lasers have been demonstrated in different cavity geometries e.g., DBR (Distributed Bragg Mirror) [37], DFB (Distributed Bragg Reflector) [38–41], VCSEL (Vertical Cavity Surface Emitting Laser)[42], micro disk[43], micro ring[44] and microsphere[45]. These resonators are attractive for compactness as well as they offer very low threshold lasing. However, one common issue shared by these resonators is poor beam quality and low output efficiency. These parameters are very important for laser applications. To solve this issue, our group introduced VECSOL (Vertical External Cavity Surface Emitting Organic Lasers)[46] where one can play with the spatial overlap between pump and

cavity mode and hence can extract maximum efficiency from the laser. In that case, a record laser slope efficiency ~ 52% was obtained with pulse energy as high as 42 µJ. Later, their wide tunability in visible wavelength [47] as well as lasing dynamics [48] were also investigated. Indeed, the diffraction limited TEM_{00} beam quality due to longitudinal pumping, high efficiency, flexible cavity parameters unlike e.g., DFB, VCSEL, micro ring lasers made VECSOL, easy fabrication process (spin-coating) made them attractive.

From above discussion, we can say that the 1970's dream to miniaturize the organic laser assembly has been accomplished. Their efficiency issue with thin film-based gain medium is also solved. However, still there are some key issues of state-of-art organic lasers which can restrict their real-life applications and can be an impediment to realize a compact, low cost, user friendly and tunable ultrafast organic lasers. These issues are going to be presented in the following.

1.3. Key issues of state-of-art organic lasers

- Applications using well-mastered optically pumped solid state organic lasers are still limited, especially because of their low photo-stability and inability to operate in high repetition rate regime. Despite numerous efforts to improve this issues, such as enhanced chemical design [49] the addition of triplet quenchers[50] encapsulation[51] or using mechanical motion [52,53] of the gain medium, a typical upper limit for stability is met around 10^6 pulses [27,54–56] for pump durations in the nanosecond range, and typical repetition rates for no-rotation system are around a few Hz [8] An exception is found in low power DFB laser using BSBCz dye where lasing life-time was, in the order of ~10^9 pulses at 80 MHz, limited by thermal degradation.

- Their CW/q-CW operation is still in dark though recently several advancements are made in this regard. For instance, q-CW lasing up to 30 ms has been achieved in a DFB laser device under diode pumping. However, from stability point of view, such device still requires to meet several challenges.

Those issues of state of art organic lasers should be solved before promoting them in real life applications.

1.4. Proposition of this thesis to solve those issues

We propose to investigate an 'off the shelf' liquid dye laser with no circulation tubing. A standalone cuvette will contain liquid dye solution to be used inside a two-mirror laser cavity. Absence of any solution circulation would make the setup user friendly as solid-state dye lasers. It is required to mention

that we are not the very first to introduce the idea of circulation-free liquid dye lasers. Few reports are found before us mainly in the direction of introducing a circulation-free liquid dye laser under diode pumping [57], investing their tunability [58] and efficiency [59]. But, those works did not comment on the photostability performance, pulse dynamics or repetition rate of circulation free liquid dye lasers.

This work, hence, starts from there to disclose those missing information about circulation free liquid dye lasers. Our work is also inspired by the recent price drop (<100$) of high-power laser diodes in blue which would be employed as the pump source of the dye laser system. Varying the pulse duration of laser diodes also opens the possibility to investigate dye laser temporal dynamics of laser under ns – qCW pumping. The integration of laser diode pumping makes this setup very comparable to the solid-state dye laser in terms of cost and compactness also. Moreover, no fabrication step is required in this laser setup and cavity geometry is flexible to investigate laser dynamics by changing cavity parameters.

Unlike solid-state dye laser where the dye molecules are immobile inside solid-state matrices, in proposed liquid dye laser even with no circulation the molecules have some intrinsic movement due to their diffusion property. We believe this might help to increase their photo-stability. If the laser is found to be photo-stable, we will try to obtain maximum repetition rate lasing from them. In liquid phase, since the dye molecules are always vibrating, lifetime of triplet states might also be short because triplet states are deactivated by vibrational relaxation. Therefore, long pulse lasing might also be possible to obtain in circulation free liquid dye lasers.

The organization of thesis is as follows:

First, we will develop diode pumped circulation-free liquid dye laser from the scratch. The gain medium will be a dye solution filled in spectroscopic cuvette without circulation tubing. This laser will be realized in a two mirror Plano-concave cavity since our group demonstrated the highest efficiency using solid-state gain medium in similar laser cavity. Moreover, such cavity offers flexible cavity parameters e.g., cavity length, output coupler mirror reflectivity etc. can be changed very easily. Following the laser design section, we will provide all types of laser characterization e.g., laser threshold, efficiency, spectrum, photostability and so on. At the end of this chapter, we will investigate their temporal dynamics under high repetition rate or long pulse (up to 10 µs) pumping. In the following chapter we will try to obtain high repetition rate lasing from circulation-free liquid dye lasers. Finally we will investigate their long pulse operation though the thesis will end by showing some future perspectives and pathways towards the continuation of this work.

2. Diode pumped circulation-free liquid dye lasers

This chapter focuses on laser design and characterization. The design section details on basic laser components e.g., pump source, gain medium and cavity while laser characterization provides information regarding laser efficiency, beam quality, pulse duration, photo-stability and so on. As mentioned earlier, poor photo-stability and short pulse duration (typically few hundreds of ns) are two key issues in solid-state organic laser, therefore, those features of circulation-free liquid dye laser will be compared with its solid-state counterpart using same material, comparable absorption, same cavity and pump configuration. This chapter will end by showing some limitations of such laser device, which will eventually raise the interest for the following chapters.

2.1. Laser design

The laser design incorporates a combination of diode lasers to longitudinally pump circulation free cuvette filled with laser dye having high absorption at laser diode wavelength. The laser cavity consists of two mirrors having enough reflection in laser wavelength to provide optical feedback. Here we will present a complete laser design followed by the details of pump, gain medium, cavity separately.

2.1.1. Pump

The pump source is a combination of two 445 nm laser diode (5W each) beams, coupled by polarization beam splitter (PBS) as shown in Figure 2.1. Very recently, high power laser diodes at this specific wavelength[60] are available at < 100$. Besides, almost all organic molecules exhibit high absorption at blue-green region of spectrum.[8] Anyway, the pump laser diodes are mounted inside aluminum heat sinks and driven through a pulsed laser diode driver (PCO-7120) bought from Directed Energy, INC as shown in the inset of Figure 2.1. This driver is able to drive CW laser diodes in pulsed mode (20 ns – 10 µs) resulting peak power around several tens of Watts as shown at the inset of Figure 2.1. Reduced thermal load on laser diode at pulsed regime compared to CW results in such peak power which is advantageous to easily reach threshold ~ kW/cm^2, after focusing on gain medium, typically seen in an external cavity organic laser we intend to build. Rise time of those pulses, as short as 10 ns, also indicates the advantage of using these drivers over traditional mechanical chopper for this work where typical rise time of each pulse is several µs. Long rise time of pump pulses can significantly increase organic laser threshold as well as affect their performance (efficiency, pulse duration or high repetition rate operation etc.) due to the accumulation of triplet states ($\tau_T = \mu s - s$). For similar reasons e.g., to have low threshold and efficient laser, beam quality of the pump laser is also an important issue to be considered in ahead of their employment in laser set-up. Classically, laser beam quality is determined by the value of M^2.

Details regarding significance and calculation of M^2 of a laser beam will be given in laser characteristics and performance section. It is important to note that, a diffraction limited TEM_{00} ($M^2 = 1$) beam is always desired to longitudinally pump laser medium to decrease laser threshold, increase efficiency[61,62] and so on. Unfortunately, the beam quality of a laser diode is not diffraction limited, rather highly elliptical with an additional feature of astigmatism – a phenomenon of resulting in two waists (w_x & w_y) in two orthogonal directions along propagation axis (z). Difference between these two waists is called astigmatism. An astigmatic beam is not optimal for pumping gain medium. Therefore, to know whether our laser diodes also possess such astigmatism, one of the diode beams is

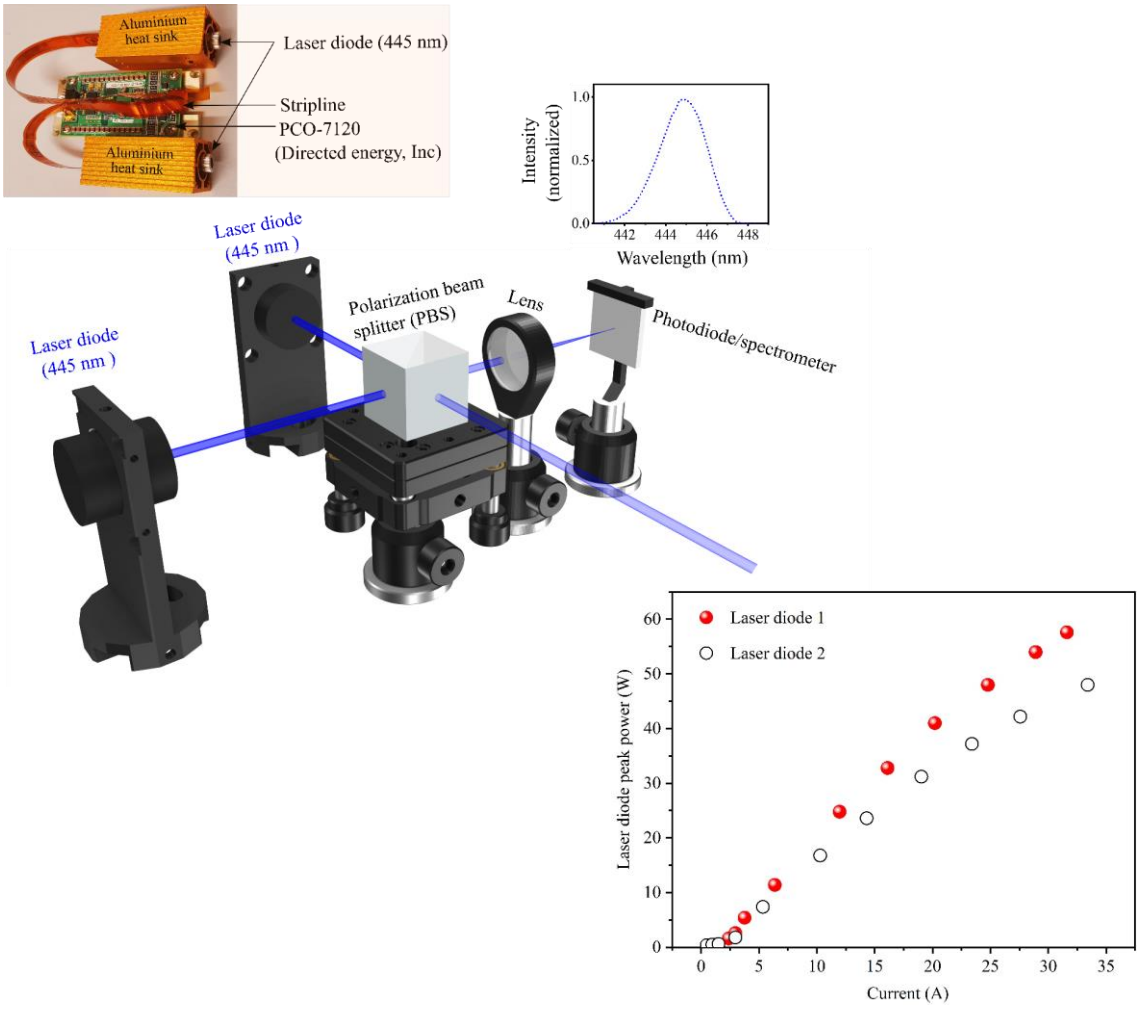

Figure 2.1: Two 445 nm (see spectrum) (5W each) laser diode beams are combined using polarization beam splitter. A small part of the beam owing to coupling losses in beam splitter is focused to a photodiode or spectrometer to monitor pulse duration or laser spectrum, respectively. Upper inset: Practical connection of laser diode, mounted inside aluminum heat sink, to PCO-7120 (Directed energy, Inc) using low loss striplines. Lower inset: Laser diode power (W), measured separately (by blocking one diode while measuring the power of another and vice versa) when operated with 50 ns pulse duration, as a function of current (A).

focused by placing 150 mm lens after PBS. Beam radii at different positions before and after the focus of the lens, measured using CCD camera, is depicted in Figure 2.2. The diode beam clearly shows two waists associated with very different beam divergences in x and y axes determined by their M^2 of 17.76 and 1.88 respectively; since far field laser beam divergence is related to M^2 by following equation (2.1),

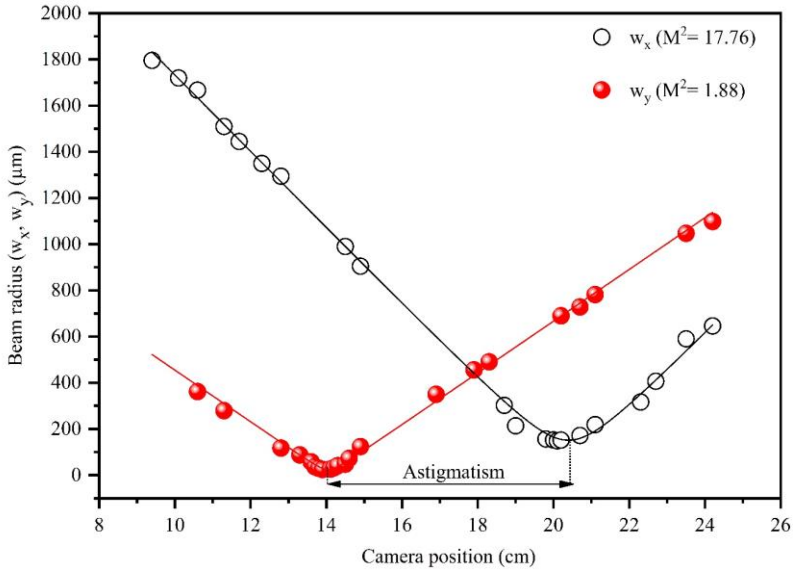

Figure 2.2: Laser diode beam radius (μm) recorded with CCD camera at different positions (mm) after 150 mm focal length plano-convex lens.

$$\theta = M^2 \frac{\lambda}{\pi w_0} \tag{2.1}$$

Where, θ is the beam divergence half-angle, λ is laser wavelength and w_0 is the beam waist radius (at $\frac{1}{e^2}$ point of laser intensity). One of the popular methods to correct astigmatism is to use a pair of cylindrical lenses of suitable focal lengths to collimate the beam by correcting its divergence in both axes. In this regard, the value of M^2 in two orthogonal axes can be useful to predict cylindrical lens focal lengths to be employed. However, it is often difficult to find cylindrical lenses of suitable focal lengths for this purpose. Moreover, the entire set-up becomes very sensitive to the position and alignment of cylindrical lens pair. In the end, even if the beam collimation is perfect, non-centrosymmetric shaped pump is expected on the gain medium, which does not match perfectly to a diffraction limited circular cavity beam produced in a Plano-concave laser cavity to be used in our study. Mismatch between pump and cavity beam affects the laser threshold and efficiency which will be shown in laser performance section. However, from this discussion, we can conclude that, astigmatism correction and beam circularization would make the diode beam optimum for pumping. Therefore, to reject their inherent

astigmatism as well as to homogenize them, we injected the combination of diode beams into a multimode optical fiber (100 µm core diameter, 0.22 NA) with the help of a 20 mm focal length aspheric

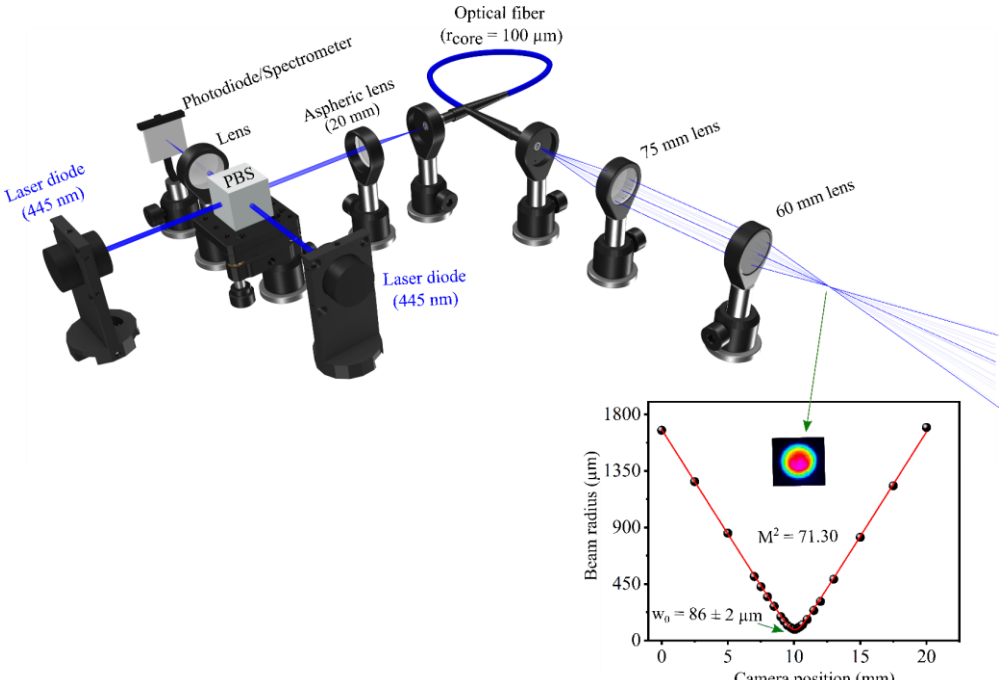

Figure 2.3: Laser diode beam is injected into a multimode optical fiber (100 µm core radius, NA = 0.22) with the help of 20 mm focal length aspheric lens. At fiber output, the beam is collimated and focused using 75 mm and 60 mm focal length lens respectively. Inset: M^2 of the beam calculated from the beam radii (µm) at different positions (mm) after 60 mm focal length lens.

lens as shown in Figure 2.3. Though 10% - 15% of diode power is sacrificed during injection process, the output beam from the fiber looks perfectly homogeneous and free from astigmatism as can be seen at the inset of Figure 2.3 where the output of the fiber is collimated and focused to a single waist unlike two waists found in Figure 2.2. However, M^2 = 71 measured after fiber refers to a highly diverging beam with short Rayleigh length. Considering this, the cuvette path length should also be equal or shorter than pump Ryleigh length but also the absorption of solution inside such short path length should be enough to get lasing. All of these will be discussed in the section of gain medium.

2.1.2. Gain medium

A well-known laser dye 4- Dicyanomethylene-2-methyl-6-p dimethylaminostyryl-4H-pyran (DCM) is chosen as the gain medium considering its high absorption at pump wavelength (445 nm) as shown in Figure 2.4. This figure also shows that its fluorescence has a large stoke shift in red resulting very small spectral overlap between absorption and fluorescence spectra which ensures negligible ground state

absorption during lasing operation. Moreover, its lasing property is well investigated in literatures which might be interesting for comparison perspectives. Anyway, to use this dye as a gain medium, a solution

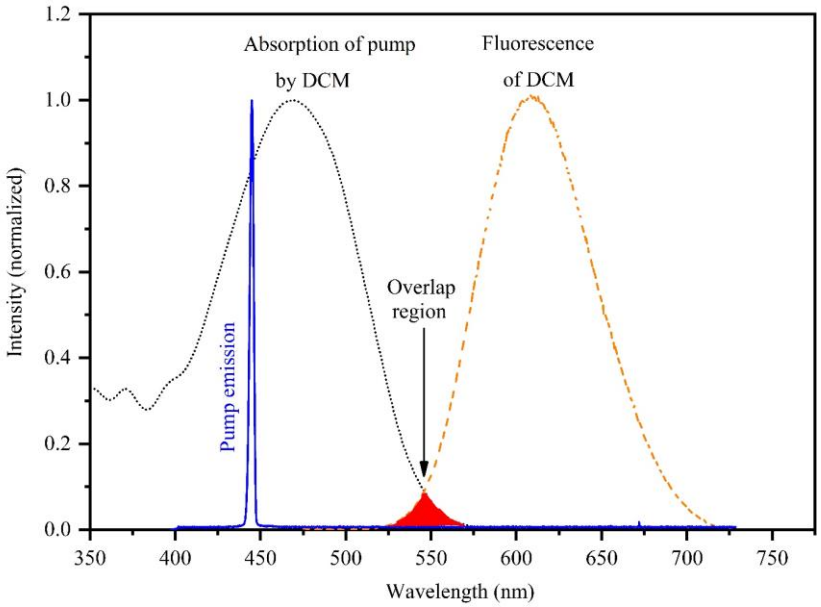

Figure 2.4: Absorption and emission properties of DCM dye solution (in propanol 2).

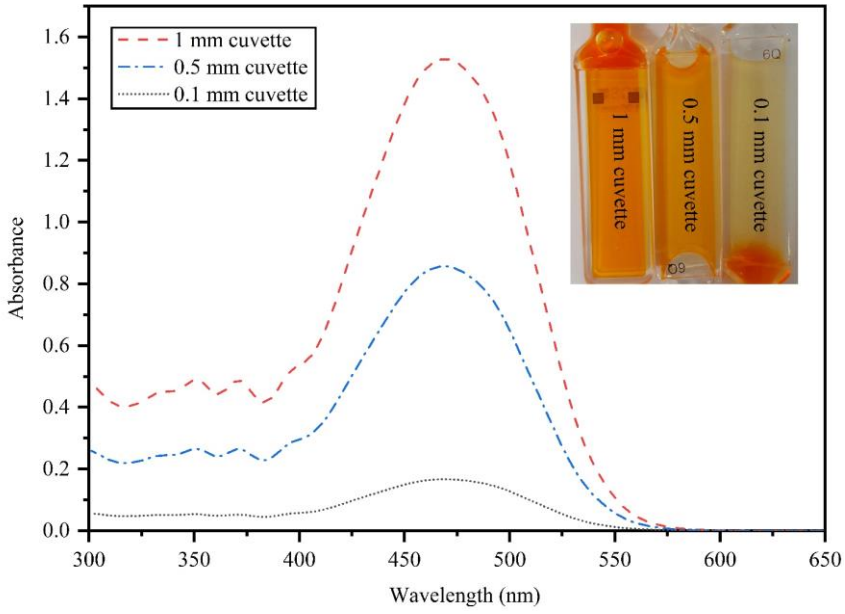

Figure 2.5: Absorbance (a.u.) of the highest concentration of gain medium (DCM in propanol-2) inside spectroscopic cuvettes of different path-lengths (0.1 mm, 0.5 mm and 1 mm).

of DCM in propanol-2 was contained in a spectroscopic cuvette, to be directly used inside laser cavity without attaching to a circulation circuit. Considering short Rayleigh distance of the pump circular beam

after the fiber ($Z_R = w^2 / (r_{core}. NA)$ = 0.16 mm), 100 µm path-length cuvette seems a good choice for this work. But solubility limit of DCM in propanol does not allow enough absorption of pump inside such short ~ 100 µm light path to obtain lasing using our laser diode. To show pump absorption inside different path length cuvette, we prepared a completely saturated solution of DCM in propanol-2 and measured its absorption inside 0.1 mm, 0.5 mm and 1 mm cuvettes as shown in Figure 2.5 . This information might be useful to show on one hand that DCM shows solubility limit in propanol and on the other hand find cuvette path-length having sufficiently high absorption of pump to get lasing easily. To prepare such solution, 11 mg of DCM is added to 20 mL of propanol-2 solution inside a beaker and kept overnight on a magnetic stirrer. Following day, a highly concentrated solution is found which showed some insoluble DCM molecules at the bottom of the beaker ensuring the saturation of solution. Even such highly concentrated DCM solution shows absorption as low as 27% (insufficient absorption for lasing with our pump power density) inside such 100 µm light-path cuvette shown in Figure 2.5. In contrast, 1 mm and 0.5 mm cuvette provide 95% and 82% absorption respectively at pump wavelength. But it is found inconvenient to work with 0.5 mm (as well as 0.1 mm cuvette) due to surface tension of its closely spaced glass facets which does not allow to change solution easily. Last but not the least, cuvette volume also has an influence on the photo stability of such laser devices which will be detailed later. Taking all these into consideration, 1 mm path-length cuvette is chosen for our work where DCM dye is dissolved in propanol-2 solvent (1.76×10^{-6} M) to provide optimum absorption (80% - 85%)[63] at pump wavelength.

2.1.3. Laser cavity

The concept of laser cavity design is adopted from the previous work of our group demonstrating Vertical External Cavity Organic Laser (VECSOL) with record ~ 52% slope efficiency [46]. Our laser cavity is formed with commercially bought plane mirror (>80% transparent at 445 nm) with 99.9% reflectivity at 600 - 660 nm and concave mirror as output coupler. The advantage of such cavity with external mirrors is its flexible design parameters e.g., cavity length, output coupler radius of curvature as well as reflectivity. For instance, they can easily accommodate intracavity elements, may be interesting for application like wavelength tunability,[47] and second harmonic generation (SHG).[64] In this work, we used output coupler with different reflectivity e.g., 99%, 98%, 94% etc. at 600 - 660 nm to show the impact of output coupler reflectivity on laser efficiency and threshold which will be detailed in laser characterization and performance section. The radius of curvature of concave mirror is chosen based on pump and cavity mode overlap calculation on gain medium. Briefly, a concave mirror acts as a lens due to its radius of curvature and creates cavity beam waist on plane mirror. Usually, radius of curvature of concave mirror is chosen such that the cavity beam size on gain medium is equal or bigger than the pump size to obtain efficient spatial overlap between pump and cavity mode resulting efficient lasing with diffraction limited TEM_{00} beam quality. Considering this, we choose 100 mm radius of

curvature (ROC) output coupler which creates around 95 µm (in radius) cavity beam on cuvette in a short ~ cm sized cavity while our pump size is 60 µm (in radius) µm using an achromatic doublet lens of 35 mm focal length. The reason to choose such short cavity length will be discussed in the following.

2.1.3.1. Cavity length (L_{cavity})

It is well known that efficiency of a CW laser depends on pump intensity, active material concentration, mode matching, etc.[8] However, organic lasers need to be operated in pulsed mode which has been discussed before. In pulsed laser, cavity length also influences laser efficiency in addition to above parameters.[48] When pump pulse is sent to excite gain medium in laser cavity, lasing does not start at the same time when the pulse hits the gain medium. Instead, a time duration is required to build-up laser oscillation inside cavity from the time when pump pulse first hits the gain medium. This is because the cavity photons require some time to complete several round trips (inside cavity) to achieve a gain that overcomes all losses of the laser cavity. This time duration is termed as laser build-up time which depends on cavity length, pump pulse duration, pump intensity etc. Indeed, as our laser cavity is composed of a plane and concave mirror enclosing 1 mm light path active medium, laser photons spend most of the round-trip time in air rather than in active medium which indicate that the highest efficiency should be obtained for short cavities, intense/long pump pulses.[8] Therefore, started our work by designing ~ cm sized Plano-concave laser cavity as mentioned earlier. But the influence of increasing cavity length on laser efficiency will be shown in laser performance and characterization section of this work. Though a Plano-concave cavity can be made as short as possible, designing long cavity requires to consider stability issues. This is discussed in the following.

2.1.3.2. Calculation of laser cavity stability

Stability of any laser cavity is an important aspect since it ensures the confinement of light rays or laser photons inside cavity after multiple round trips. Classically, cavity stability is determined by calculating its transfer matrix in ray optics formalism [65]. In Ray optics, each cavity element e.g., mirror, lens, propagation through a medium etc. can be defined with the help of 2×2 transfer matrix: $\begin{pmatrix} A & B \\ C & D \end{pmatrix}$. By linear multiplication of the transfer matrix of all cavity elements, the total transfer matrix (T) of the laser cavity is determined[65]. Finally, substituting the value of A and D matrix in following laser cavity stability equation (2.2) determines the stability condition of a specific laser cavity.

$$-1 \leq \frac{A+D}{2} \leq 1 \tag{2.2}$$

To show an example of such calculation, let us consider the case of our Plano-concave laser cavity assuming no gain medium for simplicity as shown in Figure 2.6. Here each cavity element is defined by their individual transfer as also shown in Figure 2.6 . Therefore, transfer matrix (T) of the whole system can be written as,

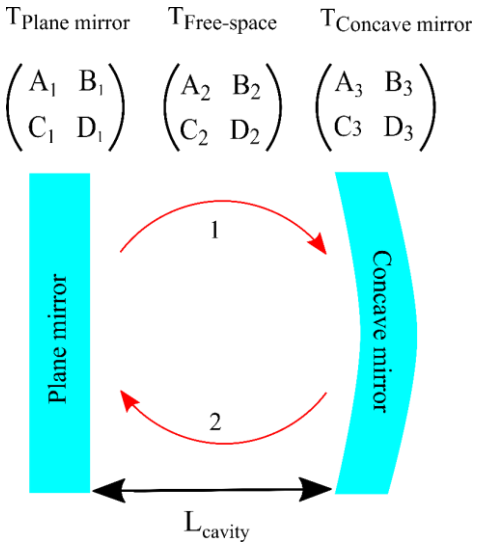

Figure 2.6: Transfer matrix calculation of a plano-concave laser cavity for one round trip. Each element inside cavity e.g., plane mirror, concave mirror, propagation in free space etc. is defined by 2×2 transfer matrix. Arrow 1 mentions that the ray travels through free space from plane mirror to concave mirror and bounces back towards plane mirror to complete single round trip which is shown by arrow 2.

By substituting the values of transfer matrix of free space propagation: $T_{Free\text{-}space} = \begin{pmatrix} 1 & L \\ 0 & 1 \end{pmatrix}$, concave mirror with radius of curvature (R): $T_{Concave\ mirror} = \begin{pmatrix} 1 & 0 \\ -\frac{2}{R} & 1 \end{pmatrix}$, plane mirror: $T_{Plane\ mirror} = \begin{pmatrix} 1 & 0 \\ 0 & 1 \end{pmatrix}$, equation (2.3) reduces to,

$$T_{cavity} = \begin{pmatrix} A_1 & B_1 \\ C_1 & D_1 \end{pmatrix}\begin{pmatrix} A_2 & B_2 \\ C_2 & D_2 \end{pmatrix}\begin{pmatrix} A_3 & B_3 \\ C_3 & D_3 \end{pmatrix}\begin{pmatrix} A_2 & B_2 \\ C_2 & D_2 \end{pmatrix} \tag{2.3}$$

$$T_{cavity} = \begin{pmatrix} 1-\frac{2L}{R} & L(1-\frac{2L}{R}) \\ -\frac{2}{R} & 1-\frac{2L}{R} \end{pmatrix} = \begin{pmatrix} A & B \\ C & D \end{pmatrix}_{cavity} \tag{2.4}$$

By substituting the value of A and D matrix from equation (2.4) in equation (2.2), the stability condition for this cavity becomes,

$$L_{cavity} < R \tag{2.5}$$

Adding a gain medium inside cavity does not change this condition significantly which will be shown below. Interestingly, above calculation can be easily performed in reZonator software which is free as

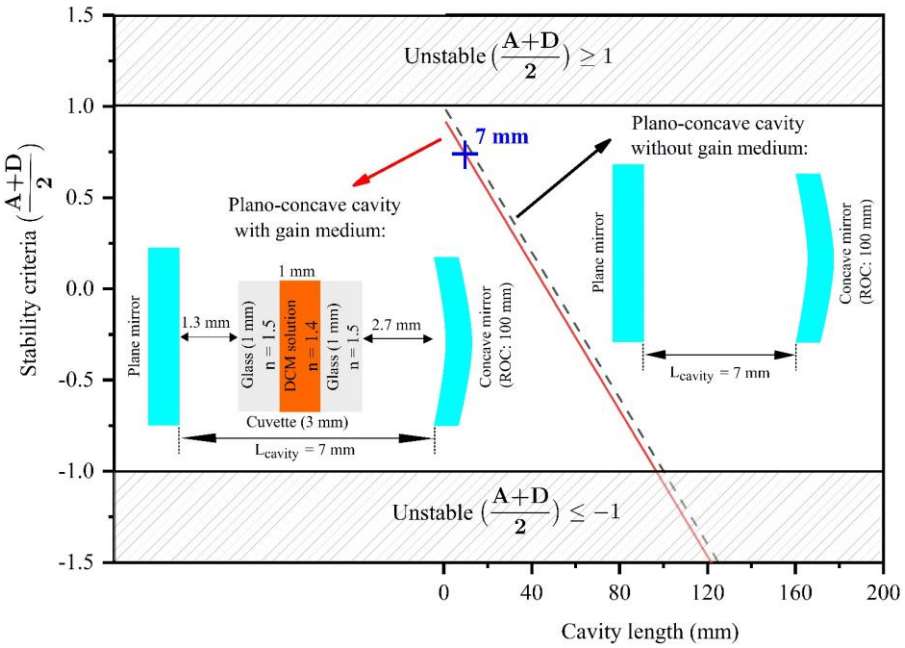

Figure 2.7: Stability (red line and red dashed line) of a laser cavity using plane mirror and a concave mirror (100 mm ROC) as a function of cavity length (mm). Upper inset: Plano-concave cavity without gain medium. Lower inset: Plano-concave cavity including a cuvette having liquid gain medium.

well as powerful tool for designing laser cavities. It is even more intuitive to perform such cavity stability simulation in reZonator since we can also check laser stability by inserting intra cavity elements e.g., cuvette, lens and so on without going through in hand matrix calculation as shown above. Figure 2.7 shows such an example where stability (dashed line) of a Plano-concave laser cavity (schematic is given in right inset of Figure 2.7), exactly what was explained in Figure 2.6, is plotted against cavity length. The cavity is found to be unstable when cavity length becomes larger than ROC of concave mirror – same as what is found from round trip transfer matrix calculation in equation (2.5). As mentioned before, the stability (red line) of the same Plano-concave cavity as a function of cavity length is almost same when a cuvette with DCM solution is numerically inserted inside cavity (schematic is given in left inset of Figure 2.7). From the result of cavity stability simulation using 100 mm coupler, we show that our laser cavity is stable for the chosen short cavity length ~ 7 mm for which the laser threshold should be minimum and efficiency is also expected to be higher as discussed before. Moreover, choosing such ROC output coupler also opens the possibility to increase cavity length up to several tens of centimeters

to compare laser performance (threshold, efficiency etc.) for short and long cavity. All of these issues will be discussed in the laser performance and characterization section.

2.1.4. A simple, compact, user-friendly dye laser system

Figure 2.8 shows a complete laser set-up where a laser dye (DCM in propanol 2) solution filled circulation free cuvette is pumped by a combination of two 445 nm laser diodes. The cuvette is placed orthogonal to pump, instead of Brewster angle, close to the plane mirror of a Plano-concave laser cavity for several reasons. Firstly, cuvette at Brewster angle might add some astigmatism and ellipticity[59] to laser beam and secondly, since the concave mirror creates cavity beam waist on mirror, placing cuvette far from the plane mirror would significantly disturb mode overlap between pump and cavity. Moreover, this design scheme is also very comparable to the case where a solid-state gain medium is spin coated

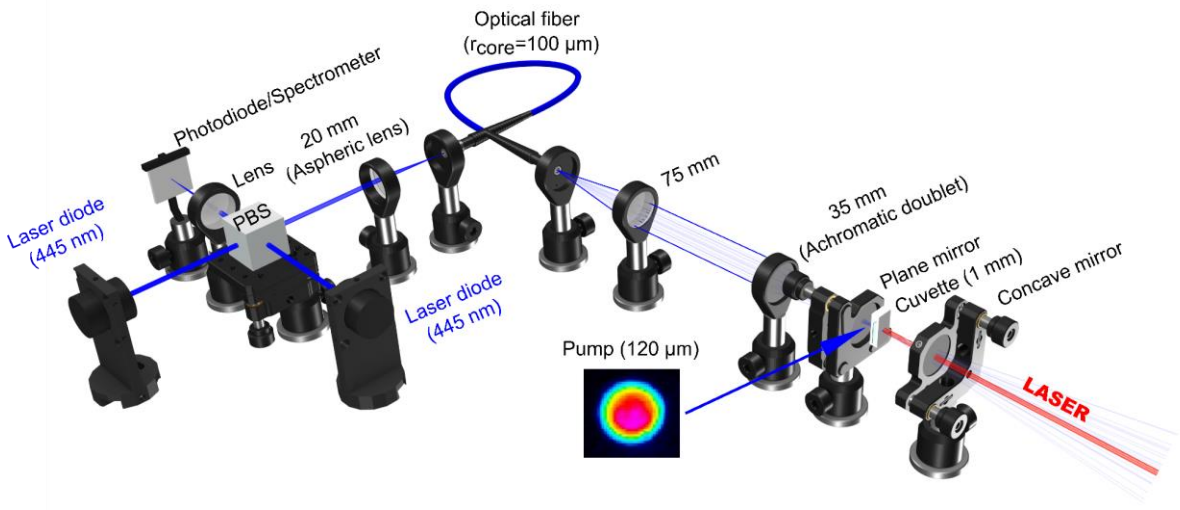

Figure 2.8: Schematic of complete laser design. PBS: Polarization beam splitter.

on the plane mirror when designing solid-state organic laser using Plano-concave laser cavity.[7,46,48] Therefore, our laser design lets the field open to compare liquid organic laser performance with a solid-state one with same material under similar pump and cavity configurations. However, the cavity length is as short as ~1 cm but can be changed easily and the total footprint of the actual setup was 29 cm by 18.5 cm and could easily be made much smaller. This design makes this laser very easy to implement with no technological step for device fabrication, and no circulation tubing. Simplicity of the setup makes the laser design especially attractive for any research application that requires pulsed light at an "unconventional" wavelength not accessible with Standard lasers.[47,58] The easy replacement of the gain medium makes it convenient for screening new organic dyes to evaluate their lasing potential directly from a solution.[66] Indeed, novel molecules have been tested in this set-up to reveal their lasing properties

for the first time. It is also valuable for educational purposes as the laser structure can be built from scratch with the nice advantage of having both pump and laser wavelengths in the visible range.

2.2. Laser performance and characterization

This section will present performance and characterization of circulation free liquid dye laser from the point of threshold, efficiency, beam quality, photo-stability and so on. Some limitations of this laser device will also be discussed at the end of this section.

2.2.1. Laser threshold and efficiency

One of the defining characteristics of any laser is its threshold – a condition where the gain in the laser medium equals all type of losses in the cavity. If we skip excited state losses of organic molecules, cavity losses may arise from finite reflectivity of output coupler mirrors, scattering in cuvette (due to any defects), etc. Therefore, modulating cavity losses will have direct impact on laser threshold and efficiency (we define here optical-optical conversion efficiency as the ratio of laser energy at output to the absorbed pump energy). Here, we will investigate our laser performance as a function of output coupler mirror reflectivity and cavity length.

2.2.1.1. Laser threshold and efficiency *vs.* output coupler reflectivity

Lasing is observed with a well-defined threshold around 23 kW/cm^2 when using a high reflectivity output coupler in a 7-mm long Plano-concave cavity as shown in Figure 2.9. Since laser threshold is a function of cavity losses, changing output coupler reflectivity to 98%, 94% and 90% resulted an increase in laser threshold to 28 kW/cm^2, 58 kW/cm^2 and 80 kW/cm^2, respectively. As expected, laser efficiency is found to be the lowest ~ 0.3% for a low threshold laser using 99.9% output coupler whereas the highest laser efficiency ~ 18% is obtained using 98% reflectivity output coupler which dropped to 13% and 9% by changing output coupler reflectivity to 94% and 90%, respectively. This is shown in Figure 2.10. From here, we can say that there is an optimum output coupler reflectivity, in our case 98%, for which laser threshold may not be the lowest but efficiency is the highest. Using this output coupler, we also obtained optical efficiencies around 17% and 14% using longer pump pulses e.g., 500 ns and 1 µs, respectively as shown in Figure 2.11.

Here, we discussed laser efficiency and threshold when the cavity length was fixed. By increasing or decreasing cavity length mode matching between pump and cavity starts to impact on laser efficiency and threshold. This issue will be discussed in the following.

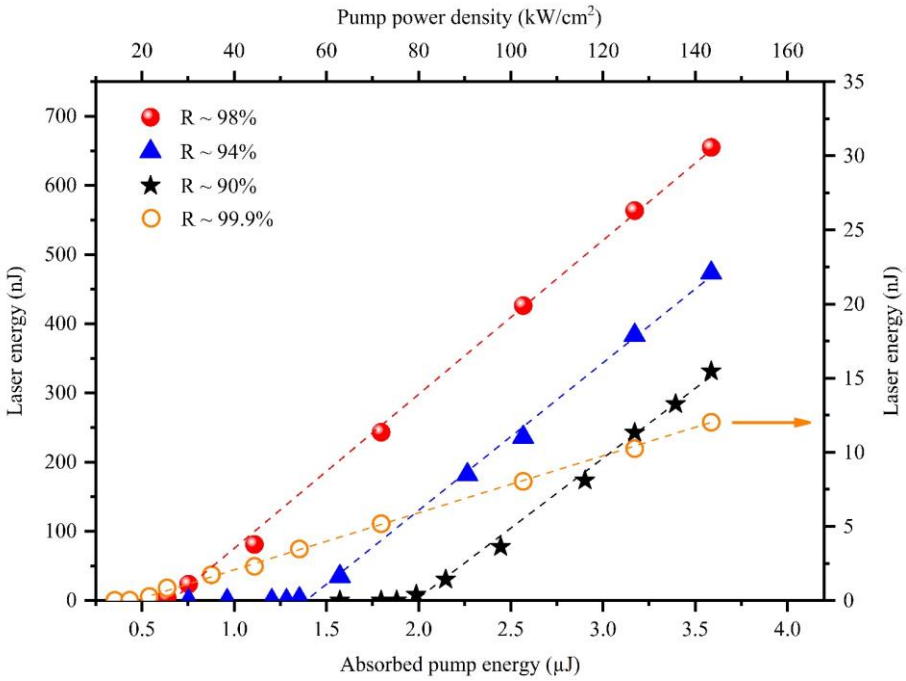

Figure 2.9: Laser energy (nJ) for different reflectivity (R) output couplers (100 mm ROC) as a function of absorbed pump energy (μJ) (bottom axis) and pump power density (kW/cm^2) (top axis) measured from absorbed pump energy using 200 ns pump.

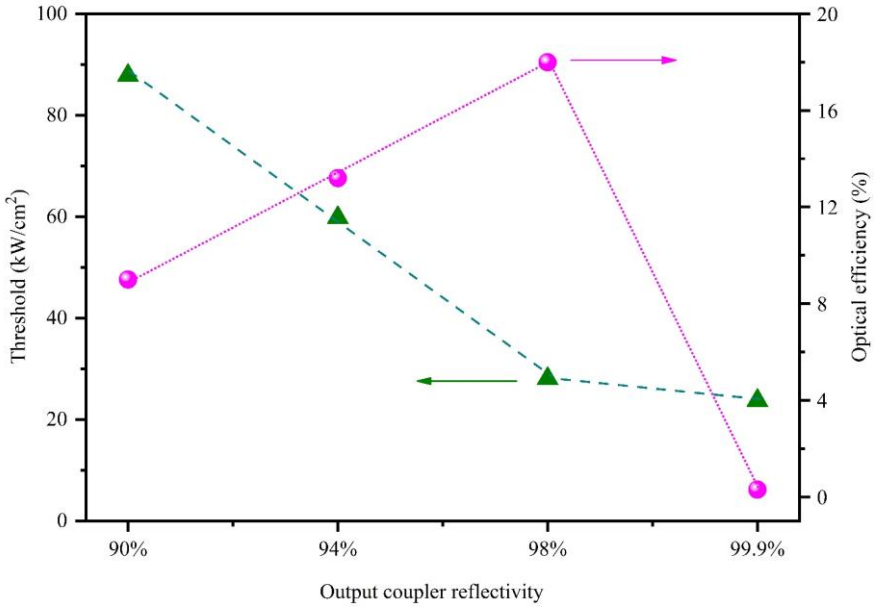

Figure 2.10: Laser threshold in kW/cm^2 (left y - axis) and efficiency (%) (right-y axis) as a function of output coupler mirror reflectivity in a 7-mm long Plano-concave cavity. 200 ns pump is used for this characterization.

2.2.1.2. Laser threshold and efficiency *vs.* cavity length

Here we show the impact of cavity length on laser threshold and efficiency using same Plano-concave laser cavity pumped by 200 ns long pulses as discussed above. For this purpose, we increased cavity length by moving output coupler mirror away from cuvette up to 90 mm such that the cavity remains inside stability zone of Plano-concave cavity (see Figure 2.7) using 100 mm (R ~ 98%). Laser energy as a function of absorbed pump energy (bottom x axis) and pump power density (top x axis) is

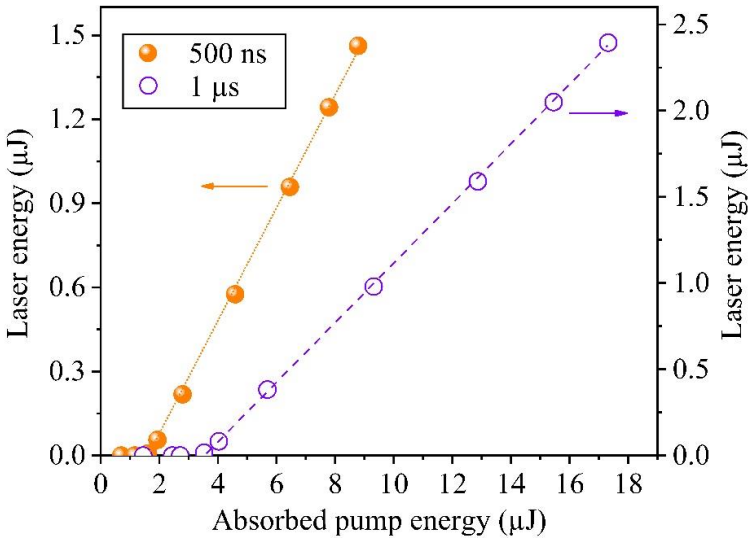

Figure 2.11: Left: Laser energy (µJ) for 500 ns pump, Right: Laser energy (µJ) for 1 µs pump as a function of absorbed pump energy (µJ).

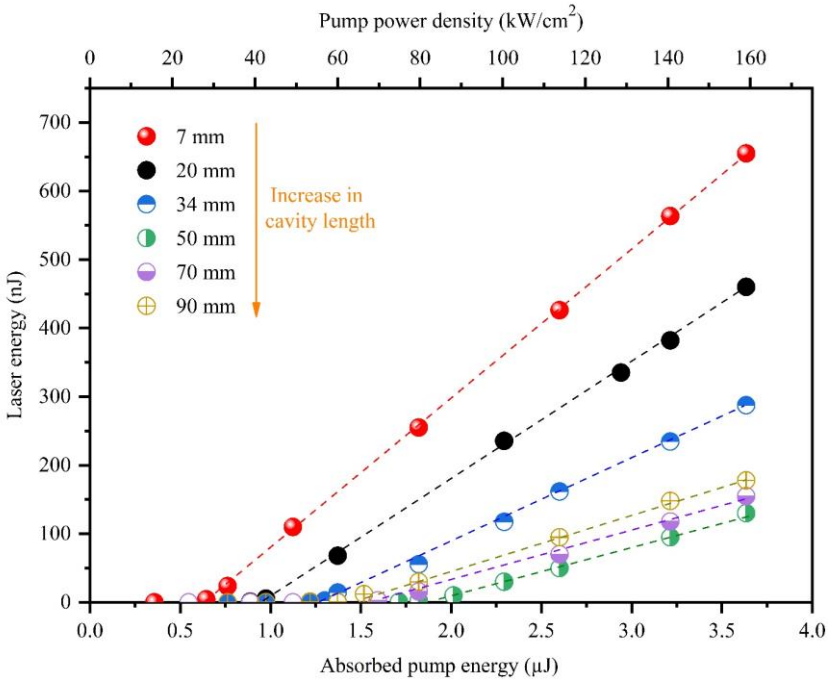

Figure 2.12: Laser energy (nJ) as a function of absorbed pump (200 ns) energy (µJ) (bottom x axis) and pump power density (kW/cm^2) (top x axis) for different cavity lengths.

showed in Figure 2.12 for different cavity lengths. For better insight, laser threshold and efficiency at those cavity lengths is plotted in left and right y-axis, respectively, of Figure 2.13. Both Figure 2.12 and Figure 2.13 show that laser efficiency drops from 18% to 4.7% when cavity length is increased from 7 mm to 90 mm, respectively.

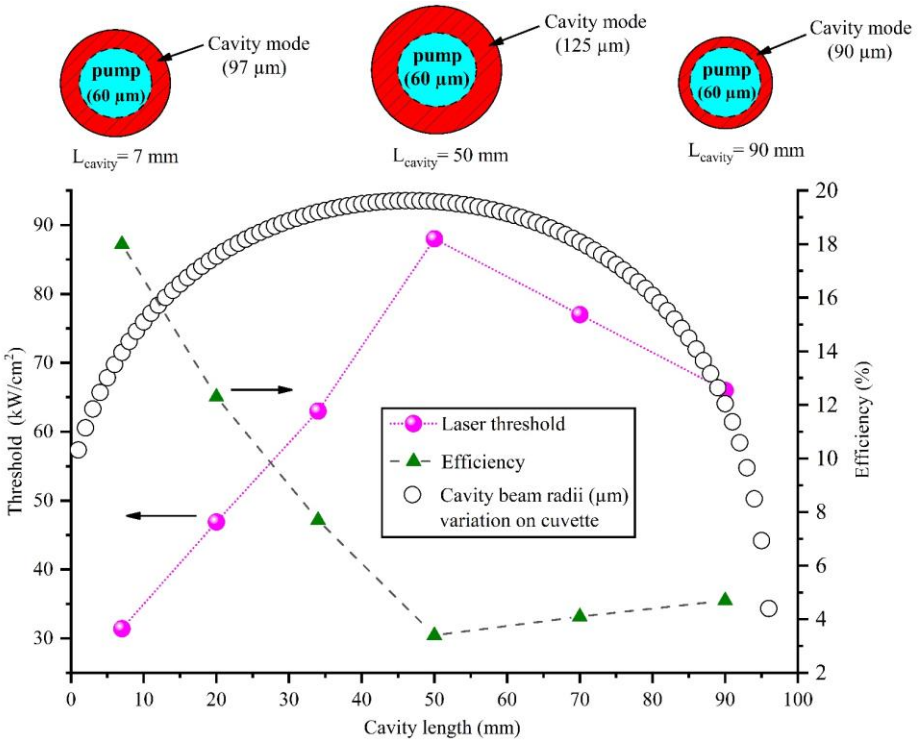

Figure 2.13 : Left y axis: Laser efficiency (%) and threshold (kW/cm^2) as a function of cavity lengths ranging between 7 mm to 90 mm. Right y axis – Variation of cavity mode (in radius) as a function of cavity length.

In contrast, laser threshold shows an increase from 31 kW/cm^2 to 66 kW/cm^2 when going from 7 mm to 90 mm in cavity length. Interestingly, such increase in laser threshold as well as the decrease in laser efficiency is not linear with the increase in cavity length (Figure 2.13). In fact, this would be linear for an ideal laser cavity where mode matching is not perturbed when increasing or decreasing cavity length. In a practical laser cavity like ours, where cavity mode variation on cuvette occurs with the cavity length is simulated using reZonator software and shown together with laser efficiency and threshold in Figure 2.13. The largest cavity mode around 125 µm (in radius) on cuvette appears at 50 mm cavity length while the pump mode is always fixed (60 µm in radius). This situation reflects an inefficient mode matching, compared to the case of other cavity lengths, resulting the highest threshold ~ 88 kW/cm^2 as well as the lowest efficiency ~ 3.4% at that cavity length. Below or beyond 50 mm, mode matching again starts to be better towards either 7 mm or 90 mm, respectively. Therefore, even for 90 mm long cavity, laser threshold is slightly lower ~ 66 kW/cm^2 as well as the efficiency is slightly higher ~ 4.7% than either of 50 mm or 70 mm cavity. One should note that, even if the optimum mode matching happens in 90 mm long cavity, it does not yield the lowest threshold and highest efficiency due to the longest laser build up time of laser oscillation inside such long cavity as already discussed above.

2.2.2. Beam quality (M^2)

Beam quality refers to how much a practical laser beam deviates from diffraction limited (TEM_{00}) perfect Gaussian beam. A diffraction limited laser beam can be focused into very tiny spot to achieve high power density. Such beam quality is also interesting for applications like high-resolution imaging, laser inscribing, laser beam injection in single mode fiber and so on. Typically, beam quality is determined by measuring the value of a dimensionless parameter M^2 where $M^2 = \frac{\theta_{Laser}}{\theta_{TEM_{00}}} = 1$ refers to diffraction limited TEM_{00} beam quality. To measure M^2 of our laser beam, beam radii at different positions after a lens were recorded using CCD camera. This experiment was performed several centimeters away from the out coupler of laser cavity. Beam radii (µm) as a function of different camera positions (mm) are plotted in Figure 2.14. Experimentally obtained beam radii are fitted using practical Gaussian beam propagation equation as given in the inset of Figure 2.14 from where the value of M^2 was extracted to be 1.04. In equation, w_0 and z_0 stand for the value of beam radius (µm) at focus and the position of focus (mm), respectively.

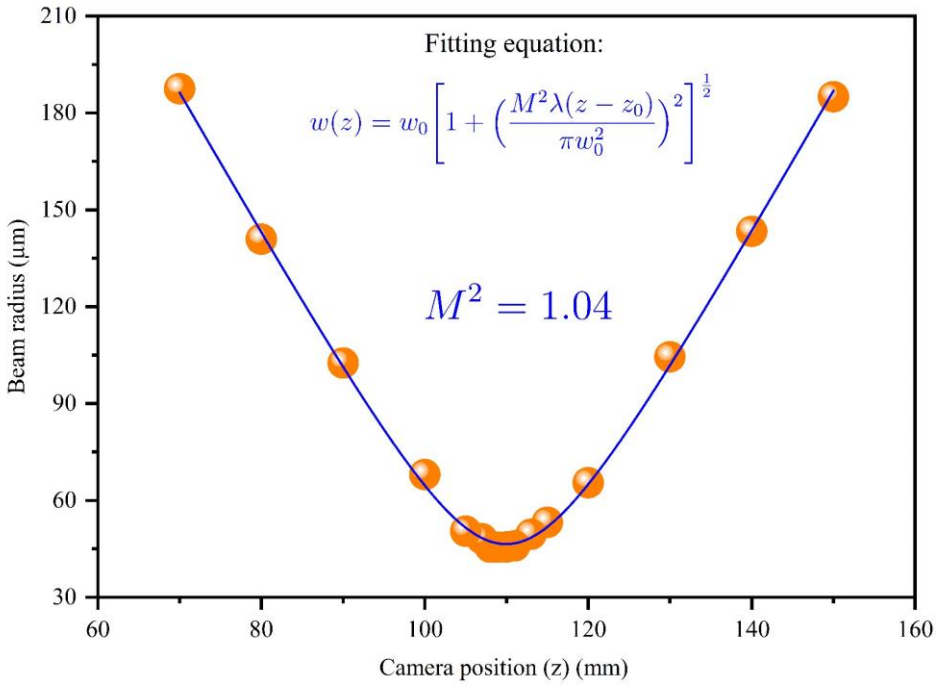

Figure 2.14 *:* Laser beam radius (µm) as a function of camera position measured after 75 mm plano-convex lens placed few centimeters away from the output coupler concave mirror. Beam radii at different positions are fitted using practical Gaussian beam propagation equation given at the inset of figure in order to extract the value of M^2.

2.2.3. Laser spectrum

Laser spectrum is recorded from a 1 cm long Plano-concave cavity using spectrometer (Ocean Optics) having 0.5 nm resolution. The spectrum consists of evenly spaced wavelength peaks within the

fluorescence spectrum of DCM (Figure 2.4) as shown in Figure 2.15. Such peaks might be related to the peaks of Fabry-Perot etalon[11] formed by two parallel reflecting surfaces with a gap between them. In a Fabry-Perot (FP) etalon, the free spectral range (FSR) between successive peaks can be written as,

$$\mathrm{FSR} = \lambda_{P+1} - \lambda_P = \frac{\lambda_P . \lambda_{P+1}}{2nL} \sim \frac{\lambda_P^2}{2nL} \qquad (2.6)^{11}$$

where λ_P and λ_{P+1} correspond to the P[th] and (P+1) [th] emission modes, respectively. L is the gap between two surfaces and n is the refractive index of medium. The value of FSR is calculated from the difference between λ_{P+1} and λ_P in Figure 2.15 is 2.5 nm. This 2.5 nm would correspond to a thickness $\sim \frac{\lambda^2}{2\Delta\lambda} =$ 80 μm which does not correspond to any relevant thickness in the set-up. Interestingly, it neither corresponds to the cavity formed by 1 mm path length cuvette nor the main two mirror cavity separated by 1 cm. For instance, if we consider (for simplicity) unity refractive index in equation (2.6), the FSR for 1 mm and 10 mm cavities would be 0.2 nm and 0.04 nm respectively which fall behind the resolution limit of our spectrometer, hence, should not be visible in spectrum. A logical way to explain the origin

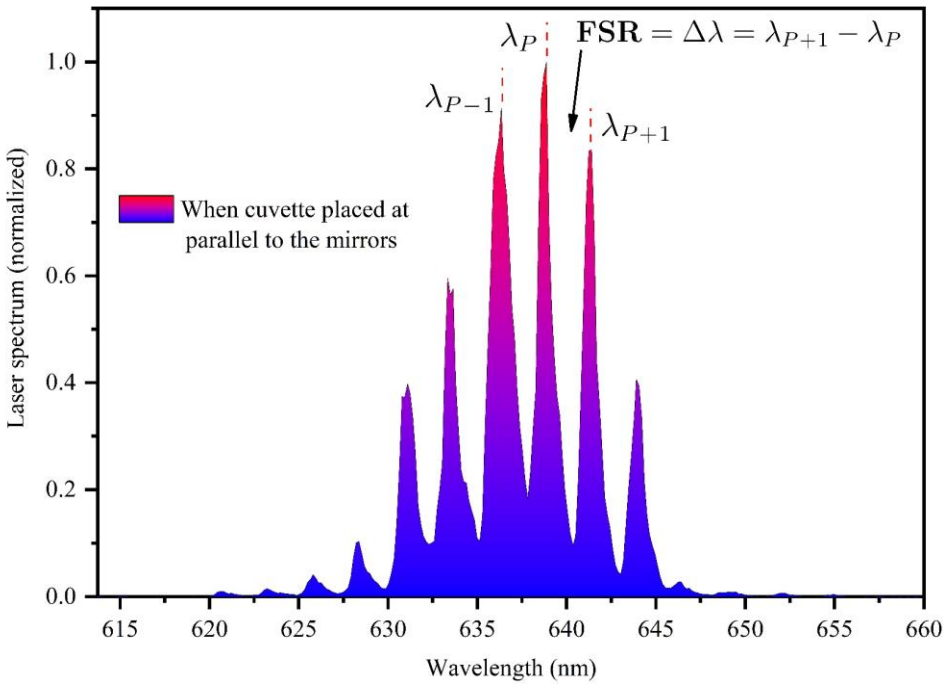

Figure 2.15: Laser spectrum when cuvette is placed at parallel to cavity mirrors.

consider Vernier Effect [67] which was first applied to vernier calipers. In vernier caliper, two measuring scales with slightly different gradation are used to improve measurement accuracy. Optical analog of those scales may be considered as interfering waves of slightly different frequencies generated in different interferometers. Such interferometers in the form of sub-cavities can also be formed inside our

laser cavity in addition to the main cavity composed of a plane and concave mirror as shown in Figure 2.16. During laser oscillation, longitudinal/transverse modes oscillate inside each of those cavities with

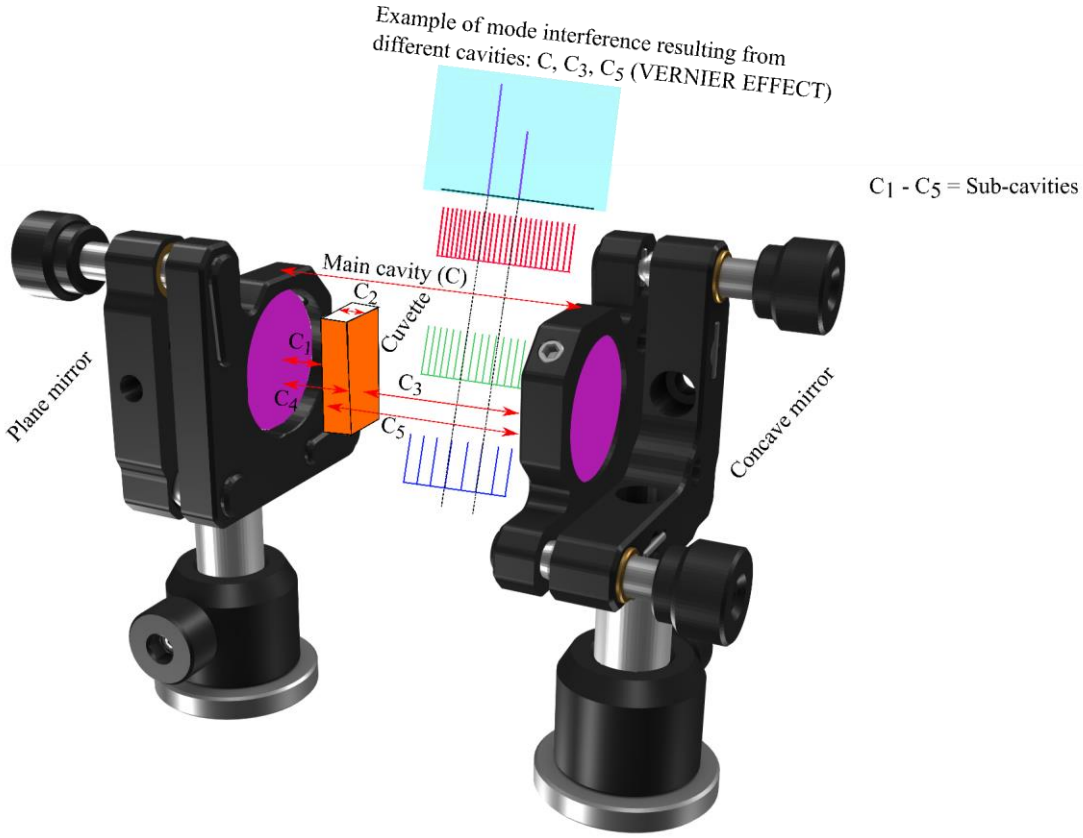

Figure 2.16: Schematic of the formation of sub-cavities (C_1 – C_5) in addition to the main Plano-concave laser cavity (C) when cuvette is placed parallel to the cavity mirrors. Interference of laser modes between different cavities (C, C_3, C_5) may create evenly spaced peaks in the laser spectrum.

slightly different frequencies or wavelengths determined by cavity lengths of those cavities. Sometimes, the modes interfere constructively to show fine periodic peaks and in the laser spectrum. An illustration is shown in Figure 2.16 where the longitudinal modes created in three cavities (C: Cavity formed by plane and concave mirror, C_3: Cavity formed between output coupler and one facet of cuvette facing the output coupler, C_5: Cavity formed between output coupler and one facet of cuvette facing the plane mirror) are interfering with each other.

However, above discussion requires experimental verification by observing any difference in laser spectrum when sub-cavity effects are significantly cancelled. One way to do that is by placing the cuvette at Brewster angle as shown in Figure 2.17. At Brewster angle, the orientation of cuvette is such that

Fresnel reflections are cancelled out for the p-polarization that is selected because of distinctive losses between S and P polarizations. Sub-cavities cannot be formed between the cuvette facets and end

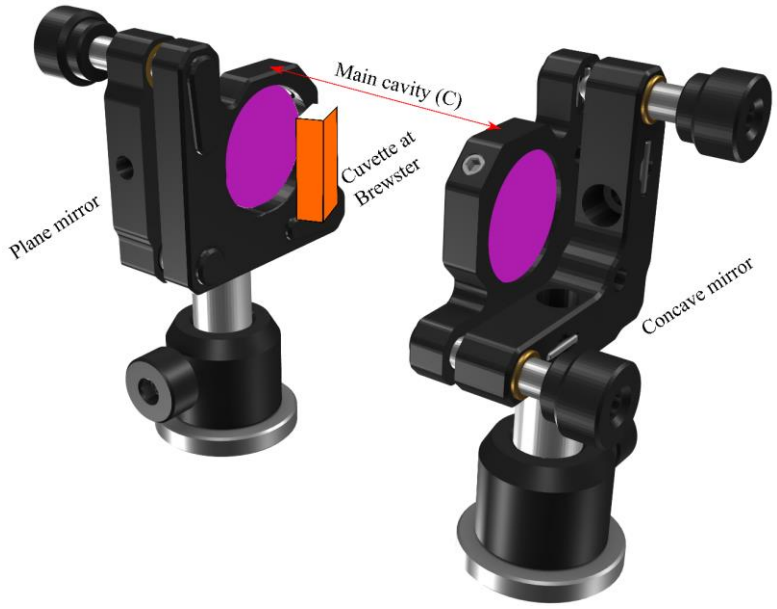

Figure 2.17 : Cuvette at Brewster angle to eliminate sub-cavities formed between the cuvette facets and end mirrors.

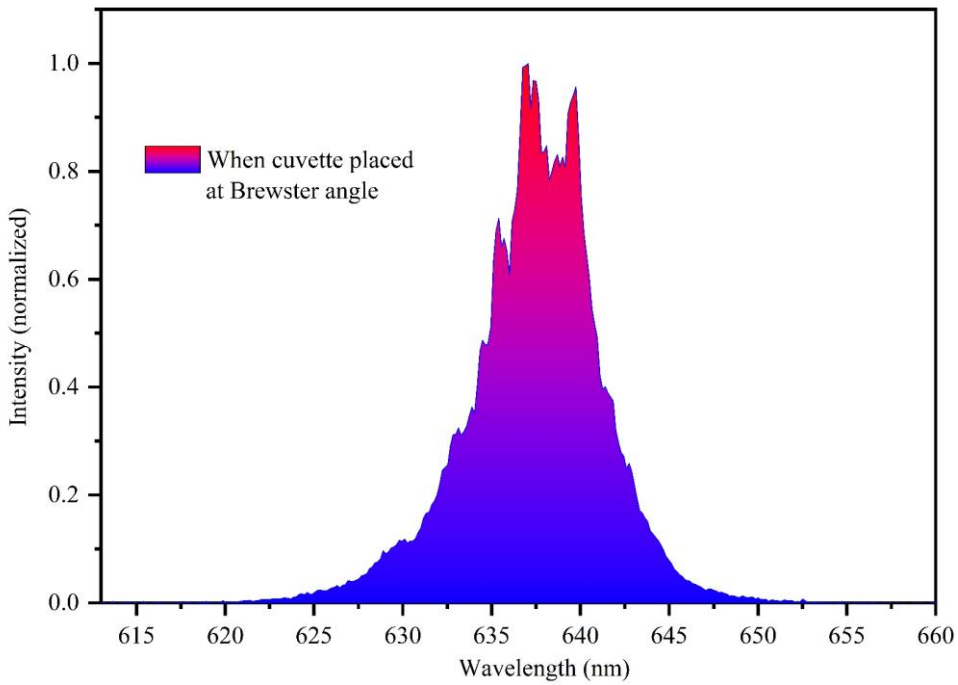

Figure 2.18: Laser spectrum when cuvette is placed at Brewster angle to cavity mirrors.

mirrors. Therefore, in laser spectrum, the separation among wavelength peaks (FSR) should not be

visible due to the resolution limit of our spectrometer as already discussed which is exactly shown in Figure 2.18.

2.2.4. Pulse duration

Typical pulse duration of solid-state organic laser is in the order of few hundreds of ns which is due to accumulation of triplet states as discussed earlier. Surprisingly, we observe here that under long pulse pumping (here 900 ns), there is almost no decrease in the laser intensity within the pump duration even under intense excitation of 153 kW/cm^2. The evolution of the laser pulse temporal profile with increasing pump power is shown in a low-threshold 7 mm cavity (using highest output coupler reflectivity R ~ 9

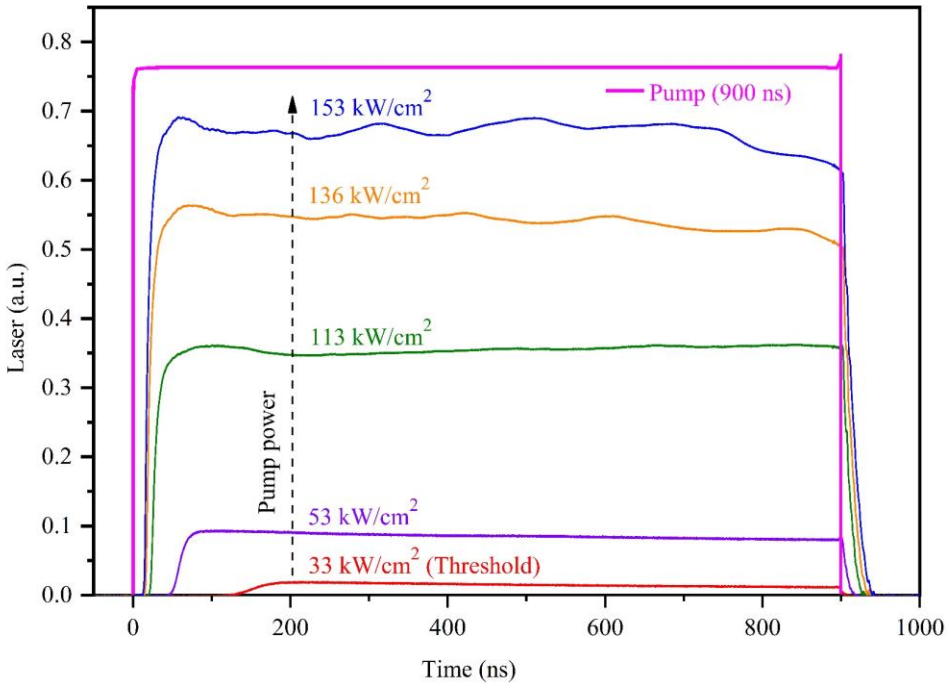

Figure 2.19: Laser temporal profile using R ~ 99.9% output coupler (100 mm) at different pump power densities under 900 ns/10 Hz pump.

9.9%). It is also noticeable that the time delay between the onsets of pump and laser pulse, which is related to oscillation build-up time inside cavity, varies with pump power density. This build-up time depends on the cavity length, the pump power density, and the cavity loss. For any laser having a fixed cavity length and loss parameters (output coupler loss), build-up time will be a function of pump power only. It is obvious that in Figure 2.19 the build-up time is higher (> than 150 ns) at lasing threshold and gradually decreases while increasing pump power. To illustrate the difference in pulse duration with a solid-state difference, we fabricated a 17-μm thick layer of DCM doped in PMMA (doping level 0.4% in weight, to ensure 83% of absorption, close to the cuvette absorption) directly spin-coated on the flat HR mirror closing the laser cavity.[7,46,48,64] The absorption of liquid and solid-state media was, thus, very comparable, as were the pump parameters and cavity configurations. It is important to notice that this

comparison between the liquid and solid-state is only for illustrative purpose here: to fairly compare lasing performance from these solid-state and liquid media, it is also required to deposit the 1-mm film (instead of 17-µm) on the HR mirror in order to ensure identical absorption coefficient, heat deposition, and intermolecular interactions in both liquid and solid-state material during lasing operation. Unfortunately, we did not succeed in making 1 mm thick DCM doped film using spin coater. Though, some thick (> 1 mm) DCM films using Epoxy Resine were prepared but those films did not come out to be clean instead having clouds of undissolved DCM molecules all along the sample. Importantly, we observed no lasing from those films probably due to strong concentration quenching by DCM clouds. For correct comparison, we should have used DCM doped PMMA blocks for instance.

However, the pulse dynamics are shown in Figure 2.20. The full width at half maximum (FWHM) of the solid-state dye laser was found to be 240 ns, whereas the liquid dye laser sustained oscillation up to more than 1 µs. But, the pulse duration of the liquid dye laser is here slightly different (not as "flat" as what is shown in Figure 2.19) because we used here R = 98% for the output coupler, corresponding to the optimal efficiency and output energy, instead of 99.9%. In this case, the additional amount of losses (2%) shortens the pulse temporal profile. To justify this statement from experiment, we inserted 150 µm

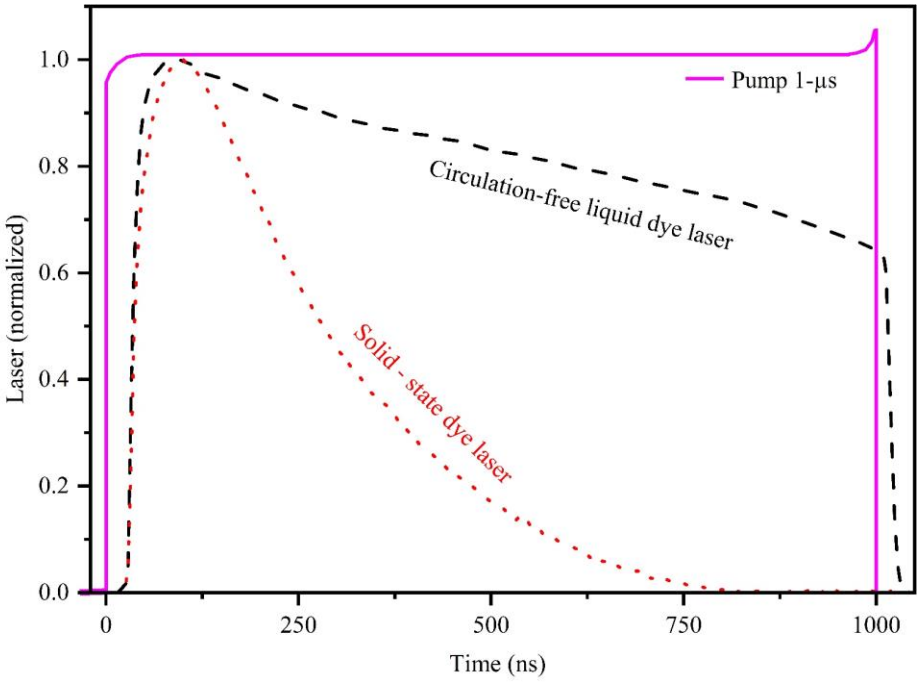

Figure 2.20: Temporal behavior of liquid and solid-state dye (DCM) laser under identical pump parameters (repetition rate: 10 Hz, pulse duration: 1 µs, power density: 113 kW/cm^2). Material (liquid and solid-state) absorption (~80%) at pump wavelength (445 nm) and cavity configuration was similar. Output coupler reflectivity was 98%.

microscope slide (glass plate) inside laser as a loss element. To keep the output coupling losses same as Figure 2.19, we used 99.9% reflective output coupler. The cavity was 74 mm long to have enough space to rotate the microscope slide inside cavity. The purpose to rotate the glass slide is to increase cavity losses and observe laser temporal behavior. Indeed, when the glass plate is aligned with the cavity mirrors and cuvette as well, cavity loss is supposed to be slightly higher compared to the cavity with no glass plate. As soon as the glass plate would rotate by known degree, fixed amount of loss will be added to the cavity due to cavity misalignment. Experimental result is presented in Figure 2.22. It is clearly seen that, when there is no glass plate inside laser cavity, laser temporal profile is as flat as pump (1 µs) exactly what we observed in Figure 2.19. As soon as the glass plate is introduced to the cavity in parallel (0°) to the cavity mirrors

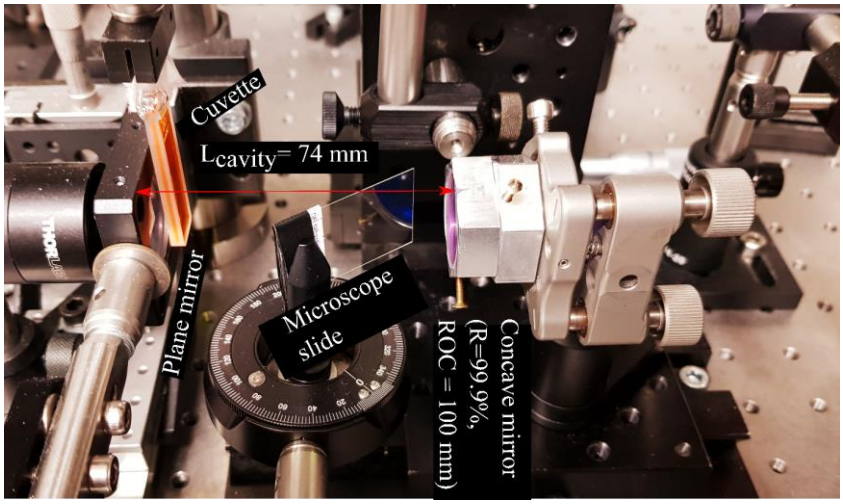

Figure 2.21: Increasing losses (in same amount) in a Plano-concave laser cavity by rotating thin (150 µm) microscope by known degree.

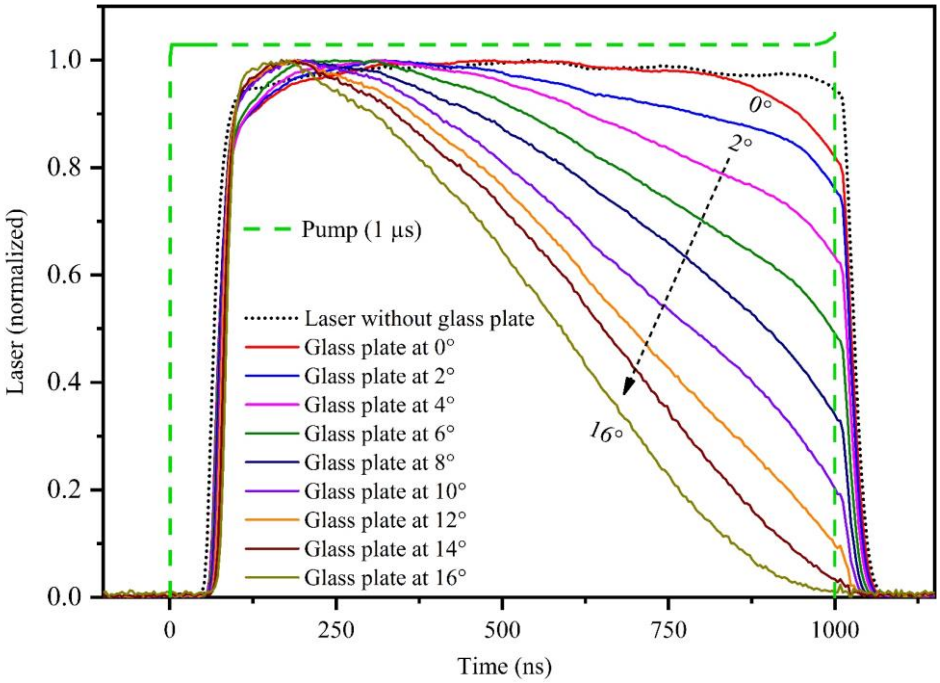

Figure 2.22: Laser temporal behavior by rotating a microscope slide (glass plate) inside laser cavity by known degrees. 1 µs (10 Hz), 120 kW/cm^2 pump power density was used for the experiment.

and cuvette, the pulse duration slightly shortens with a sudden increase in laser buildup time (Figure 2.23) from 53 ns to 60 ns compared to the case when no glass plate was present in the cavity. Still, the pulse duration remains 1 µs up to a cavity misalignment by 6° of glass plate rotation. Going from 6° to 16° rotation of glass plate, laser pulse duration decreased down to 580 ns at FWHM with further increase in build-up time (laser threshold) as shown in Figure 2.23. Since the laser threshold is higher, the singlet population is also higher and generates more triplet excitons through ISC which explains why the laser pulse duration shortened when loss was added to the cavity. This explanation is also relevant to the case of Figure 2.20 where we observed slightly different pulse duration using R~98% output coupler unlike Figure 2.19 where R~99.9% output coupler was used. Note that, cavity loss can also be increased by misaligning cavity mirrors but in that case, the degree of misalignment cannot be determined which makes our current experiment distinct. However, the reason why longer pulses are obtained in the liquid state with no circulation could be due to using a liquid gain medium without deaeration which facilitates environmental oxygen to quench triplet population rapidly enabling such long pulse (1 µs) laser. However, we observed no significant change in laser pulse duration when using a deaerated and non-deaerated solution. Other reasons may be concentration issues limiting the amount of singlet–triplet interaction in liquid experiments compared to 17 µm solid-state sample or something more complex linked to transverse laser modes which will be discussed in the third chapter.

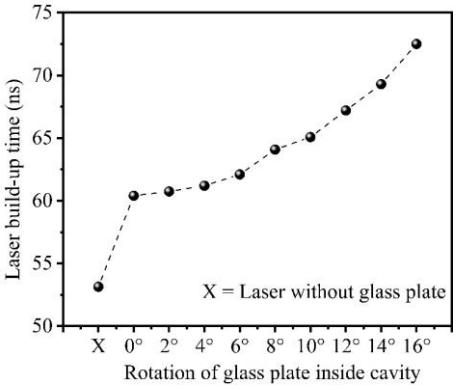

Figure 2.23 : Laser build-up (calculated from Figure 2.22) time vs orientation of glass plate inside laser cavity.

2.2.5. Photo-stability

This section will present a comparative study of photo-stability of our circulation free liquid dye laser and solid-state dye laser with same material under similar pumping (power density, repetition rates etc.) and cavity (length, reflectivity, and ROC of output coupler mirror etc.) geometry. For this purpose, we built a 11 mm long laser cavity with a plane mirror (Highly reflective at 600-690 nm) and 50 mm ROC concave mirror (99.9% reflective at 600-690 nm) as output coupler to create cavity mode around 80 µm (in radius) on cuvette where the pump mode was 60 µm (in radius).

Laser photo-stability study was performed using 50 ns pump (1 kHz) at 122 kW/cm^2 for two reasons. Firstly, a number of literatures are found (for comparison) to make photo-stability study of organic laser under ns pumping. And secondly, our laser was unable to operate at high repetition rates (e.g., 1 kHz) when pumped with 1 µs long pulse. This limitation will be discussed at the end of this chapter. The photo-stability curve is shown in Figure 2.24 using 0.03 mL of DCM solution inside 1 mm cuvette. The liquid dye device stopped lasing after 6×10^8 pulses (half-life time is around 3×10^8 pulses) with pulse-

to-pulse stability around 5%, corresponding to more than 162 hours (> 6 days and 6 nights) of non-stop operation at 1 kHz. We then filled the cuvette with 10 times more dye solution (0.3 ml), which increased the laser lifetime up to 1.3×10^9 pulses (see figure Figure 2.25) (half-life time is around 7.5×10^8 pulses) corresponding to more than 300 hours (>12 days and 12 nights) of non-stop lasing at 1 kHz. In this case,

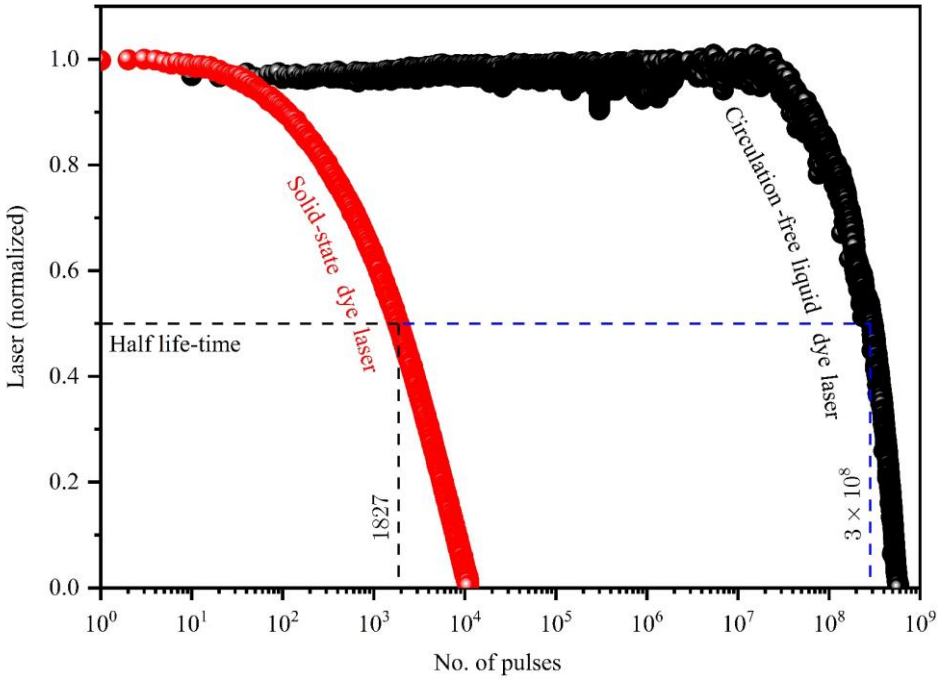

Figure 2.24: Photo-stability of circulation-free liquid dye laser (using 0.03 mL DCM solution in 1-mm light path cuvette) and solid-state dye laser (using 17-µm DCM film) at ~ 122 kW/cm^2 pump (50-ns, 1 kHz) power density. The absorption of both liquid and solid-state samples was around 83% at 445 nm.

the maximum laser output was reached only after *ca.* 10^8 pulses or 1 day, which is correlated to an increase of absorption of the sample and a small reduction of the solution volume with time, which we attribute to some evaporation of propanol through the cuvette sealing lid. We note that loss of lasing after complete photo-degradation is irreversible and cannot be recovered at any pump spot location on the cuvette as shown in Figure 2.26 where emission behavior of the degraded solution is depicted against time when we translated the cuvette horizontally as well as vertically. During translation, we waited few seconds at each point before going to the next one. Each point on the sample presents

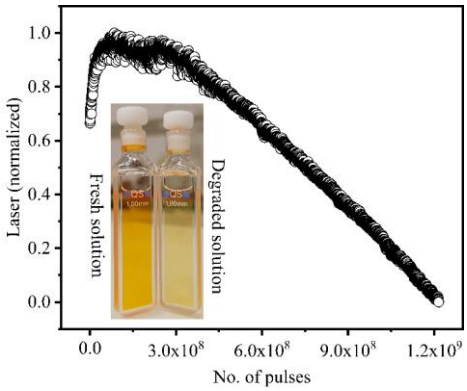

Figure 2.25: Laser photo-stability (in no. of pulses) using 0.3 mL dye solution (DCM in propanol-2 contained in circulation-free 1 mm cuvette) using 122 kW/cm2 pump (50 ns) at 1 kHz repetition rate.

similar emission behavior showing highest peak around 70 pJ which decays abruptly below 30 pJ (Figure *2.26*). This is probably lasing for few ms which is abruptly quenched by the photo-degraded products (presence of those species in degraded solution will be shown later) in the solution and cannot show steady state lasing anymore. However, such emission behavior of different positions in the degraded solution indicates that molecular diffusion has been active to replenish the pumped photoexcited volume with fresh molecules continuously. Loss of lasing does not necessarily mean that all molecules are dead in the solution. This is verified when we characterized photo-degradation by comparing their absorption before and after degradation study as shown in Figure 2.27. In addition of the $S_0 \rightarrow S_1$ absorption peak of DCM in propanol-2 at 470, a second absorption peak around 348 nm emerged in the degraded sample. This characteristic higher energy absorption band was reported earlier [68,69] and was attributed either directly to *cis* isomer, whose formation from the most stable *trans*-isomer is a distinguishing photo-physical process occurring in stilbene dyes [68,70].

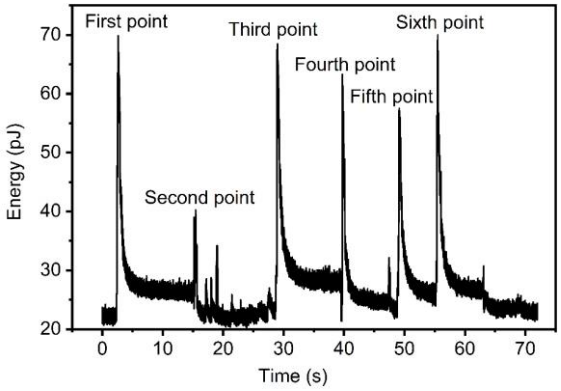

Figure 2.26: Emission behavior of the degraded sample when translated horizontally (first – third point) and vertically (fourth – sixth point).

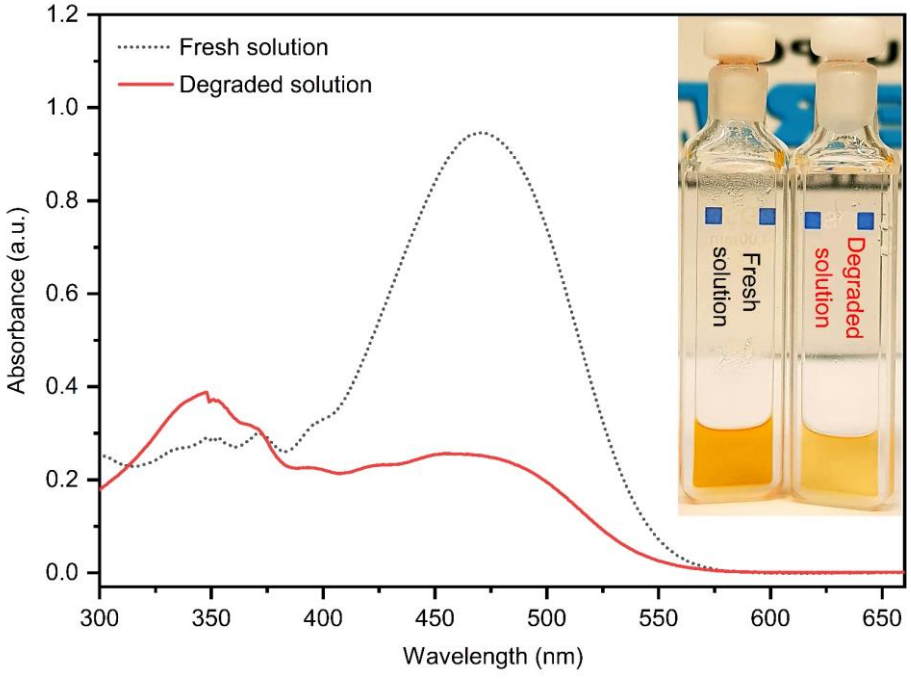

Figure 2.27: Absorbance of 0.03 mL dye solution (DCM in propanol-2 contained in circulation-free 1 mm cuvette) before and after laser photo-stability study using 122 kW/cm^2 pump (50 ns at 1 kHz).

As a comparison, we used the same setup to pump a solid-state sample discussed in the context of Figure 2.20. The solid-state laser degraded much faster (half-life of 1823 pulses only) when pumped at same peak power density (122 kW/cm^2). Let's note that comparison with solid-state is not straightforward, as the dye concentration was much higher in the solid than in the liquid form (1.57×10^{-1} M vs 1.76×10^{-4} M) in order to achieve high enough absorption on a shorter path length. These results however confirm a well- established order of magnitude for solid-state laser stability. Another comparison point can be taken from the work of Hu *et al.*[71] who reported DCM dye laser with a 3-mm thick solid-state film using ORMOSIL gel, where the dye concentration was 4×10^{-4} M, is very much comparable to the concentration we used. They showed a 10% decrease of lasing output energy after only 2×10^4 pulses, a drop in intensity which happens in our case after 5×10^7 pulses.

So far, we showed photostability study using short pump pulse duration. There might be a question why we did not show laser photo-stability under 1-µs long pump. Since it is rare to find organic lasers that lase at such pulse duration, therefore it is interesting to know their photostability under 1 µs pumping. Moreover, according to several reports degradation of organic molecules occur from triplet states [72,73] hence, traditionally they are pumped with short pulses (< 100 ns) to prohibit their accumulation in triplet states. Considering above reasons, we ran a stability test using 1 µs/122 kW-cm^{-2} pump at 50 Hz repetition rates. It is important to mention here that, we did not get 1 µs lasing at 1 kHz repetition rate which will be discussed right after this section. However, in this case we found no efficiency drop up to 1.4×10^6 pulses corresponding to 8h of non-stop lasing operation (Figure 2.28) similar to what is seen in Figure 2.24. 50 Hz is a low repetition rate compared to kHz used in previous photostability study (under 50 ns pumping) which took almost 15 days. Therefore, we did not run the stability test for longer time under 1 µs pulse at 50 Hz but we can still say that they also show great photostability even under 1 µs long pump.

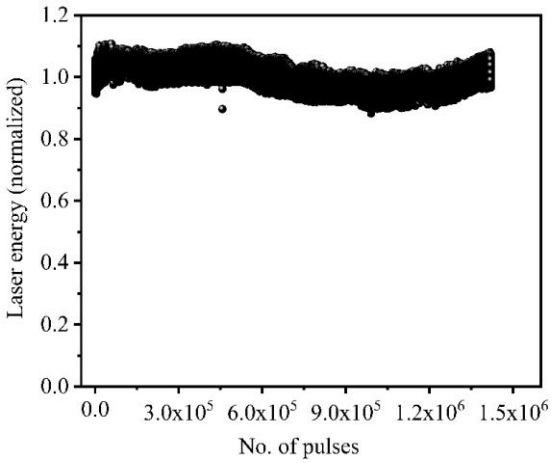

Figure 2.28: Photostability of a liquid dye laser at 113 kW/cm^2 pump (1-µs, 50 Hz) power.

2.3. Limitations of circulation-free liquid dye lasers

One of the distinct properties of circulation free liquid dye lasers over solid-state dye laser is their ability to produce longer than 1 µs lasing whereas solid-state thin film-based dye lasers are limited to a few

hundreds of ns pulse durations. Surprisingly, above 1 µs, their pulse duration does not follow the pump anymore and rather decreases when pump pulse duration is increased (beyond 1 µs). Similar decrease in laser pulse duration is also found when pump repetition rate is increased beyond 10 Hz at fixed pump pulse duration (1 µs). Despite very high photo-stability, these can be considered as limitations of those lasers since their high repetition rate or long pulse operation might be desired for many applications. In this part, we are going to discuss those issues to find the reason behind those limitations using the same laser cavity explained in Figure 2.8.

2.3.1. Limitation in pulse duration

To show such limitation, pump repetition rate was fixed at 10 Hz and the pump pulse duration was increased from 2 µs to 10 µs keeping the pump peak power fixed (113 kW/cm^2). The results are displayed in Figure 2.29 where laser pulse shortening is observed with the increase in pump pulse

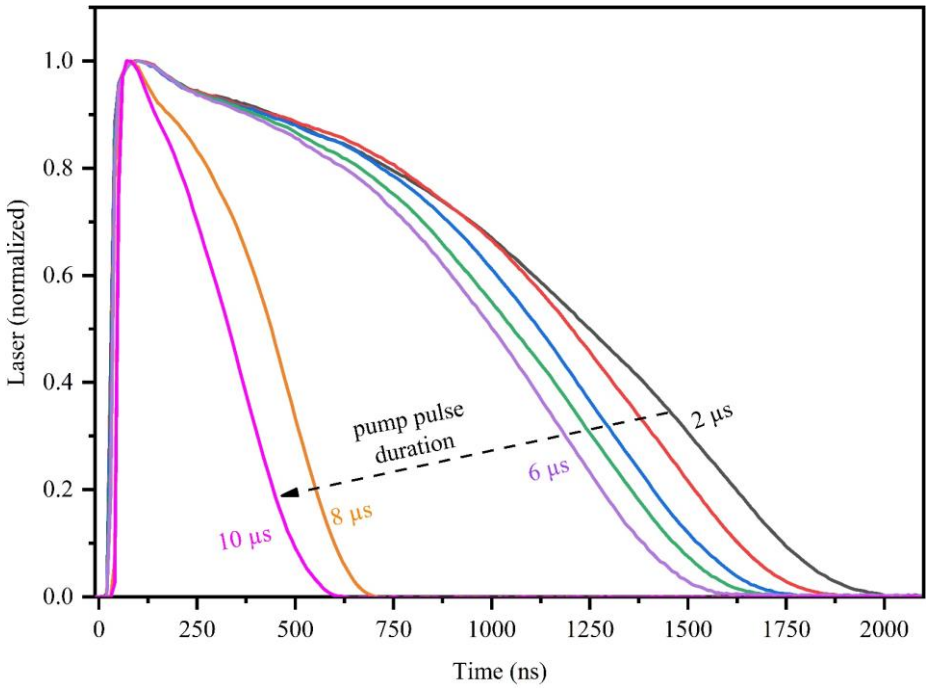

Figure 2.29: Laser temporal profile as a function of pump pulse duration. Peak pump power (82 kW/cm^2) and repetition rate (10 Hz) were fixed. Output coupler reflectivity was 98%.

duration. Here laser temporal profiles are normalized to have an estimation of the pulse width at FWHM. Going from 2 µs to 6 µs pump, the laser pulse width decreased almost linearly (FWHM from 1246 ns to 1000 ns, respectively) as shown in Figure 2.30. This is not due to permanent degradation of dye since the traces were obtained through averaging (over 512 traces) and were stable from pulse to pulse. However, beyond 6 µs, the shortening was much more significant, down to 333 ns. It is instructive to

relate this to a change in the laser oscillation build up time, as also plotted in Figure 2.30. A sudden buildup time increase (from 10 to 30 ns) is observed beyond 6 µs duration, which indicates, as pump peak power and cavity mirror losses are fixed, the loss level has increased at this point. The source of this loss could be related to pump induced thermal load that cannot relax to room temperature and hence influences the next pulse especially when 6 µs or longer pump was used. This thermal load is generally considered as function of average power.[74] To verify whether such lasing behavior is due to thermal effect, hence average pump power, we maintained same average power ~ 0.57 mW by choosing different

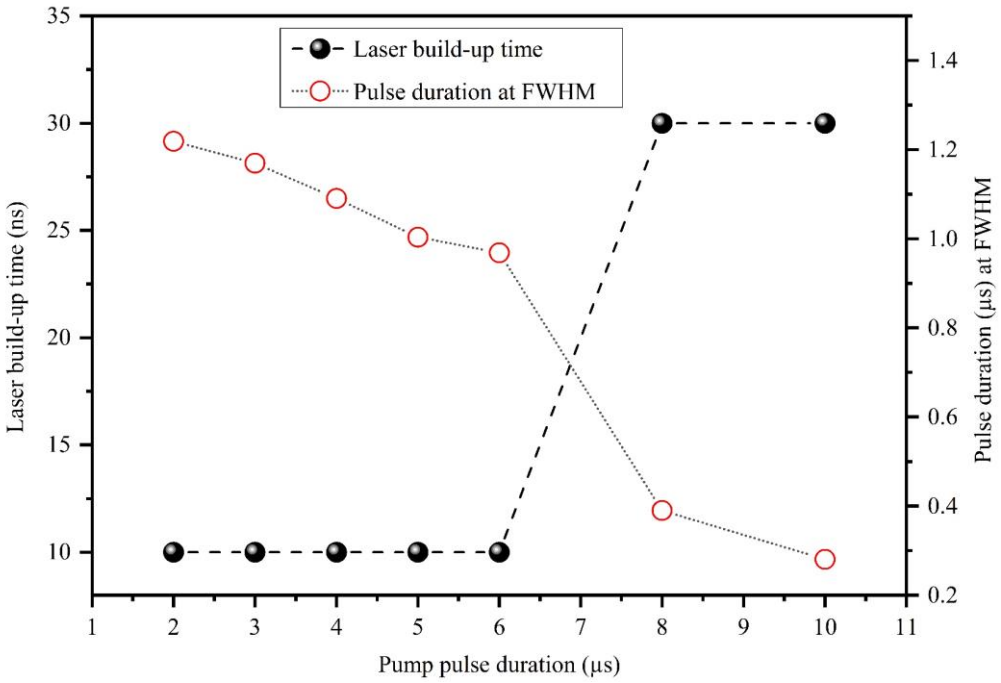

Figure 2.30: Laser build-up time (left y axis) and pulse duration at FWHM (right y axis) (calculated from Figure 2.29) as a function of pump pulse duration (2 µs -10 µs).

combinations of pump pulse duration and repetition rates when pumping the gain medium. The result can be seen in Figure 2.31. Interestingly, even if the average pump power remained same, the pulse durations were actually very different, and the lowest laser pulse duration was found for the highest pump repetition rates (100 Hz) used in this experiment. From here, it can be said that this is not a thermal effect linked to the average temperature ($\propto\ average\ power$) but a dynamical thermal stuff that occurs between pulses. Because under 10 µs pump at 5 Hz, laser pulse duration was around 900 ns at FWHM (Figure 2.31) which was found to be 300 ns when using the same pump duration at 10 Hz (Figure 2.29). Therefore, it is quite clear that thermal effect is more important when pump repetition rate is increased instead of pump pulse duration (at low repetition rate). An approach to obtain longer pulses at low repetition rate (10 Hz) will be discussed in third chapter while in the following, we will investigate the impact of pump repetition rate on laser pulse duration.

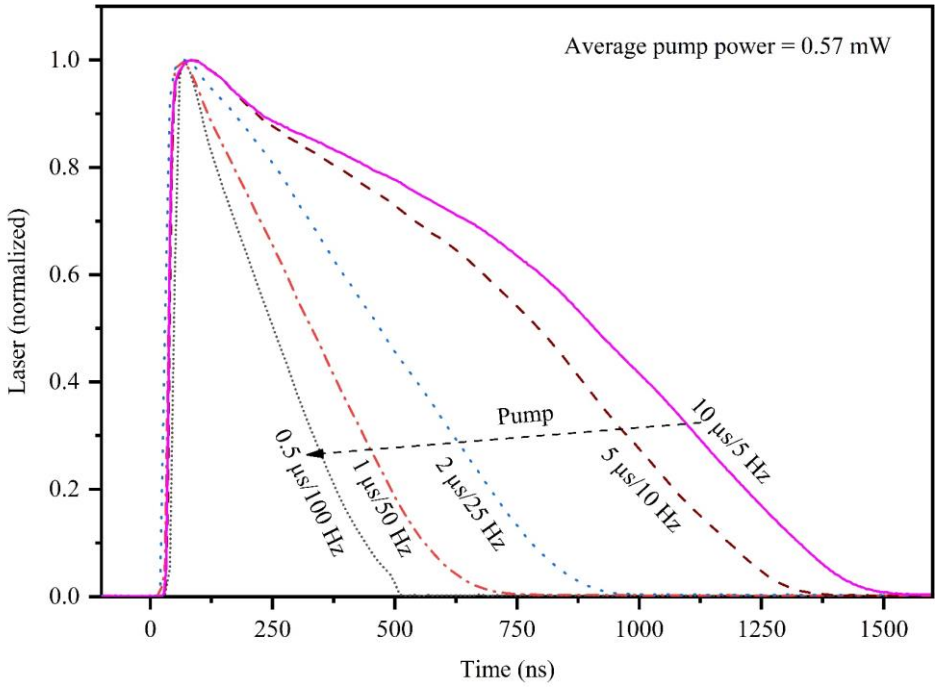

Figure 2.31: Laser temporal profile as a function of same average pump power (0.57 mW) (using different combinations of pump repetition rate and pulse duration). The output coupler reflectivity was 98%.

2.3.2. Limitation in repetition rates

In this case, we increased pump repetition rate beyond 10 Hz keeping pulse duration fixed ~ 1 µs at 113 kW/cm^2. The results are shown in Figure 2.32 and Figure 2.33. We observed a decrease in pulse duration from 1 µs to 69 ns at FWHM when the repetition rate increased from 10 Hz to 70 Hz respectively. Such decrease in pulse duration was also associated with an increase in laser build-up time from 24 ns to 86 ns when pump repetition rate increased from 10 Hz to 70 Hz, respectively. No more lasing was observed at and beyond 80 Hz. This once again proves the existence of a source of losses. Indeed, the physical origin of short pulse lasing under CW pumping is well known in organic systems and is related to triplet states (triplet absorption and singlet–triplet annihilation). Typical pulse widths are in the sub-µs range in the absence of a triplet quencher. However, it is here unlikely that shortening observed when the repetition rate is varied could be directly linked to an accumulation of triplet population between pulses, as the involved relaxation time (>10 ms for 70 Hz) is three orders of magnitude higher than the triplet lifetime (31 ± 5 µs)[68] of DCM in solution. We also rule out the possibility of a permanent photoisomerization or photobleaching scenario as the pulse durations are identical from pulse to pulse. It is obvious that when the repetition rate is increased at constant pump energy per pulse, the average power is higher, so is the thermal load inside the gain medium. After pump-induced heating during one pulse, the temperature relaxes down to room temperature with a typical timescale,

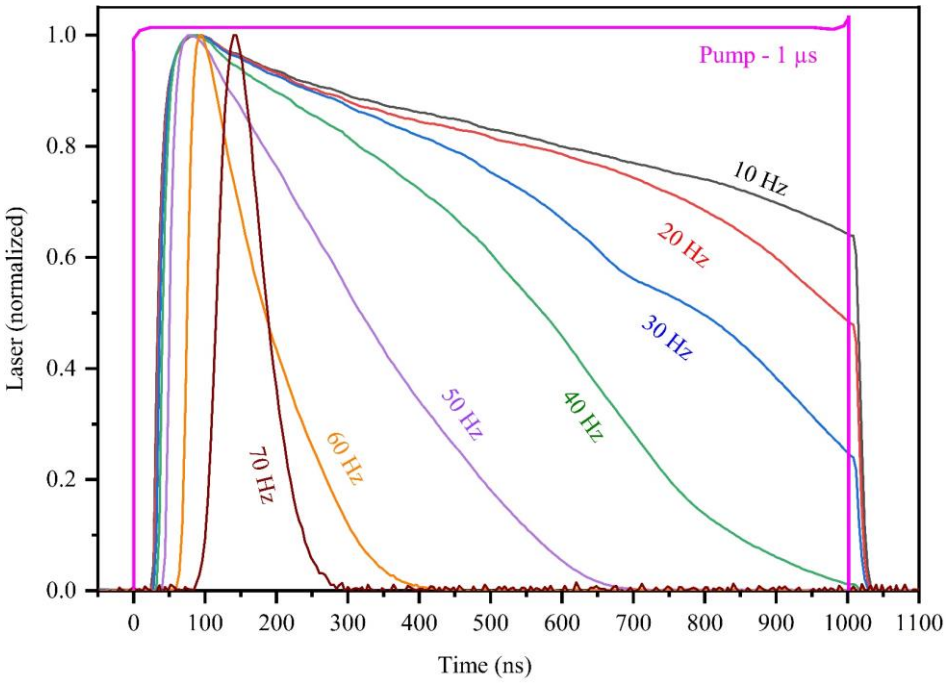

Figure 2.32: Laser temporal profile as a function of pump repetition rate (Hz). Peak pump power was 113 kW/cm^2. Output coupler (100 mm ROC) reflectivity was 98%.

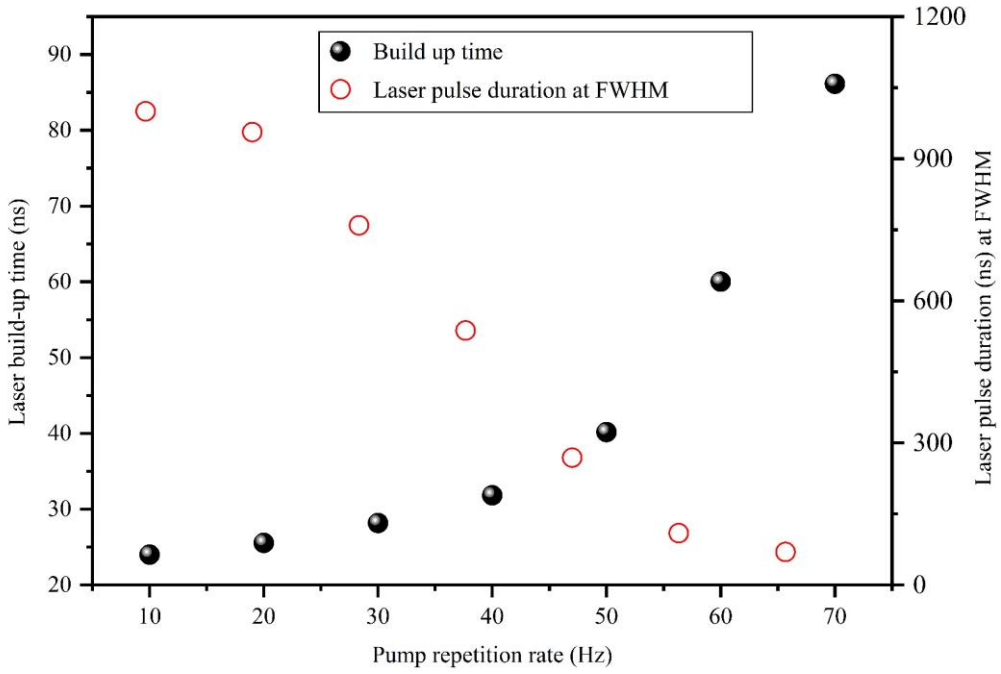

Figure 2.33 : Laser build-up time (ns) (left y axis) and pulse duration (ns) at FWHM (right y axis) as a function of pump repetition rate. Laser build-up time and pulse duration at FWHM is calculated from Figure 2.32. Pump pulse duration was fixed ~ 1 µs at 113 kW/cm^2.

$$\tau_T = \frac{w^2}{4D_T} = \frac{w^2 \rho c}{4K_c} \quad (2.7)$$

where w is the pump radius (60 μm), D_T is the thermal diffusivity, ρ is the density, c is the specific heat, and K_c is the thermal conductivity. From thermal values of ethanol (K_c= 0. 171W. m^{-1}. K^{-1}; ρ = 789 kg. m^{-3}; c = 2.46 kJ. Kg^{-1}. K^{-1}); τ_T is ~10 ms. This time scale suggests that thermal effecs are certainly the origin of thermal lensing of laser medium is the source of loss that tends to destabilize laser cavity and terminates lasing action when pump repetition rate is increased after 70 Hz in this case. In next chapter, we will show the existence of thermal effect at those laser experimental conditions and also try to solve this problem to push their current repetition rate limit.

2.4. Conclusion

We have designed a low cost, compact, user-friendly circulation-free liquid dye laser from commercially available elements (cavity mirrors, laser diodes as pump source etc.) The laser system is very much comparable to the current state-of-art organic thin film based solid-state lasers in terms of efficiency (18%) and beam quality (M^2 = 1) without compromising simplicity, compactness, and cost. The photo-stability of liquid laser device was found to be 5 orders of magnitude higher when compared to the photo-stability of a solid-state laser with same material, absorption, pump and cavity configuration. Such high photostability is attributed to molecular diffusion that efficiently replenishes photo bleached molecules from the pump area between each pulse. Surprisingly, their photo stability can be increased by increasing the volume of lasing solution whereas the solid-state dye laser stability depends on the pump volume. Another distinct property of liquid dye laser was 1 μs stable and efficient lasing when it was operated at 10 Hz. Unfortunately, laser pulse duration did not follow the pump anymore and rather decreased when longer (2 μs – 10 μs) pump pulses were used in the system. Similar behavior (shortening of laser pulse duration) was also observed when pump repetition rate was increased keeping the pump pulse duration fixed (1 μs). While the reason behind laser pulse shortening when repetition rate increased can be explained from a characteristic time ~ ms to build up thermal effect in laser medium, precisely thermal lensing diffraction losses, laser pulse shortening under long pulse at low repetition rate is still not very clear. Since their limitation to provide high repetition rate lasing is related to thermal lensing o laser medium, high repetition rate operation from them can be achieved by correcting thermal lens. In the next chapter, we will first explore the existence of thermal effect in laser medium and take necessary measures to correct it for the demonstration of high repetition rate operation of circulation free liquid laser.

3. Toward high repetition rate circulation-free liquid organic lasers

3.1. Introduction

In this chapter we will provide possible pathways to operate circulation free liquid dye lasers at several kHz. So far, we have found that increasing pump (1 μs) repetition rates leads to shorter laser pulses and terminates lasing after several tens of Hz. Triplets cannot be responsible to impose such limitation in laser repetition rate in our case. Because, unlike solid-state organic gain medium where triplet lifetimes can be in the *ms* range or longer,[8] they are typically much shorter in liquids, especially when solutions are not deaerated to eliminate molecular oxygen, which acts as an effective triplet quencher. From the lifetime ~ 31±5 μs[68] of triplet states of DCM in a deaerated DMSO solution we can estimate that lasing will be fundamentally perturbed by triplet states roughly after 30 kHz. Therefore, we will only consider losses from thermal lensing of laser medium to impose such limitation. Briefly, when pump repetition rate is such that the gain medium does not get enough time to return to room temperature between two pump pulses, temperature inside gain medium starts to rise pulse after pulse [75] until reaching an average steady state value. This results a refractive index gradient (follows temperature gradient profile) which acts like a lens. Though thermal lens is often aberrative in nature[76,77] its quadratic part can be corrected using suitable opposite focal length lens. This possibility will be investigated in this chapter in detail.

The beginning of this chapter investigates the existence of thermal effect in laser medium under similar pumping condition of previous chapter where lasing terminated after 70 Hz at 1 μs pumping. In the next, lasing under 30 ns pump (the shortest pulse duration could be produced by PC0-7120 laser diode driver was 20 ns) is investigated in order to reach the maximum laser repetition rates intrinsically from our Plano-concave laser cavity. This is followed by a pump-probe experiment to measure the static thermal lens focal length at different repetition rates under 30 ns pump to direct a pathway to correct it. At the end of this chapter, the role of cavity design is shown to obtain high repetition rate lasing without the need of any correction lens. Finally, a brief discussion is made regarding which procedure of thermal lens correction is better, future perspectives etc. in the conclusion part of this chapter.

3.2. Experimental

This section provides experimental details. Since our main concern is the thermal lensing of laser medium which disturbs cavity stability, simple Plano-concave laser cavity stability simulation is also shown here in relevance to the experiments.

3.2.1. Design of Michelson Interferometer to ensure the presence of thermal effect in laser medium

An interferometer provides the resultant of two or more waves superimposed on each other while travelling through same medium. The resultant appears as interferometric fringes or constructive and destructive interference in other words. Fringe intensity occurring from a constructive interference is higher than the either of interfering waves while a dark fringe appears when waves interfere destructively. Constructive and destructive interference of two waves depend on the distance/path lengths travelled by each wave before interfering, provided that the observation point is fixed for the resultant wave. If their path lengths are equal or multiple of one wavelength, constructive interference occurs. Oppositely, if their path length differs by a half wavelength or multiple of one wavelength plus a half wavelength, destructive interference occurs. Therefore, the condition of constructive and destructive interference can be written as follows:

$$D = m\lambda \text{ (Constructive interference)} \tag{3.1}$$

$$D = (m + \frac{1}{2})\lambda \text{ (Destructive interference)} \tag{3.2}$$

Where, D is the difference in path lengths travelled by two waves before interfering, m (m= 0, 1, 2...) is an integer and λ is the wavelength of the interfering waves. From these equations, we can say that very small difference (order of half wavelength) between the path travelled by two waves will change the interference from constructive to destructive and vice versa. Hence this tool can be very sensitive to observe temperature induced refractive index change in our laser solution by looking at the change in interference pattern under different pumping conditions (pump power, repetition rates etc.)

Therefore, we designed one of the simplest forms of light interferometer called 'Michelson Interferometer' where a He-Ne (632.8 nm is not absorbed by DCM) beam is split (using 50/50 beam splitter (BS)) into two parts - one hits a moveable mirror while another is directed to a fixed mirror as shown in Figure 3.1. The interferometer was designed in the same diode pumped laser setup (Figure 2.8) by just removing cavity mirrors. The cuvette was placed inside the beam path of fixed mirror at 45° with respect to the pump beam/interferometer beam as shown in Figure 3.1. Approximate radius of He-

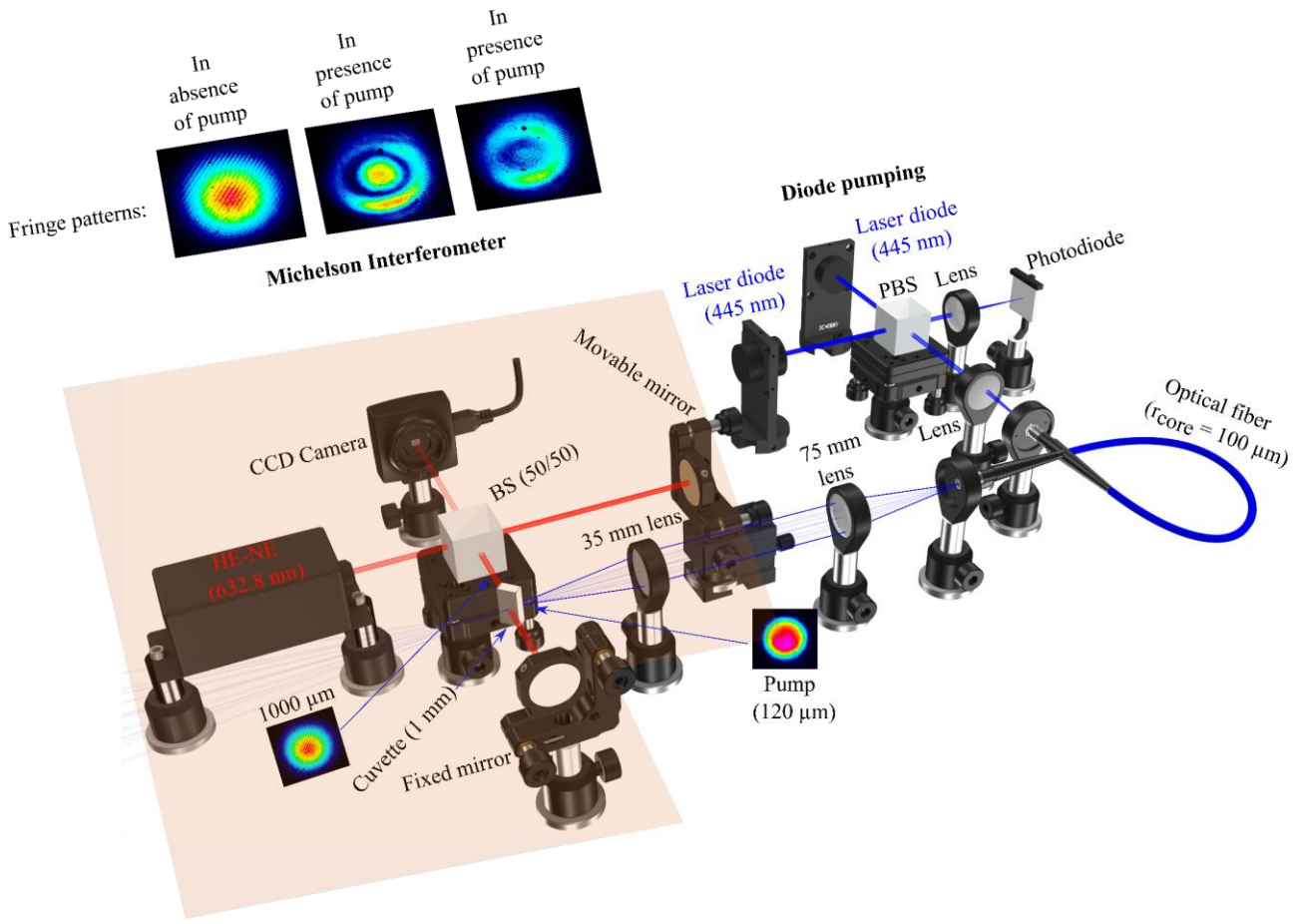

Figure 3.1 : Michelson interferometer set-up designed in the same same laser experimental setup by removing cavity mirrors to probe pump area on gain medium using He-Ne laser (632.8 nm). Pump beam originates from two polarization coupled laser diode (5W each) beams. CCD images have been inserted above CCD camera in the schematic. Left most represents probe beam (He-Ne) at no/low (≤10Hz) pump repetition rate. Rest of the images represent distortion at the middle of probe beam when the pump was operated at higher repetition rates (80Hz, 200Hz). The appearance of few black dots on the CCD images were due to dead pixels at those points.

Ne beam was around 450 µm with which it travels through 60 µm pump spot on the cuvette. However, two reflected beams (from fixed and movable mirrors) were combined in the BS to see interferometer fringes on a CCD camera. First, in absence of pump, the movable mirror was adjusted so that the resultant beam (left most image above CCD camera) on CCD camera looked like the He-Ne beam itself indicating no difference between the path length of two interfering beam. As soon as we started pumping at repetitions rates like 80 Hz or 200 Hz, bright and dark fringes (see above CCD camera) started to appear in the middle of the probe beam indicating a distortion of the He-Ne beam wave front due to the change in the refractive index at the pump area. It is necessary to mention here that we choose 1 µs long pump pulse in these experiments, since using such pump pulse duration no lasing was observed beyond 70 Hz as shown at the end of previous chapter. However, to further quantify our findings, a power meter was placed at the center of the probe beam and the pump power was increased for different repetition

rates (10 Hz, 80 Hz, and 200 Hz). The result is shown in Figure 3.2. It appears that at 10 Hz, almost no thermal effect is present in the solution, while at 80 Hz a phase variation of π (from a bright to a dark fringe) was observed for 82 kW/cm^2 pump fluence. At 200 Hz, a 2π dephasing was achieved for 113 kW/cm^2 of pump fluence only. Fringe patterns (seen inside the probe beam) are depicted above CCD camera in the schematic of Interferometer setup. Calculating the corresponding variation of the optical path gives a change in the refractive index of 6.42×10^{-4}, which corresponds to a temperature gradient of 1.64 K $\left(\frac{dn}{dT}\right.$ of ethanol is $\left. -4.5 \times 10^{-4}\right)$.

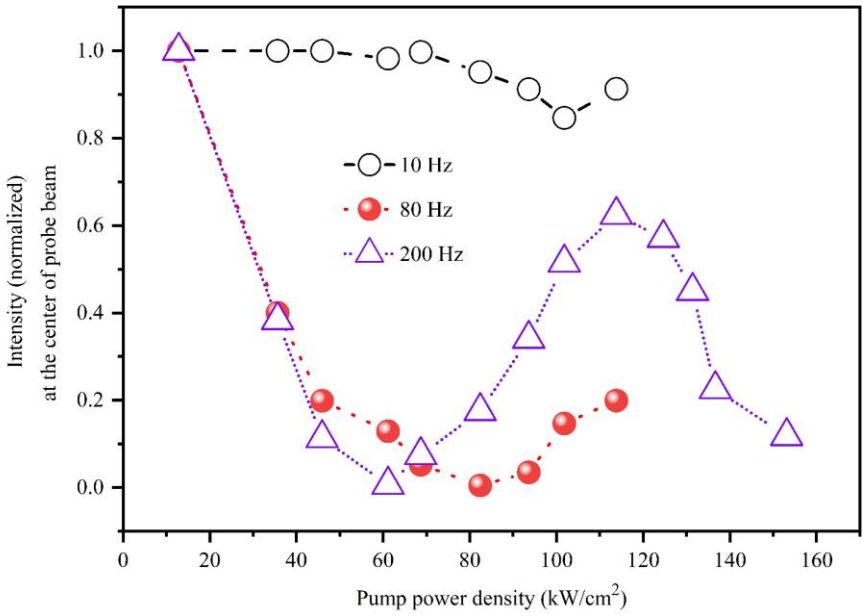

Figure 3.2 : Variation of the probe beam intensity (at center) as a function of pump (1 µs) power density (kW/cm^2) for different repetition rates.

These results ensured the existence of thermal effect inside the pump area of liquid dye laser solution when pumped at several tens of Hz using the power density and pump pulse duration similar to laser experiments shown in chapter 1. Using short pump pulses (ns/ps) instead of 1 µs, where thermal effect is negligible inside each pulse, this lasing limitation in repetition rates could be pushed beyond tens of Hz. Therefore, we used 30 ns pump for the rest of the study of this chapter.

3.2.2. Laser experiments under short pulse (30 ns) pumping

In this section, we are mostly interested to investigate maximum lasing repetition rate using 30 ns pump. Although, same Plano-concave laser cavity shown in chapter 1 was used for that purpose, still there were few modifications in the cavity parameters e.g., cavity length, output coupler mirror ROC etc.

Therefore, we start by a brief explanation of the laser set-up which will be followed by showing laser efficiency, threshold before going to the investigation of lasing repetition rates.

3.2.2.1. Laser design

Figure 3.3 shows the schematic of the laser experimental setup very similar to what we discussed in chapter 1. Same 1 mm light path spectrophotometric cuvette (Hellma analytics) filled with a solution of

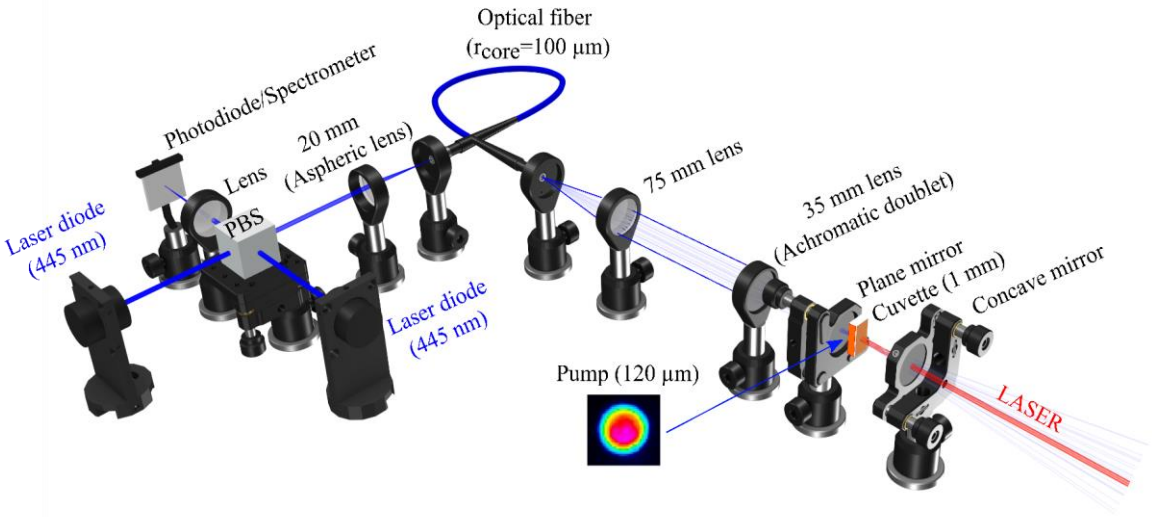

Figure 3.3 : Schematic of laser experimental set-up. Two 445 nm (each 5W) laser diode beams are coupled using polarization beam splitter (PBS) to inject into a multimode fiber with 100µm core radius. Output beam from the fiber is collimated and focused into 120 µm spot on the gain medium (organic dye dissolved in solution) inside 1 mm (light-path) cuvette using 75 mm and 35 mm lens respectively. A plane mirror (> 80% transparent for pump wavelngth and 99.9% reflective at lasing wavelngth) and a concave mirror (>95% reflection at lasing wavelength) form the laser cavity.

4- Dicyanomethylene-2-methyl-6-p dimethylaminostyryl-4H-pyran (DCM) in propanol-2 (1.76×10^{-4} M, 84% absorption at 445 nm) was used as the gain medium. Another dye, Coumarin 540 dissolved in propanol-2 (1.6×10^{-4} M, 85% absorption at 445 nm in 1 mm cuvette) was also investigated as a second gain medium to compare laser performances when relevant. The cuvette was set as close as possible from a plane mirror (reflectivity R ~ 99.9% at 600-680 nm, transmission T > 80% at 445 nm); the cavity was 11.8 mm long (easily adjustable) and closed by a concave output coupler (R ~ 99.9% at 600-680 nm) with a 50 mm radius of curvature. The fundamental cavity mode was around 80 µm in radius, enabling a good matching with the pump mode (60 µm in radius) along the cuvette.

3.2.2.2. Laser threshold and efficiency

Figure 3.4 shows laser peak power (W) as a function of absorbed pump peak power (W) for DCM and Coumarin dye using 30 ns pump. It is necessary to clarify here that we will mainly focus on DCM

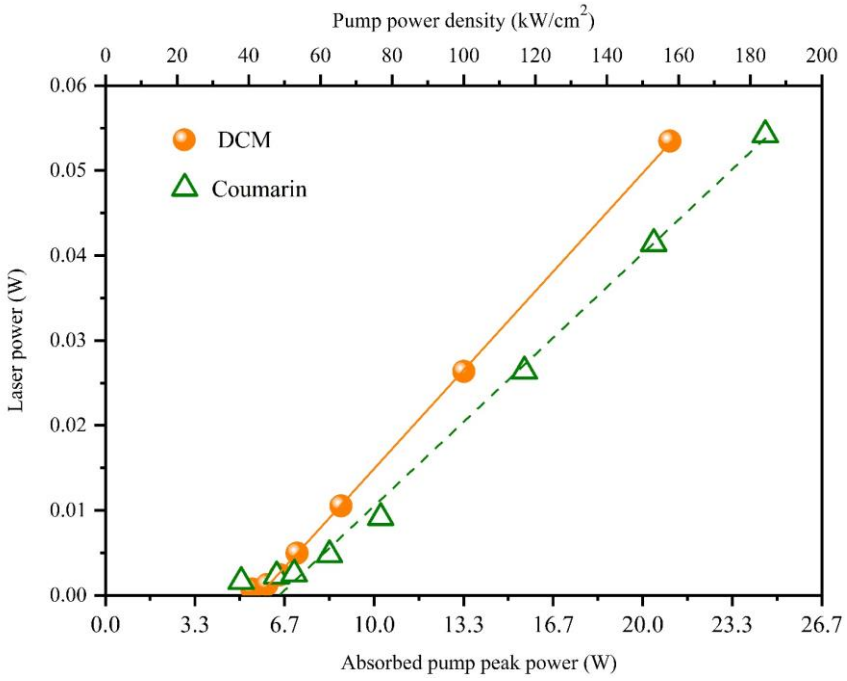

Figure 3.4 : Laser peak power (W) using DCM and Coumarin-540 dyes as a function of absorbed pump peak power (W) (bottom x-axis) and pump power density (kW/cm^2) (top x-axis). Output coupler radius of curvature is 50 mm with reflectivity 99.9% at laser wavelength.

laser since previous chapter investigated such laser in detail. Performance of Coumarin laser will only be shown when relevant for the perspective of comparison. However, lasing was obtained with a clear threshold around 48 kW/cm^2 and 53 kW/cm^2 for DCM and Coumarin respectively. Slope efficiency of each laser was calculated to be ~ 0.3% (approximately) while optical conversion efficiency was ~ 0.2% (calculated from the ratio of maximum laser peak power to corresponding pump peak power). Although we had an efficient overlap between pump (60 µm in radius) and cavity mode (80 µm in radius) on the gain medium, such low efficiency is the result of using highly reflective ~ 99.9% (at laser wavelength) output coupler. This phenomenon is already discussed in chapter 1 where ~ 18% optical efficiency was obtained by using output coupler with 98% reflectivity at lasing wavelength. However, this laser cavity is intended for high repetition rate lasing experiments where thermal lensing of laser medium would certainly result additional cavity losses, therefore highly reflective output coupler mirror was chosen to keep the cavity losses as low as possible.

3.2.2.3. Laser repetition rates

Following laser design and threshold characterization, we were interested to investigate the maximum lasing repetition rate achievable intrinsically from our circulation-free liquid dye (DCM in propanol-2)

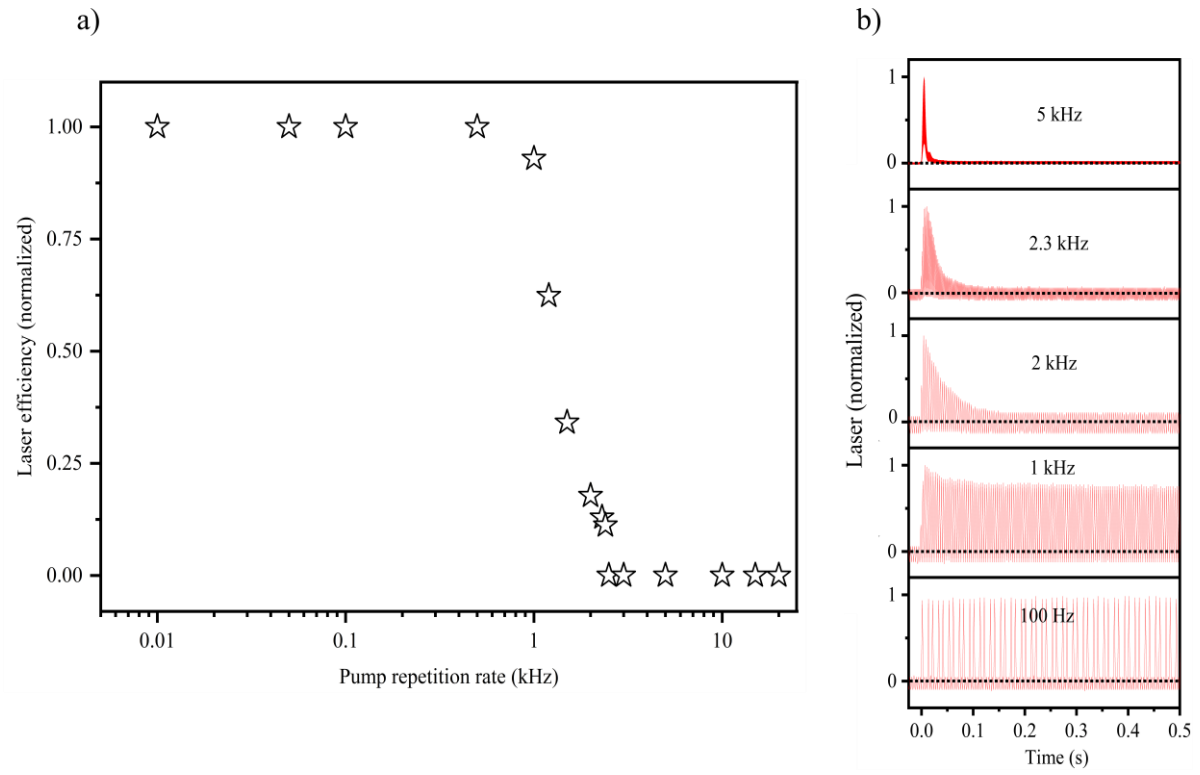

Figure 3.5 : (a) DCM laser efficiency (normalized) vs pump (30 ns) repetition rates (kHz) measured at absorbed pump peak power ~ 83 kW/cm^2. (b) Laser behavior for the first 500 ms at different repetition rates.

using 30 ns long pump. Figure 3.5 shows laser efficiency (normalized) vs repetition rates (kHz) measured at 83 kW/cm^2 pump power density. Such pump power, approximately 1.7 times above laser threshold is chosen to keep thermal load (when operating pump at several kHz high repetition rates) as low as possible. However, no efficiency drop is observed up to 500 Hz. As soon as the pump repetition rate went beyond 1 kHz, laser efficiency started to decrease significantly. This phenomenon is more understandable from the oscilloscope trace showing laser behavior recorded during the first 500 ms of lasing at different pump repetition rates as depicted in Figure 3.5. Anyway, no lasing was obtained when the pump was operated beyond 2.4 kHz. Coumarin dye also showed up to 3 kHz lasing using 30 ns pump at 95 kW/cm^2 (1.8 times above laser threshold) which is quite close to the maximum repetition rate obtained for DCM. This is shown in Figure 3.6.

By recalling the lifetime ~31 µs[68] of triplet states of DCM in solution, we can say that 2.4 kHz cannot be attributed to fundamental limit in repetition rates resulting from the accumulation of triplet states but

a logical explanation may be thermal lensing of laser medium, which completely destroys cavity stability beyond such repetition rates. To verify such hypothesis, we performed Plano-concave laser cavity stability simulation by numerically inserting (inside cuvette) a diverging lens of variable focal lengths (-200 mm to -1 mm) using reZonator software. The schematic of the laser cavity is shown in Figure 3.7. Negative value of dn/dT of propanol 2[78] is the reason to choose diverging lens in the simulation. Figure 3.8 shows the result of such simulation where cavity stability is determined from the value of $\frac{A+D}{2}$ as already discussed in chapter 1. As expected, it is seen here that the cavity is no more stable as soon as the thermal lens value becomes smaller than 41 mm in absolute value. Although this simple simulation confirms our hypothesis, that thermal lens can destroy our Plano-concave laser cavity stability, we do not have any information regarding the value of pump induced thermal lens focal length inside our solution during laser experimental conditions (pump power,

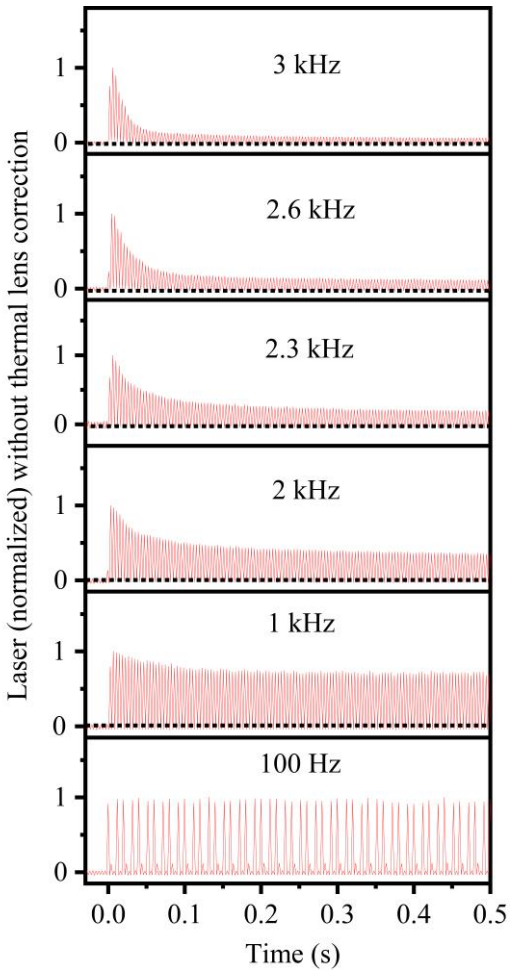

Figure 3.6: Coumarin laser behavior for first 500 ms using pump peak power 95 kW/cm^2.

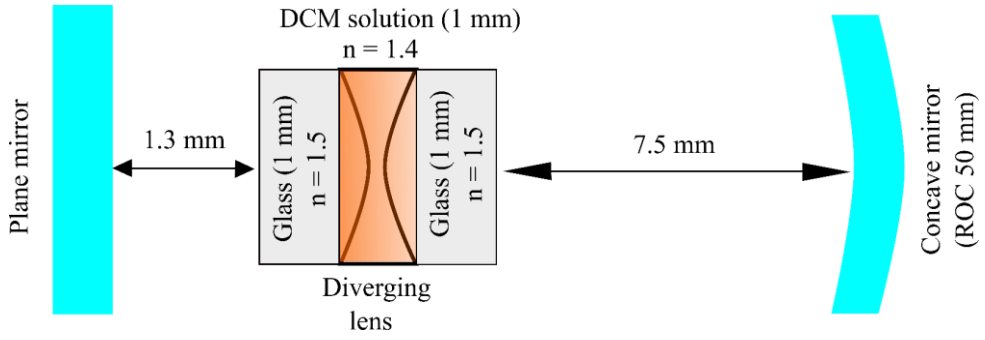

Figure 3.7: Schematic of Plano-concave cavity used for the cavity stability simulation as well as laser experiment. A diverging lens is placed inside cuvette to mimic pump induced thermal lens inside the laser cavity.

repetition rates etc.). Therefore, it was interesting to experimentally measure thermal lens focal lengths at different pump repetition rates keeping pump peak power/average power similar as the laser experiment shown in Figure 3.5. It would be also interesting to compare experimentally found thermal lens focal length to the focal length (41 mm in absolute value) found from simulation below which the

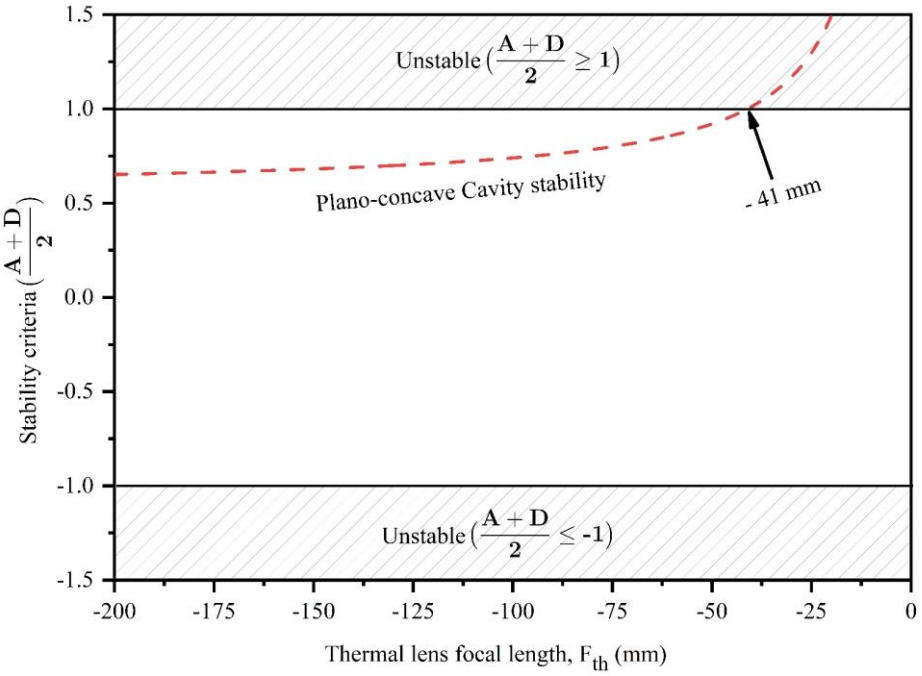

Figure 3.8: Calculation of the cavity stability criteria c = (A+D)/2 for a Plano-concave laser cavity with a diverging thermal lens; For thermal lens focal length, $|fth|$ < 41 mm, the cavity is no more stable resulting from |c|>1.

cavity the cavity was no more stable (Figure 3.8). However, knowing thermal lens focal length values at repetition rates beyond their current lasing limit (2.3 kHz) might open up the possibility for lasing at higher repetition rates by compensating thermal lens correction.

In the following, we show the design of a pump-probe experiment to measure thermal lens focal lengths for different pump repetition rates used in the laser experiment (Figure *3.5*).

3.2.3. Pump-probe experiment to measure thermal lens focal length

Pump-probe technique is one of the popular methods to characterize pump induced thermal lensing of any absorbing medium.[79–81] This method relies on the principle that a pump and probe beam overlaps on each other inside the medium (solid-state/liquid) of interest, which strongly absorbs the pump while being 100% transparent for probe beam wavelength. A photodiode/CCD camera is placed after the sample to monitor the probe beam intensity/size variation at a fixed distance after sample. From probe

beam intensity or size variation after sample one can understand the nature of thermal lens (converging/diverging) and also calculate thermal lens focal length.

Figure 3.9 shows the schematic of pump-probe experiment which was performed in the laser experimental set-up by just removing the output coupler (concave mirror). A CW He-Ne laser (632.8 nm) was used as the probe beam since this wavelength is not absorbed by DCM dye. The pump and probe beam, coming from opposite ends, collinearly overlapped each other inside 1 mm cuvette containing the lasing solution (DCM in propanol 2). A 75 mm lens was used to focus the probe beam before cuvette to create 110 µm (in diameter) spot on the cuvette while the pump diameter on cuvette was 120 µm. Pump and probe beam diameters were kept comparable to have a better photo thermal signal.[80] A CCD camera was placed 7.7 cm after the sample to record probe beam size in absence and presence of pump (30 ns, 77.4 kW/cm^2) at different pump repetition rates ranging from 0.3 kHz to 5 kHz. When pump repetition rate exceeded beyond 5 kHz, probe beam diameters appeared to be larger than the camera sensor.

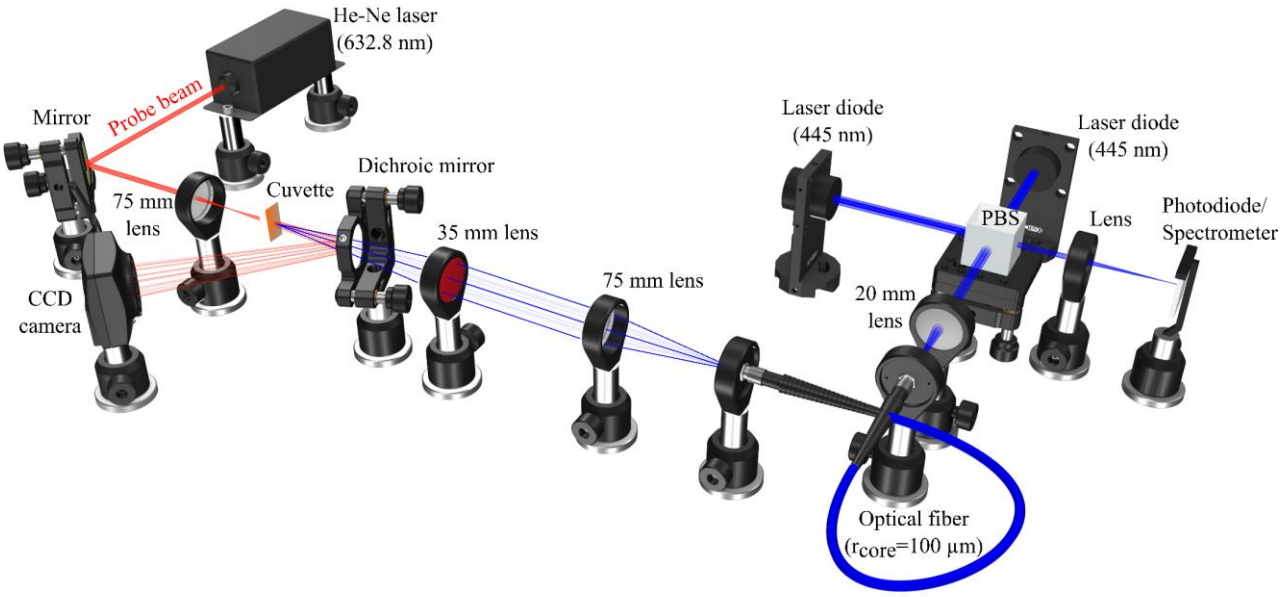

Figure 3.9: Schematic of pump-probe experiment performed by removing the cavity mirrors of laser experimental setup. He-Ne laser (at 632.8 nm) is chosen to probe the pump spot on the cuvette since DCM does not absorb at this wavelength. The pump and probe beam collinearly overlapped onto the liquid cuvette from opposite ends with spot sizes around 120 µm and 100 µm in diameters, respectively. A CCD camera was placed at 7.7 cm after the sample to monitor probe beam size when increasing the pump repetition rate at a fixed pump peak power ~ 77.4 kW/cm^2(~1.6 times the laser threshold).

Thermal lens focal lengths for different pump repetition rates were calculated by modelling the propagation of probe beam starting from the source (HE-NE laser whose M^2 was taken to be 1) to the CCD camera (calculating the transfer matrix of each element that changes probe beam path due to having different refractive index e.g., lens, cuvette, etc.). The schematic used for modelling is presented in Figure 3.10. We validated our modelling by comparing (in absence of pump) practically measured probe beam sizes at different positions (e.g., at the entrance of lens, cuvette etc.) inside its propagation path with the beam sizes at those positions found from modelling (Figure 3.12). The plot of probe beam radius after 75 mm lens, as a function of d_2 (distance between lens to cuvette), cuvette and d_3 (distance between cuvette to camera) is also given in Figure 3.12. The reason to keep the cuvette few mm away

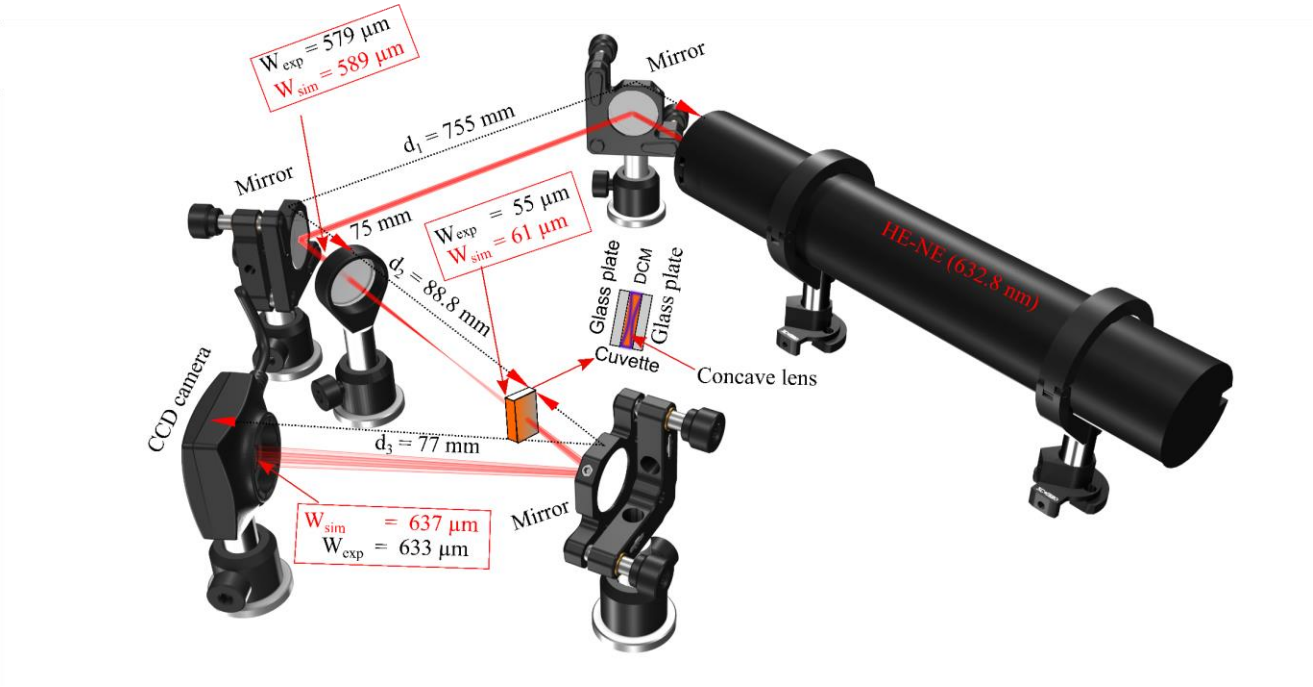

Figure 3.10: Schematic of the probe beam propagation, including a focusing lens (75 mm) and cuvette, from source (HE-NE 632.8 nm) to the CCD camera. A concave lens is numerically inserted inside liquid cuvette (see cuvette design) to mimic diverging thermal lens created in the laser medium during a real pump-probe experiment. Thus, varying the focal lengths of this lens, different probe beam radii were numerically created on camera (at certain distance after cuvette) to match the probe beam radii, at same distance after cuvette, at different repetition rates during pump-probe experiment. w_{sim} or w_{exp} at different positions (e.g., before lens, cuvette, on camera) correspond to probe beam radii from simulation and experiment, respectively.

(one Rayleigh length after focus) from the focus of probe beam was to increase the sensitivity of the measurement. To show this, we present a simulation in Figure 3.11 where we kept 10 mm (in absolute value) diverging lens containing cuvette at the focus of probe beam and at the position used in our experiment. Here, we can clearly see that the probe beam remains almost unchanged after it meets

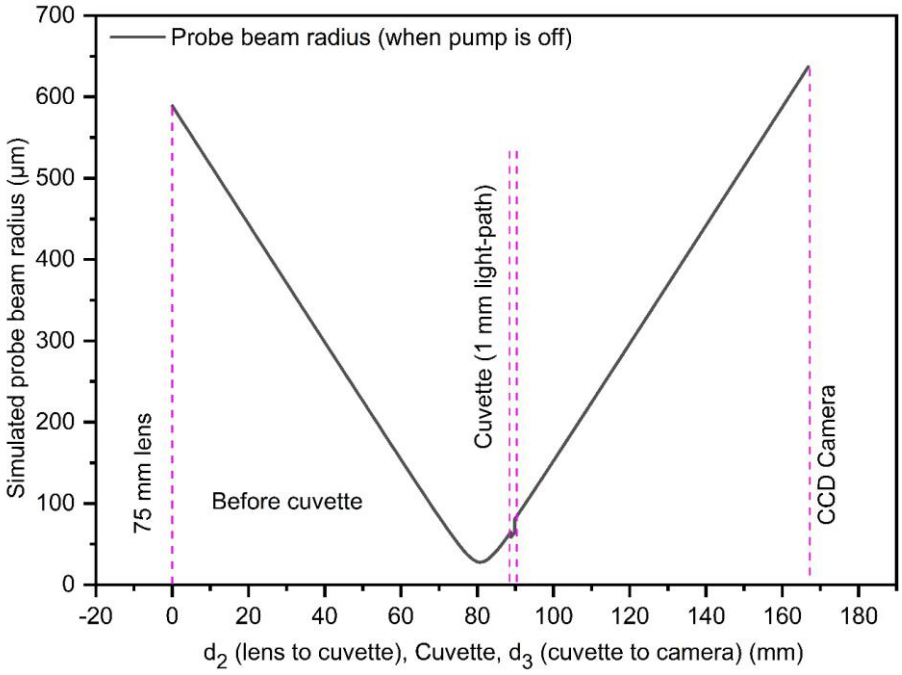

Figure 3.12: Propagation of simulated probe beam from 75 mm lens to a CCD camera. Probe beam radii before lens, on cuvette and CCD camera obtained from this simulation is used in Figure 3.10.

the cuvette, hence, the diverging lens at its focus. On contrary, when the cuvette is placed few mm after focus as we did in our pump-probe experiment, the probe beam diverges significantly indicating the sensitivity of our measurement.

However, our thermal lens focal length measurement and simulation were very close (comparative values are given in Figure 3.10) demonstrating a good agreement between our experiment and modelling. Following this, we numerically inserted a concave lens with variable focal lengths inside the cuvette as presented in the inset (2D diagram) Figure 3.10 since the thermal lens was presumed to be diverging as already mentioned before. Different probe beam radii on CCD camera as a function of

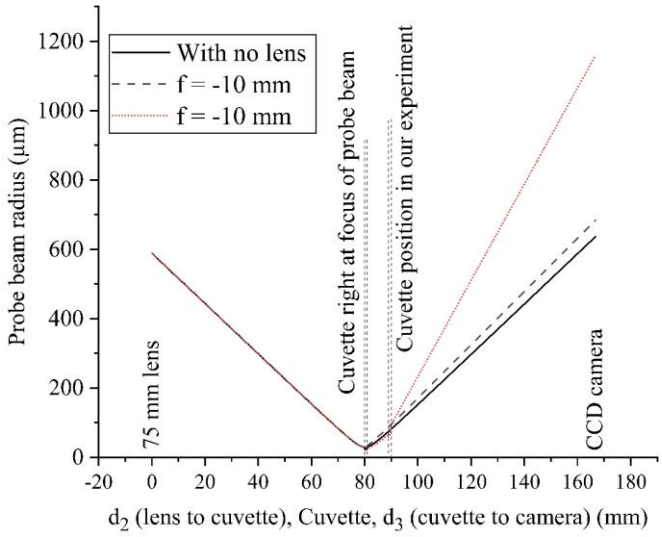

Figure 3.11: Here the cuvette contains a 10 mm (in absolute value) diverging lens. Probe beam divergence (after cuvette) remains almost insensitive to such diverging lens when the cuvette is placed right at the focus of probe beam. When the cuvette is placed one Rayleigh length after focus as used in our experiment (Figure 3.9, Figure 3.10, Figure 3.12), significant divergence of probe beam indicates the sensitivity of our measurement.

pump repetition rates recorded from pump-probe experiment were recreated numerically by changing the focal lengths of the concave lens. Those focal lengths. represented the values of thermal lens focal lengths at different pump repetition rates. The results are discussed below.

- **Results of pump-probe experiment**

Experimentally obtained probe beam radii for different pump repetition rates were recreated by suitable focal length diverging lenses in a simulation as detailed above. Figure 3.13 shows the result of such simulation where one can see the variation of probe beam radius when it propagates from 75 mm lens to the camera by traversing through the pump area on cuvette. In absence of pump, probe beam radius on camera remained almost similar as its radius at lens position. To show the effect of negative thermal lens as soon as the pump was applied at different repetition rates (0.3 kHz-5 kHz), we numerically inserted diverging lens of different focal lengths to match the experimental values of probe beam radii (at those repetition rates) recorded on CCD camera during experiment. Thermal lens focal lengths used in this simulation are plotted as a function of different pump repetition rates in Figure 3.15.

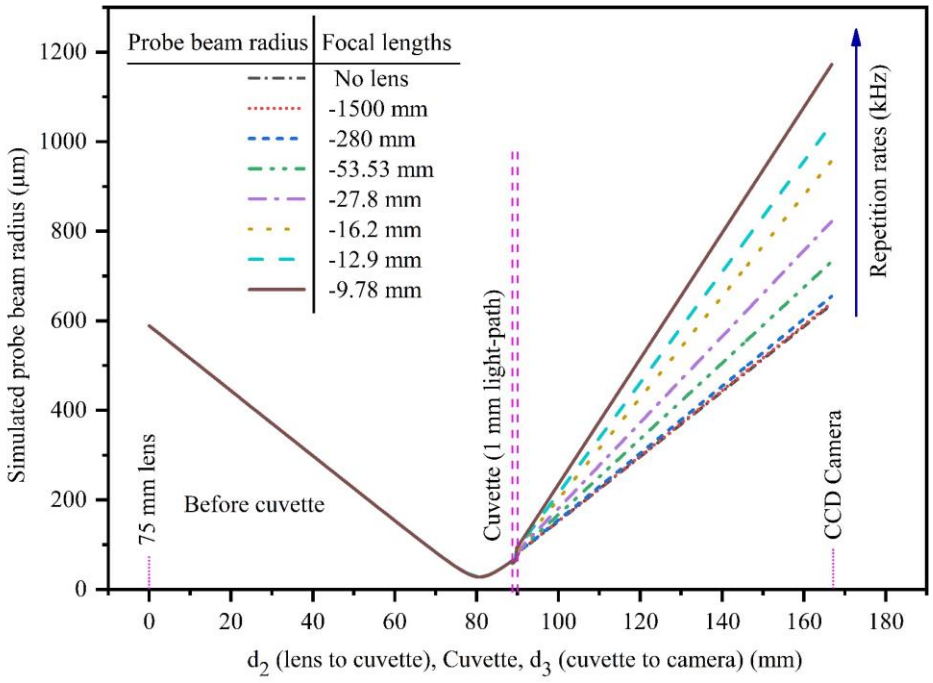

Figure 3.13: Propagation of simulated probe beam from 75 mm lens to a CCD camera by varying the focal length of diverging lens numerically inserted inside cuvette in order to match the probe beam radii on camera at certain repetition rates (0.3 kHz – 5 kHz) during pump-probe experiment.

As expected, we observed an increase in probe beam radii (left y-axis) and corresponding thermal lens dioptric powers (right y-axis) as a function of pump repetition rates ranging between 0.3 kHz to 5 kHz.

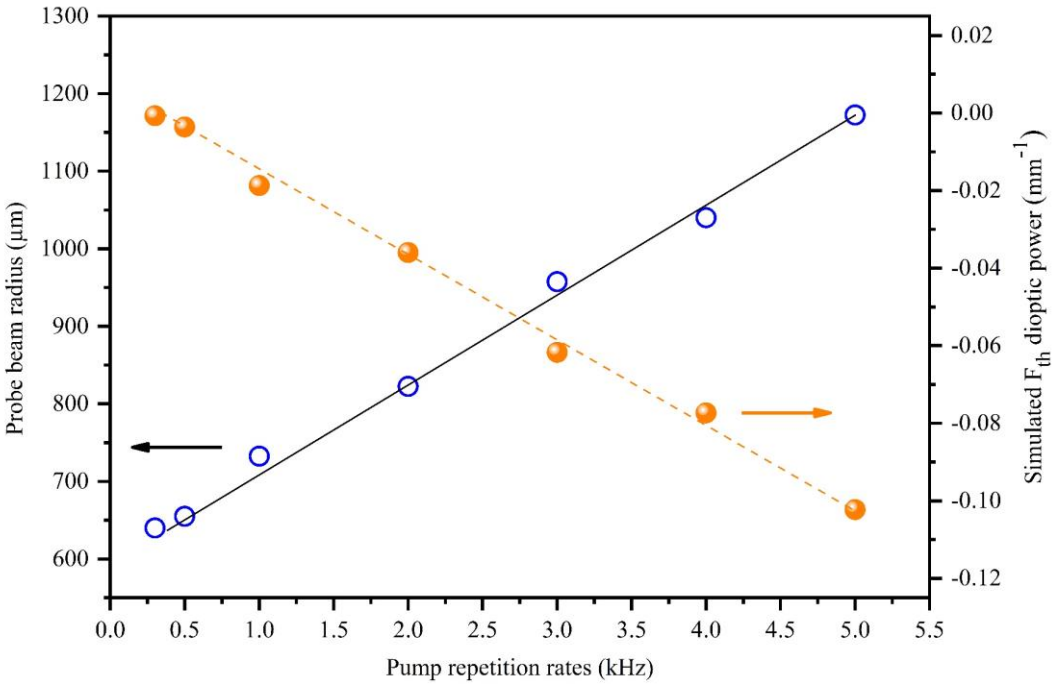

Figure 3.15: Probe beam (HE-NE 632.8 nm) radius (μm) (left x-axis) and simulated thermal lens dioptric power (mm-1) (right-y axis) as a function of pump (445 nm, 30-ns, 77.4 kW/cm2) repetition rates (0.3 kHz – 5 kHz) (x-axis).

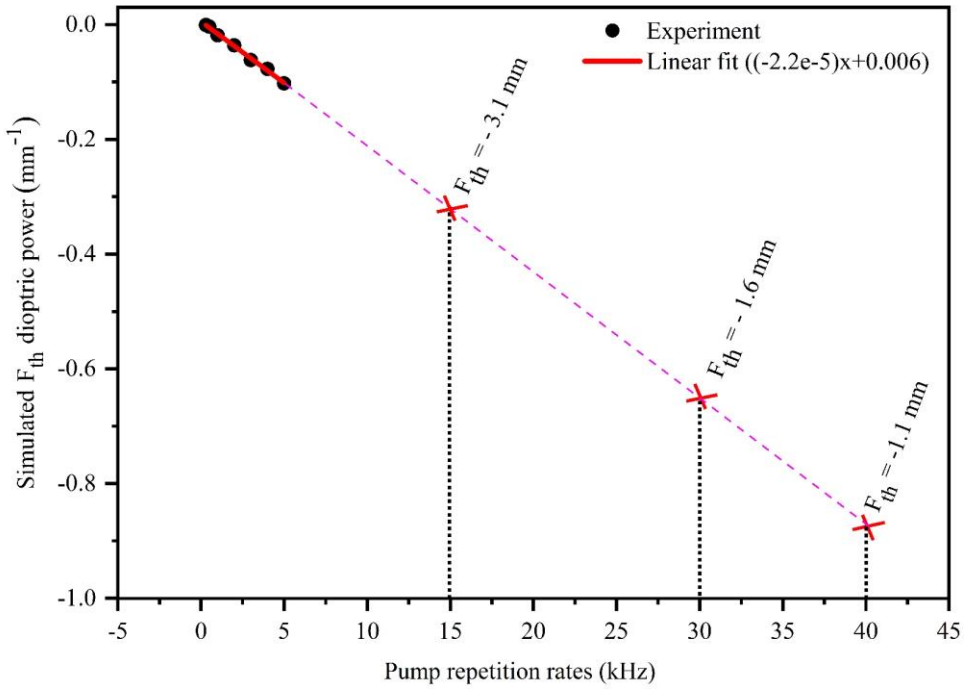

Figure 3.14: Linear fitting of thermal lens dioptric powers (from Figure 3.15) as a function of pump repetition rates (0.3 kHz to 5 kHz). Thermal lens dioptric powers, hence focal lengths, at higher (>5 kHz) repetition rates are estimated by extending the linear fit up to 40 kHz.

Such behavior of increasing probe beam radius with pump repetition rates verifies the temperature

induced refractive index change of propanol-2 is negative as found from literature. It is important to mention that, at 2.4 kHz (maximum repetition rate of our laser) thermal lens focal length extracted from this experiment is 25 mm in absolute value which is comparable but slightly higher than 41 mm (in absolute value) found in simulation (Figure 3.8) below which the cavity was no more stable. While thermal effect was found to be insignificant below 0.3 kHz (corresponding thermal lens focal length 1500 mm in absolute value) pumping, beyond 5 kHz (corresponding thermal lens focal length 9.78 mm in absolute value), the probe beam diameter appeared to be larger than camera sensor. However, thermal lens dioptric power at higher repetition rates (beyond 5 kHz) can also be estimated from its linear have been fitted using linear function (bold red line) and extended to estimate thermal lens dioptric powers, hence focal lengths when pump repetition rates go beyond 5 kHz (dashed line). Quadratic relationship with pump repetition rates as shown in Figure 3.14. Here, thermal lens dioptric powers thermal lensing, unlike higher order thermal aberrations, can be readily compensated by compensation of thermal lens effect. This possibility will be investigated in the following with the objective to push maximum repetition rate (under 30 ns pump) of our laser device beyond 2.4 kHz by thermal lens compensation.

3.2.4. High repetition rate circulation-free liquid dye laser by thermal lens correction

In this section we are interested to compensate steady-state thermal lensing of laser medium by introducing a correction lens inside Plano-concave laser cavity. For this purpose, the focal length of the correction lens was decided to be 3 mm to achieve up to 15 kHz lasing as can be understood from Figure 3.14. In this regard, we were stick to the same Plano-concave laser cavity (Figure 3.7) which showed maximum 2.4 kHz lasing, except that here a 3 mm focal length aspheric lens was used inside cavity as

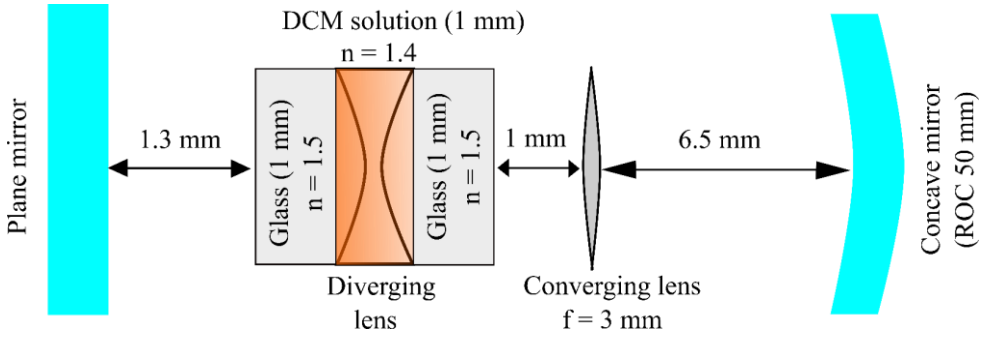

Figure 3.16: Design of a Plano-concave laser cavity by employing an extra converging lens (f = 3 mm) to compensate thermal lens effect of the laser medium.

a thermal lens compensator. The schematic of the laser cavity is shown in Figure 3.16. Prior to laser experiments, it would be interesting to verify if the 3 mm lens can enhance the stability zone of the laser resonator compared to the case when no such correction lens was used (Figure 3.8). Cavity stability

simulation for both cases (with and without thermal lens correction) is depicted in Figure 3.17 for a wide range of thermal lens focal lengths (-200 mm to -1 mm). It is clear from Figure 3.17 that with this additional lens, the cavity becomes stable for a wider range of thermal lenses down to 3.2 mm in absolute value. As a direct consequence, experimentally we observed 14 kHz lasing (Figure 3.18, Figure 3.19) using an intracavity 3-mm aspheric converging lens (experimental cavity design parameters are based

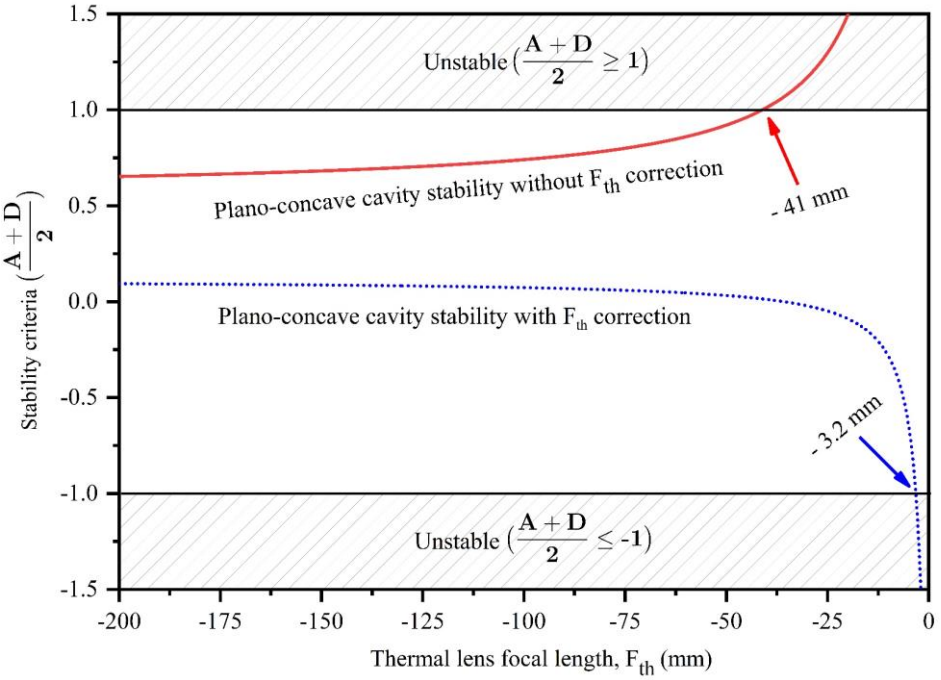

Figure 3.17: Calculation of the cavity stability criteria c = (A+D)/2 for a plano-concave laser cavity with a diverging thermal lens; in absence of correction (red solid curve), $|c|>1$ for thermal lens focal lengths $|fth|>41\ mm$; with an additional 3-mm positive lens, the stability domain is extended to $|fth|<3.2\ mm$ (dotted line).

on Figure 3.16). Interestingly, using 3 mm correction lens we expected to obtain 15 kHz (Figure 3.14) lasing which is very close to 14 kHz obtained experimentally. Figure 3.18 shows a comparative plot of laser efficiency vs pump repetition rate with and without correction of thermal lens. In both cases, although no efficiency drop was observed up to 500 Hz, the laser having no thermal lens correction lost 50% of its initial efficiency when operated at 1.3 kHz which happened at 9 kHz for the thermal lens compensated laser – a proof that thermal lensing played the major role to terminate the laser just after 2.4 kHz when no correction lens was used. It is worthwhile to mention that correction of thermal lens with a lens of fixed focal length implies that the resonator is optimized (in terms of matching cavity and pump modes inside the gain medium) for a single repetition rate, which is here around 3 kHz where the efficiency is slightly higher, although lasing was obtained over the whole stability domain up to 14 kHz. A more comprehensive insight can be found in Figure 3.19 with the oscilloscope traces during the

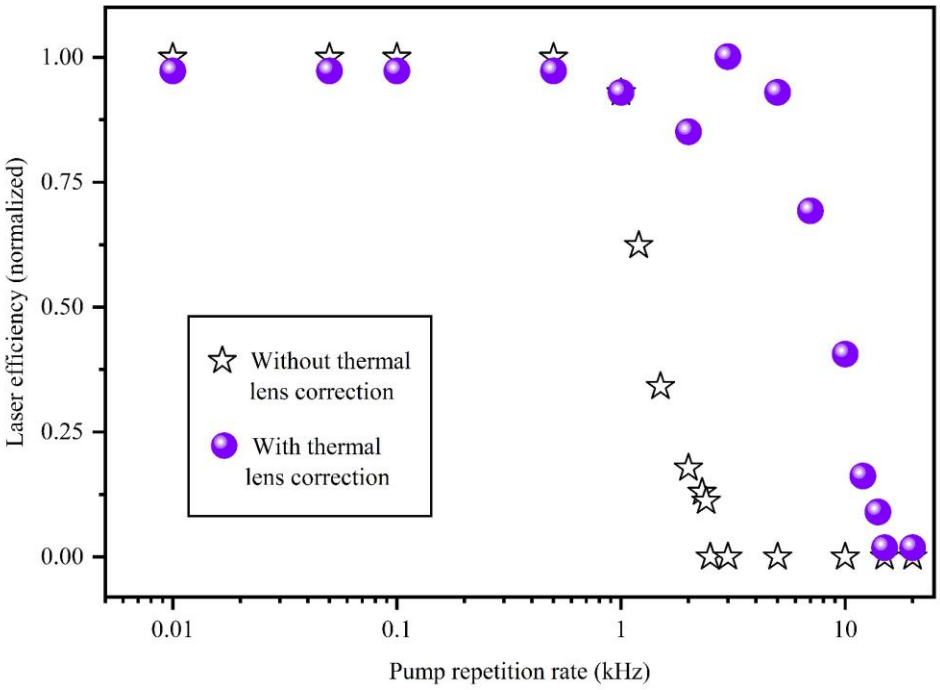

Figure 3.18: Laser efficiency (normalized) vs pump (30-ns, 83 kW/cm^2) repetition rates in a Plano-concave cavity with and without intracavity thermal lens compensation.

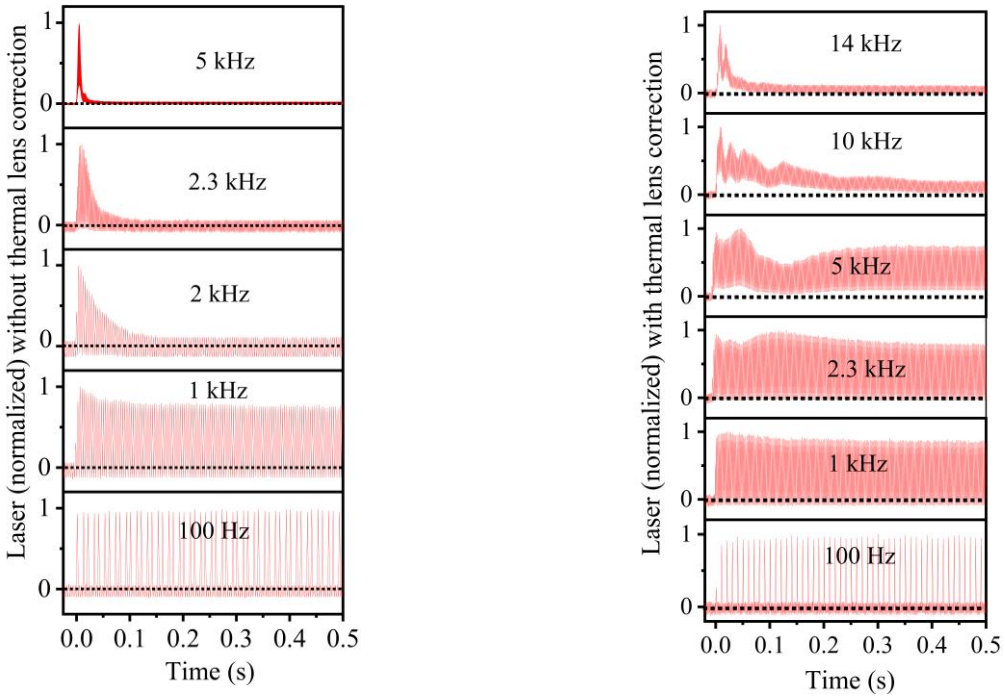

Figure 3.19: Oscilloscope trace of DCM laser behavior for the first 500 ms at different pump (30-ns, 83 kW/cm^2) repetition rates in a Plano-concave cavity without (left) and with (right) thermal lens correction.

first 500 ms of lasing with and without TL compensation. As the repetition rate limitation due to thermal loading is a cumulative effect that builds up pulse after pulse, it is consistent to observe that the first pulses all have the same intensity irrespective of the repetition rates. The intensity however rapidly decreases to a steady-state value where the thermal lens (TL) has reached a stable dioptric power. The intensity goes to zero if the thermal lens dioptric power is so strong that it makes the cavity unstable, a situation which however allows the laser to emit a few pulses before shutdown: this situation occurs beyond 2.4 kHz and 14 kHz, respectively without and with TL correction. However, from Figure 3.14, we estimated that using a correction lens of shorter focal length (for example, 1.1 mm in absolute value), repetition rates as high as 40 kHz could theoretically be reached. At such a repetition rate however, triplet issues (together with aberrations of the thermal lens) might start to be important. In order to check whether this several kHz lasing obtained after thermal lens correction is unique to DCM dye, we ran the same experiments with coumarin-540 dye dissolved in the same solvent (to keep the thermo-optic properties similar) at a concentration of 1.6×10^{-4} M in such a way that the gain solution had a similar absorption of ~ 85% at 445 nm. The laser efficiency curve using Coumarin is already shown in Figure 3.4. We observed in this case lasing up to 18 kHz with a 3 mm converging lens and a 3 kHz limit without thermal lens correction respectively, close to the results obtained with DCM. Coumarin laser behavior for first few hundreds of ms is shown in Figure 3.20.

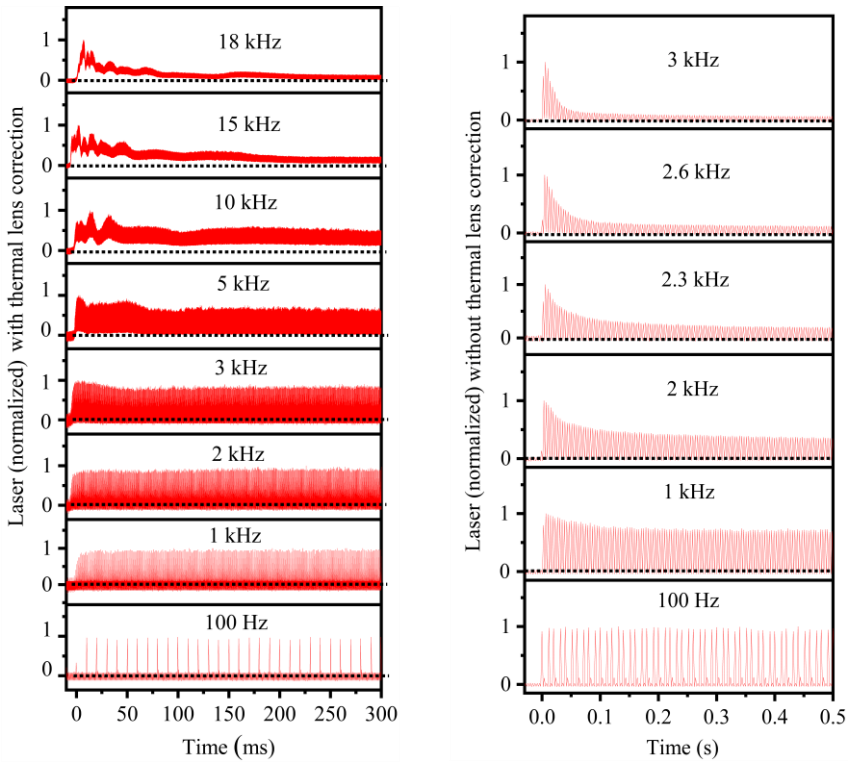

Figure 3.20: Oscilloscope trace of Coumarin-540 laser behavior for the first 500 ms at different pump (30-ns, 95 kW/cm^2) repetition rates in a Plano-concave cavity without (left) and with (right) thermal lens correction.

It is clear that several kHz operations of circulation free liquid dye lasers is not fundamentally limited by accumulation of triplet states but thermal lensing of laser medium that destabilizes laser cavity at certain repetition rate. Although, we have compensated such thermal lens effect by using an intra cavity correction lens but adding a lens inside cavity increases cavity losses and hence decreases laser efficiency as shown in chapter 1. An alternative method to compensate the effect of thermal lens may consider the design of thermal lens insensitive laser cavity. Such design concept relies on keeping cavity mode significantly smaller than the pump mode, so that the cavity mode becomes insensitive to the temperature change inside the pump area of gain medium. However, in that case, smaller cavity mode compared to the pump results inefficient spatial overlap between them (pump and cavity mode) and often possess multi-mode beam quality rather than diffraction limited TEM_{00} which falls in line with the discussion of next chapter. In the following, we will focus on resonator design to operate our laser at high repetition rates.

3.2.5. High repetition rate circulation free liquid dye laser by resonator design

In this section, the role of resonator design to withstand thermal lensing of laser medium will be investigated with the goal to achieve high-repetition rate operation intrinsically from circulation-free liquid dye lasers. A concentric laser cavity would be the most suitable candidate for this purpose. The

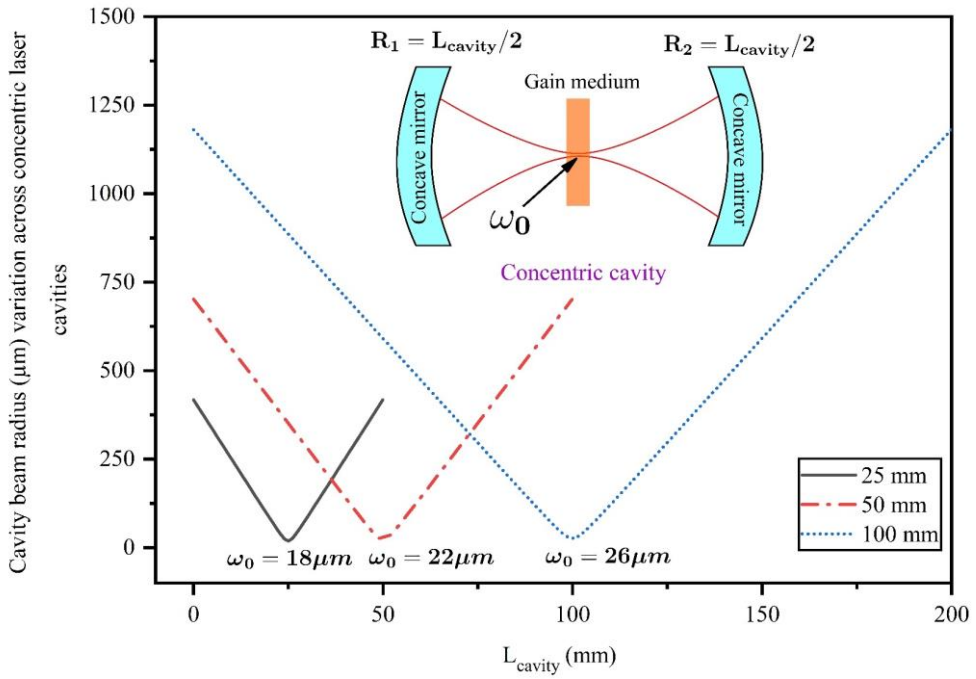

Figure 3.21: Cavity beam radius as a function of cavity length in a concentric laser cavity composed of a pair of 25 mm, a pair of 50 mm and a pair of 100 mm radius of curvature mirrors.

Schematic of a concentric cavity with two concave mirrors is shown at the inset of Figure 3.21. As one can see, the smallest cavity beam waist is created on the gain medium which makes the cavity beam less sensitive to thermal lensing. Variation of cavity beam radius as a function of cavity length using different radius of curvature concave mirrors forming the concentric cavity are also plotted in Figure 3.21. The smallest cavity beam waist ~ 18 µm on cuvette is found in the concentric cavity using twos 25 mm ROC concave mirrors. Though similar sizes of cavity beam waists can also be obtained using 50 and 100 mm mirrors, but in all cases cavity lengths are mandatorily long to fulfil the condition of concentric laser cavity. For instance, cavity length as long as 50 mm is mandatory to form a concentric cavity using two 25 mm ROC concave mirrors. The impact of cavity length on laser efficiency of a pulsed laser is already discussed in chapter 1. Besides, even if we choose the smallest concentric cavity having 50 mm cavity length for high repetition rate laser experiments, laser experiments would not be comparable to our previous experiments made with a ~12 mm laser cavity.

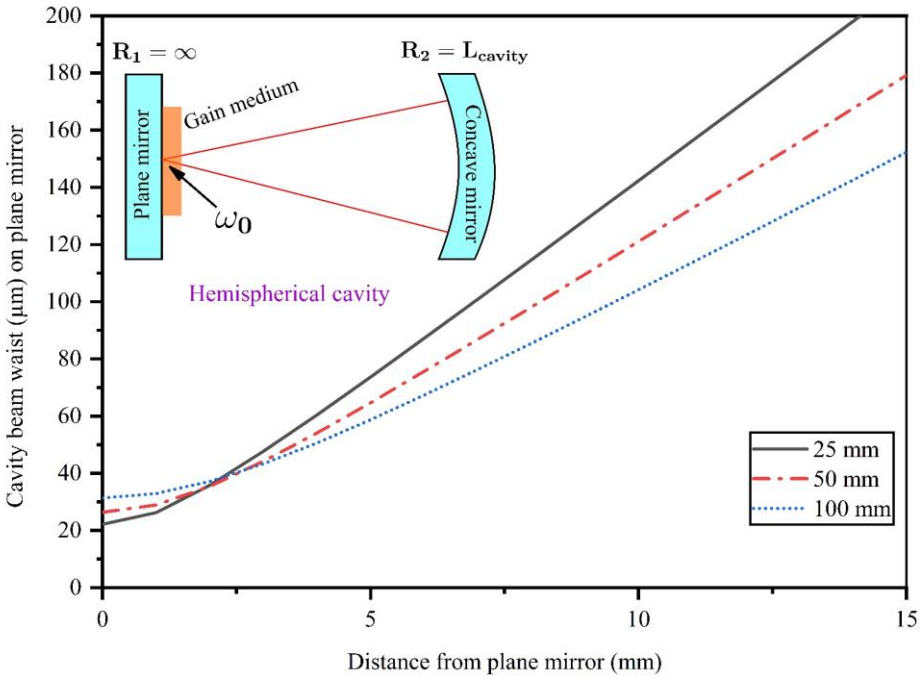

Figure 3.22: Cavity beam waist on the plane mirror of a hemispherical laser cavity formed with 25 mm, 50 mm and 100 mm radius of curvature concave mirror. Cavity beam radius increases it moves towards concave mirror.

Considering these issues related to concentric cavity, we became interested to explore a hemispherical cavity formed by a plane and concave mirror. This type of cavity forms the cavity beam waist on plane mirror. Therefore, if the gain medium is coated on the plane mirror or placed very close to it, similar objective of using concentric cavity, as discussed before, can be achieved. A schematic of such hemispherical cavity is shown at the inset of Figure 3.22. In this case, cavity beam waist on the plane mirror is also found to be similar compared to the waist sizes of concentric cavity using different concave

mirrors with an additional advantage that here the cavity length can be short using 25 mm concave mirror which is comparable with our previous experiments.

Therefore, we designed the shortest hemispherical laser cavity using 25 mm ROC output coupler and a plane mirror as shown in Figure 3.23. This cavity length might also result similar lasing threshold as

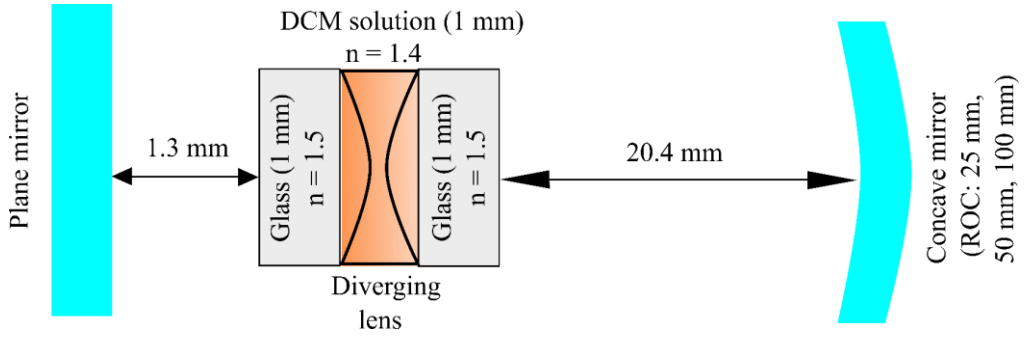

Figure 3.23: Schematic of a Hemispherical Plano-concave cavity design, with numerically inserted diverging lens as thermal lens, using 25 mm radius of curvature (ROC) output coupler. 50 mm and 100 mm ROC output coupler mirrors are also used in place of 25 mm output coupler to compare cavity stability perturbed by thermal lens focal lengths.

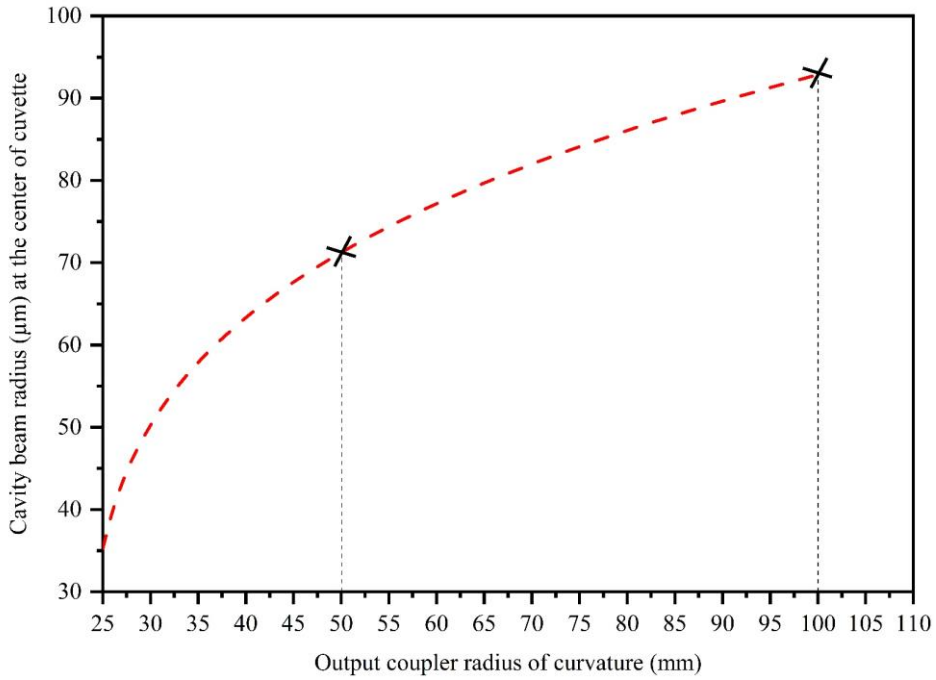

Figure 3.24: Cavity beam radius (μm) on cuvette in the case of a near hemispherical cavity configuration using 25 mm output coupler and also for the case when the output coupler radius of curvature was changed to 50 mm and and 100 mm keeping cavity length fixed.

shown in Figure 3.5. Hence, it leaves the possibility to perform high repetition rate laser experiments in hemispherical cavity using similar pump power as shown in Figure 3.18 or Figure 3.19 for comparison. However, during laser experiment, we also changed output coupler radius of curvature without changing cavity length/mirror reflectivity to see variation of cavity mode size created on the cuvette in a hemispherical and non-hemispherical Plano-concave cavity case. This is simulated in Figure 3.24 where cavity mode size is plotted as a function of output coupler radius of curvature. The smallest cavity beam around 35 µm (in radius), to be compared with our fixed pump size ~ 60 µm in radius, on the gain medium was found when the laser cavity fulfilled the condition of hemispherical cavity by using 25 mm concave mirror at a distance of 24.7 mm from the plane mirror. However, as mentioned earlier the interest of creating small cavity beam on the gain medium was to make the cavity beam less

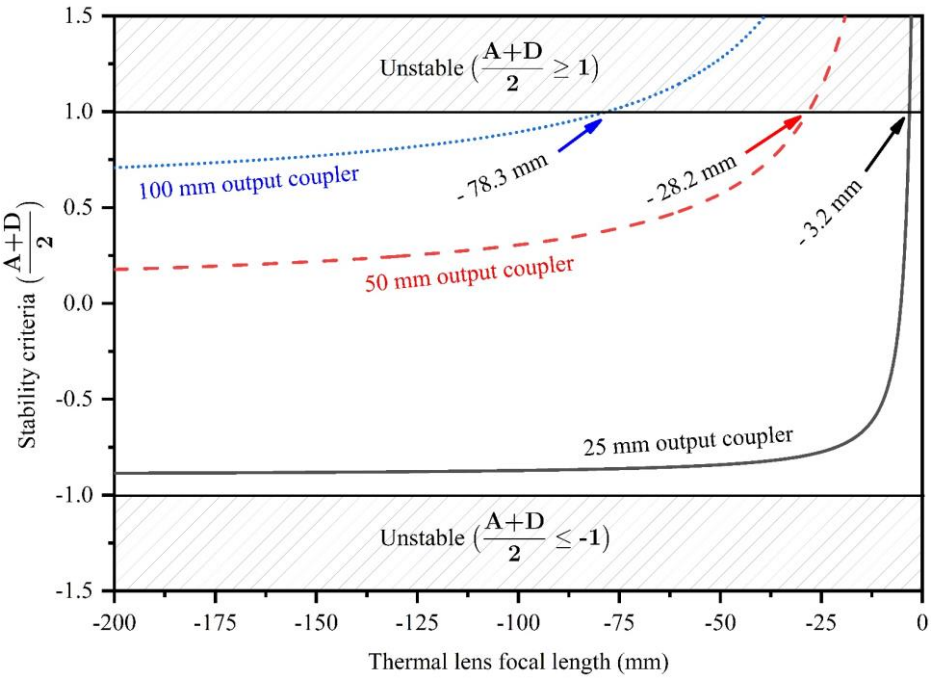

Figure 3.25: Calculation of the cavity stability criteria c= (A+D)/2 for a Plano-concave laser cavity in hemispherical case (using 25 mm output coupler mirror) and non-hemispherical case (using 50 mm and 100 mm output coupler mirrors). The hemispherical cavity is stable up to a thermal lens focal length, $|fth|$= |3.2| mm in absolute value, whereas a non- hemispherical cavity is stable up to a thermal lens focal length, $|fth|$= |28.2| mm and |78.3| mm in absolute value using 50 mm and 100 mm output couplers respectively.

sensitive to the thermal lensing of laser medium thereby enhancing the cavity stability zone towards very short focal length of thermal lens. To check such possibility, we performed hemispherical laser cavity (with 25 mm output coupler) stability simulation by inserting a diverging lens of focal lengths varied between -200 mm to -1 mm. The schematic of simulated cavity is presented in Figure 3.23. As

expected, the hemispherical cavity was found to be stable up to a thermal lens focal length 3.2 mm in absolute value, same as the value obtained in Figure 3.17 where a correction lens was employed to enhance a Plano-concave cavity stability zone by compensating thermal effect. As a clear contrast, the cavity lost its stability to much higher values of thermal lens focal lengths around 28.2 mm and 78.3 mm in absolute value when the output coupler radius of curvature was changed to 50 mm and 100 mm, respectively without changing the cavity length. The results are presented in Figure 3.25. Although, this simulation indicates the importance of cavity design to retrieve high repetition rate lasing from circulation-free liquid dye lasers, an experimental proof would confirm the validity of such claim.

Therefore, we designed hemispherical laser cavity, pumped by two polarization coupled 445 nm blue diodes as detailed in previous section as well as chapter 1, using the cavity parameters (cavity length, position of cuvette, output coupler radius of curvature (25 mm)) given as schematic in Figure 3.23. Lasing from such hemispherical cavity (Figure 3.26) was observed with a clear threshold around 58 kW/cm^2, to be compared with threshold around 48 kW/cm^2 in previous laser experiments with same material (DCM) indicates slight increase ~ 1.1 cm in cavity length (to achieve hemispherical cavity condition). Additionally, the laser efficiency from the Hemispherical cavity is slightly lower ~ 0.12%

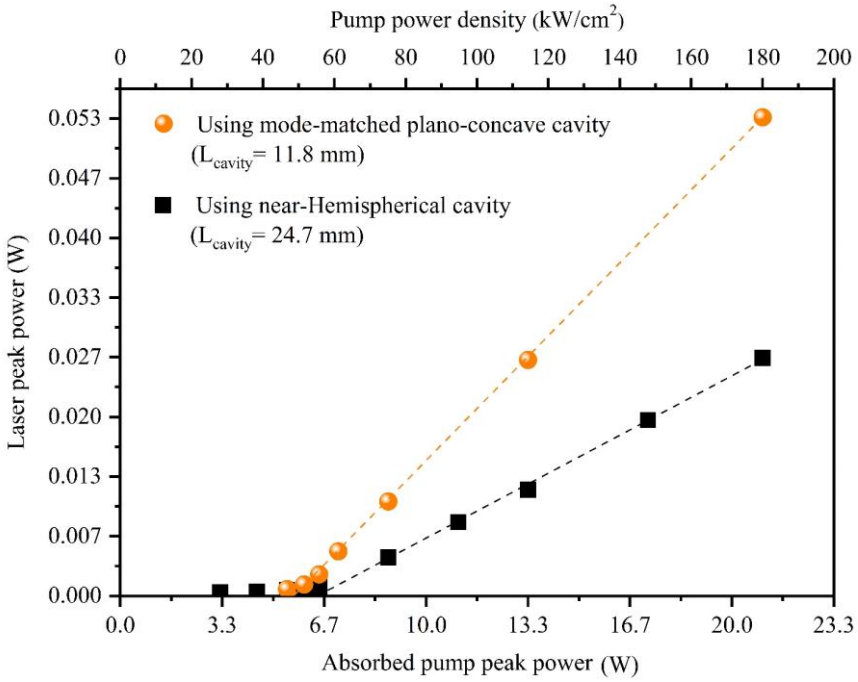

Figure 3.26: Laser peak power (W) as a function of absorbed pump peak power (W) (bottom x-axis) and pump power density (kW/cm^2) (top-x axis) for plano-concave Hemispherical cavity with 25 mm ROC mirror (99.9% reflectivity at laser wavelength) was used as the laser cavity and a mode-matched laser cavity with 50 mm output coupler.

due to inefficient spatial overlap between pump and cavity mode compared to the case of mode-matched Plano-concave cavity with same mirror reflectivity. Beam quality of such laser is not expected to be diffraction limited TEM_{00} – a topic of interest for the next chapter. Here we will only concentrate on the role of cavity mode size, by varying output coupler radius of curvature, to fight against thermal effect. However, by changing the output coupler mirror radius of curvature to 50 mm or 100 mm without

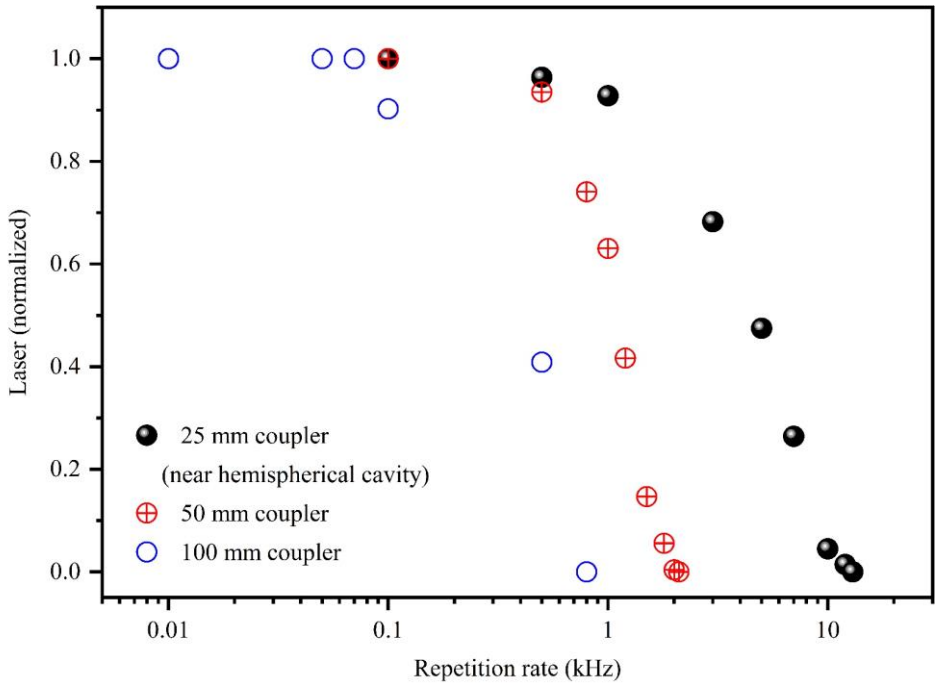

Figure 3.27: DCM laser efficiency (normalized) as a function of pump repetition rates using different radius of curvature output couplers. Laser cavity length (24.7 mm) and reflectivity (99.9% at laser wavelength) of the output coupler mirrors were same.

changing the cavity length or mirror reflectivity (99.9% at laser wavelength) should result similar lasing threshold. The high repetition rate lasing experiments were performed at pump power ~ 90 kW/cm^2 close to the pump power used in previous section for same purpose. Figure 3.27 shows laser efficiency (normalized) vs repetition rate (kHz) for different radius of curvature output couplers. Using 25 mm output coupler in a hemispherical cavity geometry, lasing was observed up to 12 kHz with 50% efficiency drop at around 5 kHz. This is a consequence of cavity design where the cavity mode remained 2 times (appr.) smaller than the pump mode (60 µm in radius) making the cavity less sensitive to thermal lensing as verified from simulation (Figure 3.25). Interestingly, 14 kHz lasing observed earlier by thermal lens correction is close to the maximum lasing repetition rate ~12 kHz we observe here. It might be due to the fact that the thermal lens focal length at those repetition rates is similar as can be seen in Figure 3.14 and Figure 3.25. But slightly higher pump power 90 kW/cm^2 corresponding stronger thermal effect in current experiment compared to 83 kW/cm^2 in previous case, can result maximum 12 kHz

lasing in current experiment. As a clear contrast, maximum 2 kHz lasing was obtained by using 50 mm output coupler whereas lasing terminated just after 500 Hz in case of using 100 mm radius of curvature output coupler mirror, with same reflectivity (99.9% at laser wavelength). Cavity mode sizes comparable (in case of 50 mm mirror) or even larger (in case of 100 mm mirror) than pump mode was probably the main reason behind such low repetition lasing operation. Laser behavior for first few hundreds of ms using different output couplers is shown in Figure 3.28.

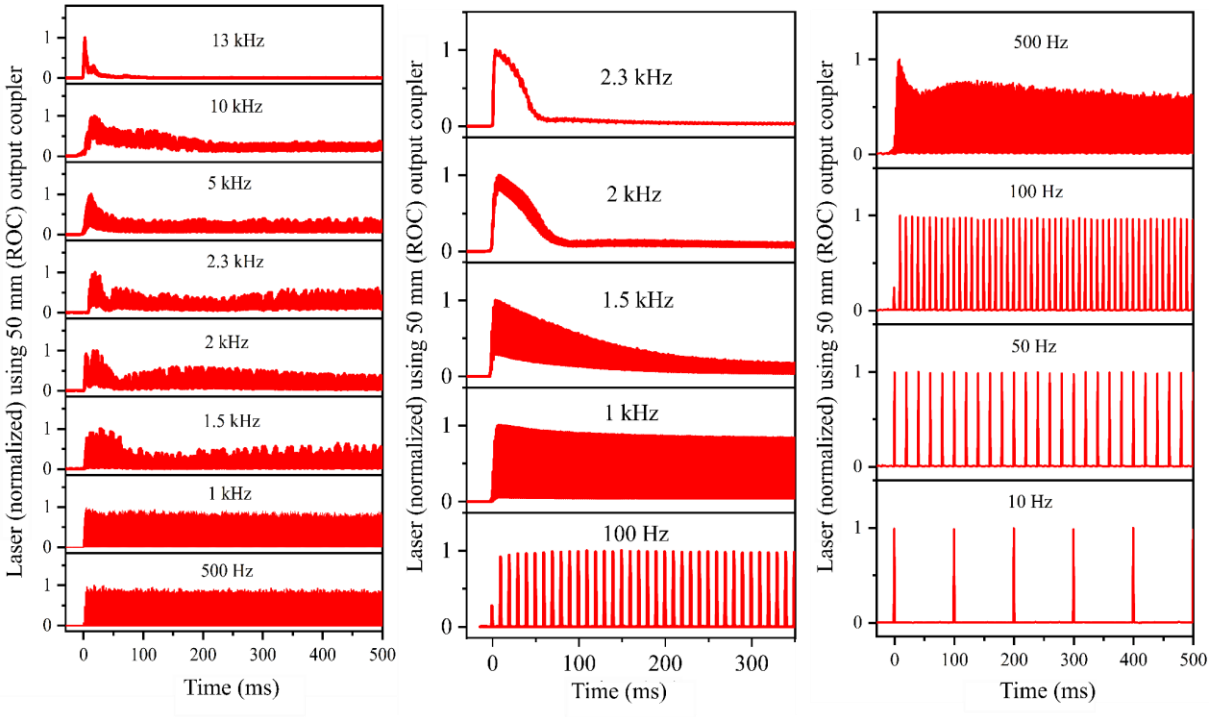

Figure 3.28 : DCM laser behavior for first few hundreds of ms in a hemispherical plano-concave cavity using 25 mm ROC output coupler (left most), and non-hemispherical plano-concave cavities using 50 mm ROC (middle) as well as 100 mm ROC (right most) output coupler mirrors where the cavity length was same in each case.

3.3. Conclusion

We have shown that low repetition operation of circulation-free liquid dye lasers is not fundamentally limited by the accumulation of triplet population but thermal lensing of laser medium. This thermal lens builds-up in the laser medium with a *ms* time scale and destabilizes a Plano-concave laser cavity used in this study. The effect of static thermal lensing can be partly compensated by resonator design with thermal lens correction arrangements. Therefore, we measured thermal lens focal lengths (created in our laser medium) at different pump repetition rates by pump-probe technique. Knowing the value of thermal lens focal length at 15 kHz pump repetition rate, we introduced a correction lens of suitable

focal length inside laser cavity. This cavity arrangement resulted 14 kHz lasing which terminated at beyond 2.3 kHz when no correction lens was used in the cavity. Interestingly, these results were not specific to the DCM dye laser because similar results were obtained when we investigated Coumarin-540 dye in the same experimental setup. This indicates the universality of the fact that, thermal lensing of laser medium is the main barrier for circulation free liquid dye lasers to be operated at high repetition rates. However, the role of cavity design is also shown to fight against thermal lens without the need of an intracavity thermal lens compensator optics. In this regard, a near hemispherical laser cavity was designed, where a small cavity mode compared to the pump enhanced the cavity stability resulting 12 kHz lasing. It is difficult to conclude which technique is better to fight against thermal lens. Both techniques have their advantages and disadvantages. For example, correction of thermal lens with a static lens requires some prior investigation to estimate thermal lens focal length, which can be skipped by just thermal lens insensitive cavity design e.g., Hemispherical, Concentric cavity. However, designing such cavities by usual cavity mirrors (25 mm, 50 mm, 100 mm and so on) might increase cavity length which decreases organic laser efficiency as discussed in chapter 1. But, with specially designed or commercially available very short radius of curvature mirrors might reduce cavity length issues but will significantly degrade the beam quality by showing multimode operation which will be broadly discussed in next chapter. Anyway, regardless of any method used to correct thermal lens focal length, higher repetition rate lasing beyond 30 kHz maybe difficult to obtain due to the fundamental limitation imposed by triplet states. This demonstration opens up opportunities for further improvements in order to reach triplet-limited repetition rates, such as a thermal-lens-insensitive concentric cavity or the insertion of an intracavity variable focal length lens.

4. Toward long pulse circulation-free liquid dye laser

Long pulse circulation-free liquid dye laser is interesting for building simple and compact mode-locked tunable organic laser. Such laser device can be very impressive for laser applications especially owing to their low-cost compared to existing state-of-art mode-locked (Ti:S) lasers. Unfortunately, the current limit of our laser pulse duration is probably not suitable to investigate mode-locking since to obtain mode-locking, the laser should be ideally CW/q-CW as already stated before. For instance, Burdukova et al. investigated mode-locking in circulation-free liquid dye laser using 400 ns laser diode pumping and realized that the pulse duration was not sufficient for building-up mode locking. Therefore, efforts should be given to investigate long pulse regime of circulation-free liquid dye lasers. Unfortunately, single literature by Cole is found on that direction which demonstrated CW lasing from Rhodamine dye solution using a specially designed microcavity liquid dye laser. In Cole's work ultra-small cavity mode volume ~ 11 μm^3 allowed efficient replenishment of dye molecules outside cavity mode through diffusion which resulted CW lasing from them. But rapid photo bleaching of dye within 180s as well as very low laser efficiency ~10^{-6} might limit their application specially to investigate mode locking in those lasers. Since we already have a highly photostable laser, attention should be given to unveil their long pulse regime in order to prepare them for building compact and user-friendly future mode locked organic sources.

Previous chapters showed that any type of losses either originating from cavity mirror reflectivity, gain medium (e.g., diffraction losses arising from thermal effects) or photo-physics of organic molecules (e.g., losses imposed by triplet states) may shorten the pulse duration of organic laser. Unfortunately, by designing a minimum loss cavity with high reflective cavity mirrors and operating the laser at low repetition rate (10 Hz) to avoid cumulative thermal effect as well as accumulation of triplet states, respectively, we could not achieve more than 1.3 µs laser (using 2 µs pump) as shown in chapter 1. However, those results were specific for the case of single transverse mode (TEM_{00}) laser resulting from a mode-matched cavity geometry. Interestingly, we observed longer pulses (> 1 µs) when the laser beam occupies multiple-transverse modes. To our knowledge, this kind of phenomena is observed for the first time in the field of organic lasers and our understanding on this is still incomplete. However, in this chapter we will discuss such phenomena in pursuit of achieving long pulse lasing from circulation-free liquid dye laser.

4.1. Longitudinal and transverse modes of a laser

Here we will briefly discuss about longitudinal and transverse modes of laser in a two-mirror cavity. In a two-mirror laser cavity, standing waves are formed upon fulfilling the resonant condition which physically implies that the waves must create their nodes on both mirrors as shown in Figure 4.1. From this figure, it is also seen that the shortest laser cavity can be in the order of half wavelength although a usual laser cavity can accommodate millions of wavelengths. Longitudinal modes of a laser are referred to those standing waves oscillating in a resonant laser cavity. These wavelengths lie within the fluorescence spectrum of lasing material and wavelength reflectivity band of cavity mirrors. Again, not all of these wavelengths/modes contribute to lasing due to cavity losses. Only the modes that are amplified such that to overcome cavity losses can lase. A simple example of longitudinal modes is depicted in Figure 4.2. It shows three longitudinal modes separated by free spectral

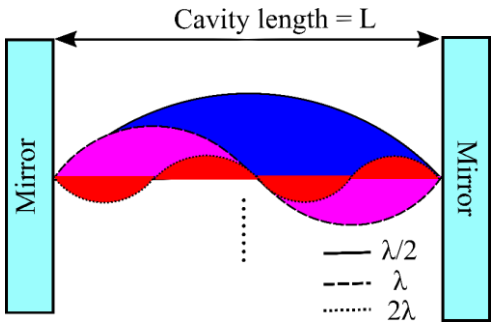

Figure 4.1 : Formation of standing wave in a resonant laser cavity.

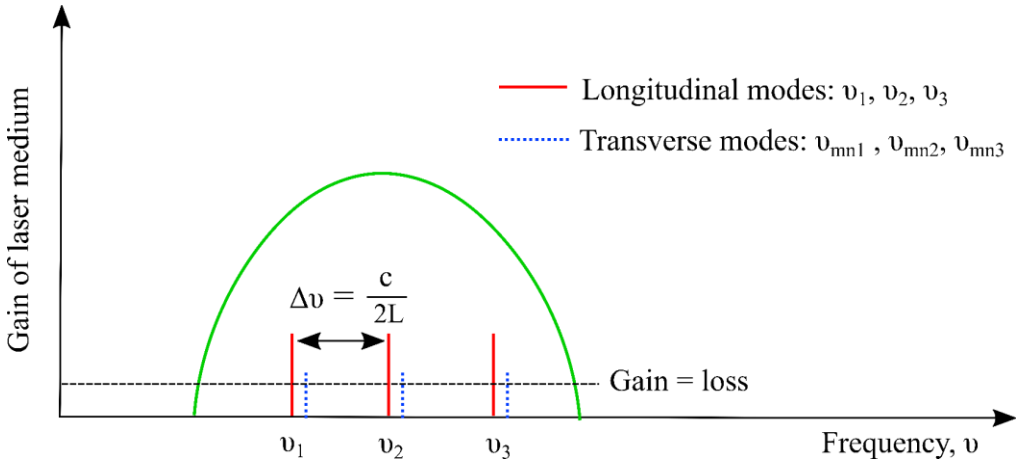

Figure 4.2: Three longitudinal modes of a resonant laser cavity are separated by free spectral range, FSR= $\Delta\upsilon = \frac{c}{2L}$. Lasing can be obtained at either of these frequencies which possess the highest gain over others.

range (FSR= c/2L) of laser cavity. The laser can oscillate in those modes since they have overcome cavity losses. Additionally, it is also seen that, each longitudinal mode is associated with transverse mode with slightly different frequency. These transverse modes define laser intensity distribution along transverse (x, y) axis to the beam propagation axis (z), where x, y and z are orthogonal to each other.

This intensity distribution is expressed by integers (e.g., m, n etc.) (Figure 4.1 and Figure 4.3) and written as TEM_{mn} where m and n denote the number of intensity nodes of the cavity mode along two transverse

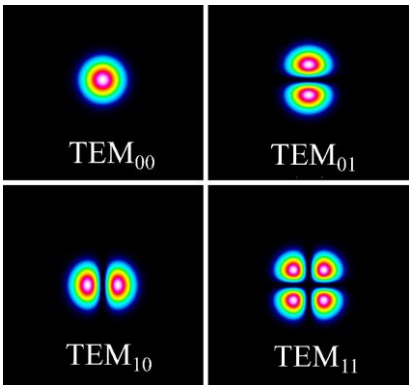

Figure 4.3: Example of laser transverse modes.

axes (x and y). The lowest transverse mode or single transverse mode in other word is known as TEM_{00} having the attractive property of the smallest beam diameter as well as far field divergence. Non-zero values of m and n indicate higher order transverse modes. An example of laser transverse modes is depicted in Figure 4.3. Here transverse modes can be easily distinguished by looking at the beam profile, but it is possible that several transverse modes can superimpose on each other resulting a mixture of laser modes with different percentage of TEM_{00}, TEM_{01}, $TEM_{11,}$ and so on in a way to confuse the beam appearance with a circular diffraction limited one in naked eye. In this case, the value of M^2 can be useful to determine whether the beam contains single or multiple transverse modes. Notably, $M^2 = 1$ indicates laser beam with single transverse mode and $M^2 > 1$ indicates laser beam higher order transverse modes. It is necessary to clarify here that, we are not interested to go into the details of laser transverse modes but to show the distinction between the pulse duration of a single transverse mode vs multi-mode laser. Note that, here multi-mode means multiple transverse modes since our laser possess multiple longitudinal modes as observed from their spectrum shown in Figure 2.15. However, mode matching (fundamental cavity mode > pump mode) between pump and cavity in addition to proper cavity alignment resulted diffraction limited single transverse mode (TEM_{00}) laser as also can be evidenced from their $M^2 = 1.04$ (Figure 2.14).

4.1.1. Physical origin of transverse modes in Plano-concave laser cavity

There are several ways to create transverse modes in Plano-concave laser cavity. Generally, transverse modes can be created from the misalignment of laser cavity mirrors as shown in Figure 4.4 (a). Though this method is simple and straightforward to generate transverse mode lasing, but misalignment of cavity mirrors increases cavity losses while any type of losses can shorten pulse duration of organic laser which

can be an impediment to obtain long pulses from them. Again, from experimental point of view, by adopting this method, same degree of misalignment (of cavity mirrors) is very difficult to maintain when changing laser cavity parameters (mirror, cavity length etc.). Therefore, fair comparison among different experiments having different cavity parameters would not be accurate. Anyway, a second method may consider inserting thin opaque object (e.g., human hair) to block some portion of cavity beam to create transverse modes. However, alignment of such thin object inside laser cavity especially when the cavity length is as short as 1 cm becomes crucial. To avoid those issues, we were interested to generate transverse modes by playing on mode geometry of pump and cavity mode as shown in Figure 4.4 (b). Once a laser cavity (e.g., mode-matched) is properly aligned, pump mode can be easily increased by defocusing the pump on gain medium to a degree until lasing can be maintained. Alternatively, the cuvette can also be moved from the lens focal plane in order to place the cuvette light path (gain medium) out of focus. Either of those methods can result lasing with transverse modes because when the pump mode is significantly larger than cavity mode, the cavity field can support not only the TEM_{00} but also TEM_{01}, TEM_{10}, etc. modes to oscillate. This method does not perturb cavity alignment with an advantage of relaxing thermal load on gain medium.

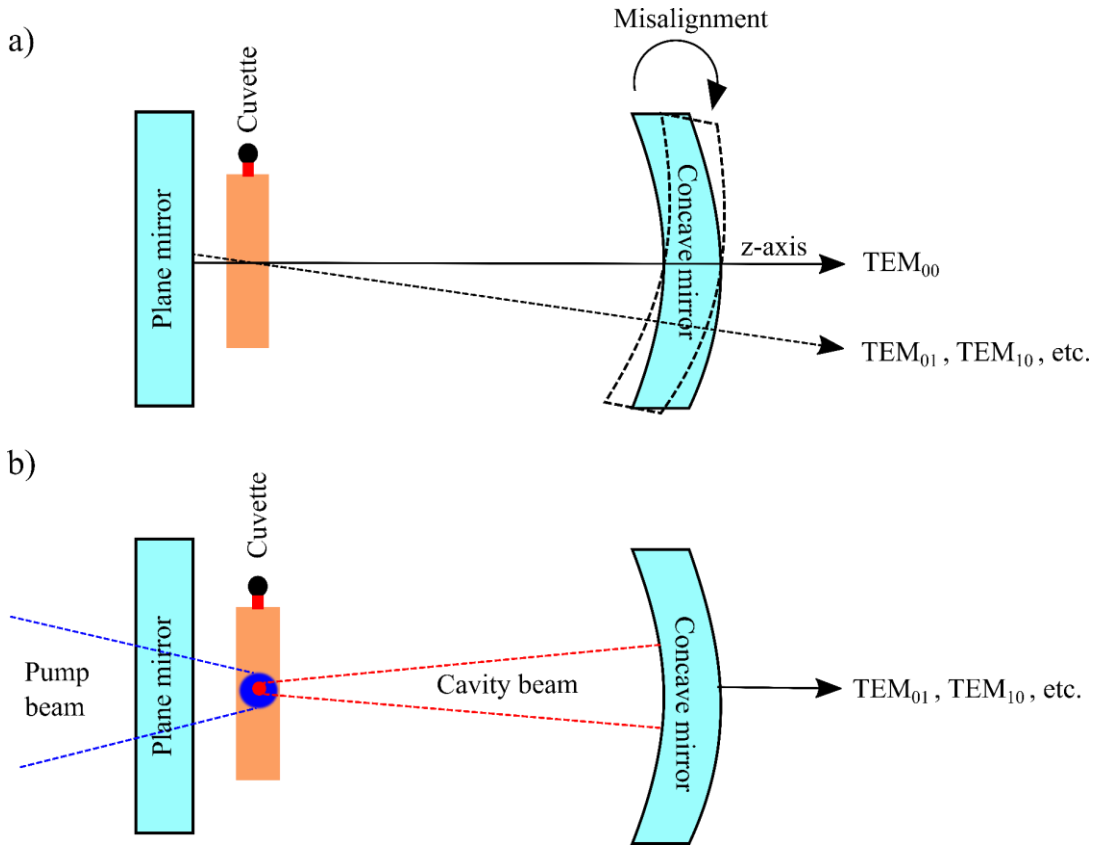

Figure 4.4: Methods to create transverse modes in Plano-concave laser cavity by a) misaligning cavity mirror by b) making pump mode bigger than cavity mode.

Therefore, in the following, we will compare pulse duration of a multimode laser resulting from a completely mode mismatched laser cavity as explained in Figure 4.4 (b), with the pulse duration diffraction limited single transverse mode laser resulting from a mode-matched cavity.

4.2. Dye laser characteristics under focused and defocused pump (10 µs) on cuvette

A mode-matched laser cavity was built by focusing the pump on the cuvette and choosing 50 mm output coupler radius to match the pump size (on cuvette) in a 12±1 mm cavity as shown in Figure 4.5. Cavity and pump mode radii were 80 µm and 60 µm respectively. Complete experimental setup is already discussed in Figure 3.3 of chapter 2. Such cavity design resulted in a diffraction limited single transverse mode laser as also shown before. However, in current setup, the 35 mm lens is attached to a one-dimensional (z) translation to defocus the pump, hence, to make a large pump area on the cuvette. Laser pulse duration was first recorded when the pump was focused on the cuvette as well as for each lens position during the course of defocusing pump. When pump was focused on the cuvette, the laser pulse duration was found to be 1.4 µs which was previously shown to be 600 ns (FWHM) in similar experiment of chapter 1. Here we used highly reflective ~ 99.9% output coupler compared to previous experiment which might explain slightly longer pulse duration here.

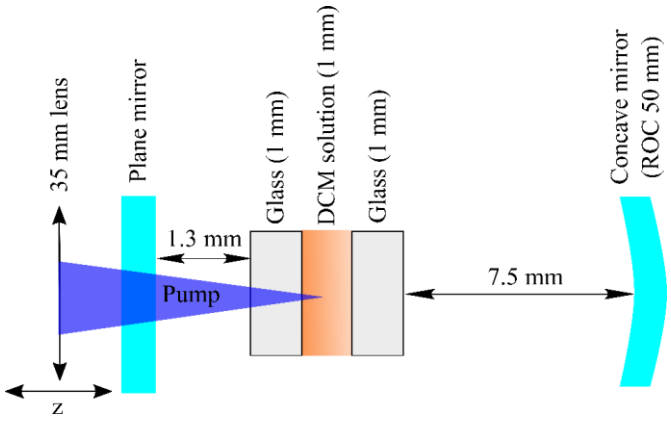

Figure 4.5: Plano-concave cavity for laser experiments. One dimensional translation is attached to lens to defocus pump on cuvette. Complete experimental set-up is explained in

Anyway, the interesting part of current experiment was, when we defocused pump on the gain medium by moving the lens backward up to 0.7 mm with 0.1 mm step, laser pulse duration (at FWHM) also increased. This is also shown separately in Figure 4.7 where it is seen that laser pulse duration is the shortest when pump was focused on the cuvette defined by the lens position 0 mm. Almost 10 µs (at FWHM) laser was obtained when the lens was moved to 0.6 mm and beyond from its original position (0 mm) as can be seen in Figure 4.7. Indeed, moving lens position from 0 to 0.7 mm significantly decreased pump power densities on the cuvette. It was challenging to determine the pump area inside cuvette during the process of pump defocusing. Therefore, we modelled pump beam propagation from

the output of fiber to the cuvette. Similar method is already discussed in chapter 2. In this modelling, M^2 of the pump beam (after fiber) was taken as 72 since it was already measured in chapter 1. Such modelling resulted pump beam waist as short as 47 µm in radius on cuvette which was experimentally

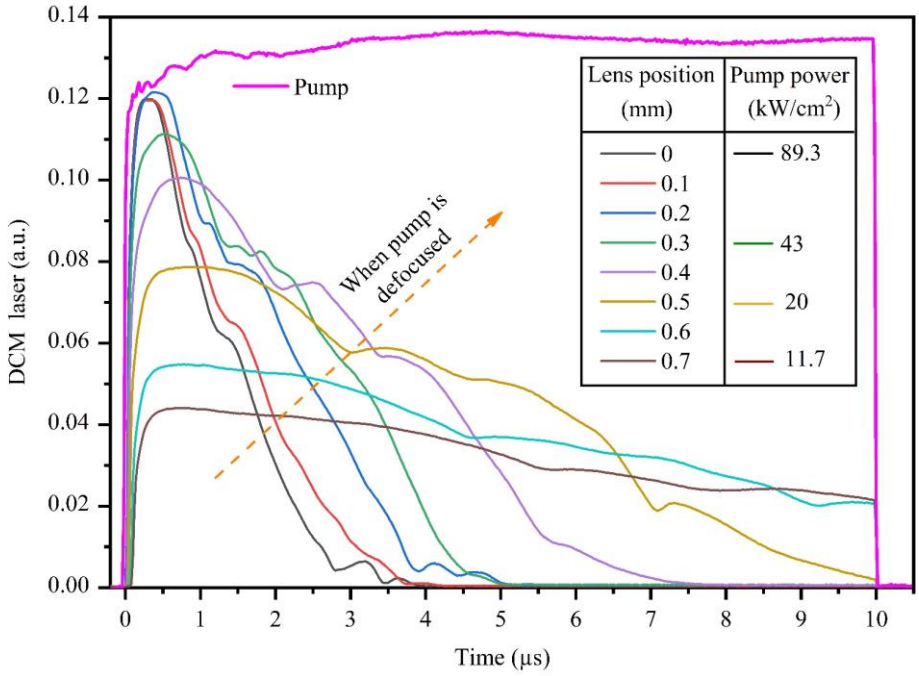

Figure 4.6: DCM laser pulse duration when 10 µs long pump is focused on the cuvette. The lens position in this case is defined as 0 mm. Then the lens is moved backward direction (e.g., away from plane mirror) up to 0.7 mm with 0.1 mm step corresponding to a decrease in pump power density (kW/cm^2). Laser pulse duration is also plotted for each lens displacement.

measured to be 60 µm. The result is given in Figure 4.8. Few micrometers uncertainty is understandable by considering the fact that we choose an M^2 value of the pump beam for modelling its propagation after a focusing lens. However, M^2 is not suited to describe top hat laser beam as the one was coming out from the fiber. But the modelling can estimate approximate beam size on cuvette when we defocused the lens. beam from here we

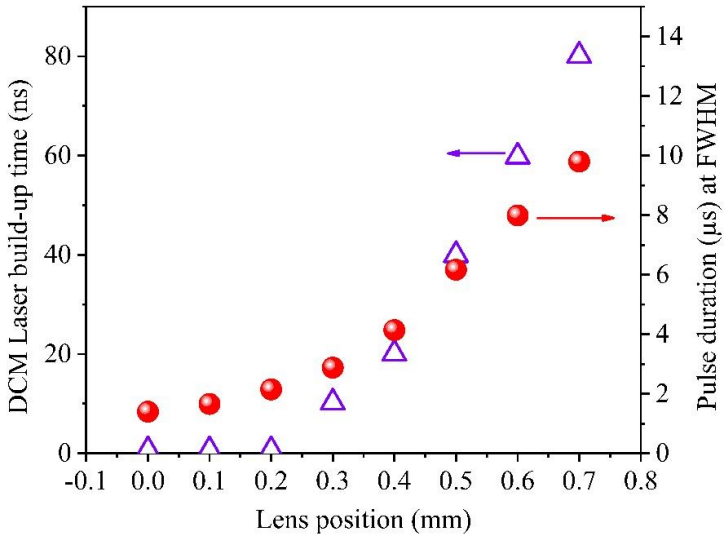

Figure 4.7 : Left: Laser build-up time, right: laser pulse duration at FWHM.

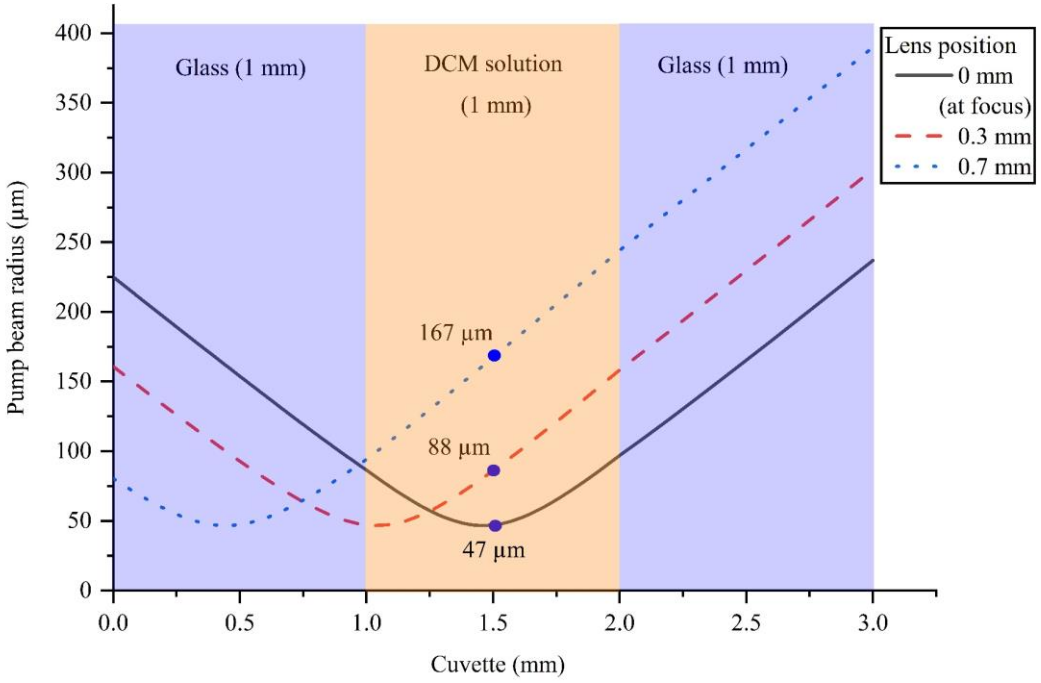

Figure 4.8: Simulation of pump beam (M^2 = 72) propagation inside cuvette when focused on the middle of the cuvette using 35 mm lens and when the focusing lens was moved 0.3 mm and 0.7 mm backward from initial position.

estimated the pump power density to be 11.7 kW/cm^2 when the lens moved to and 0.7 mm. It is also seen that the focus of the pump beam completely shifted to the 1 mm glass from DCM solution when lens was moved to 0.7 mm. However, during pump defocusing process, a decrease in laser intensity (Figure 4.6) at the same time increase in laser build-up time from 0.7 ns to 80 ns (Figure 4.7) are also observed. The shortest build-up time also indicates that the pump beam was tightly focused on the cuvette. The increase in laser build-up time and decrease in laser intensity during pump defocusing can be explained from low pump power density compared to the focused case.

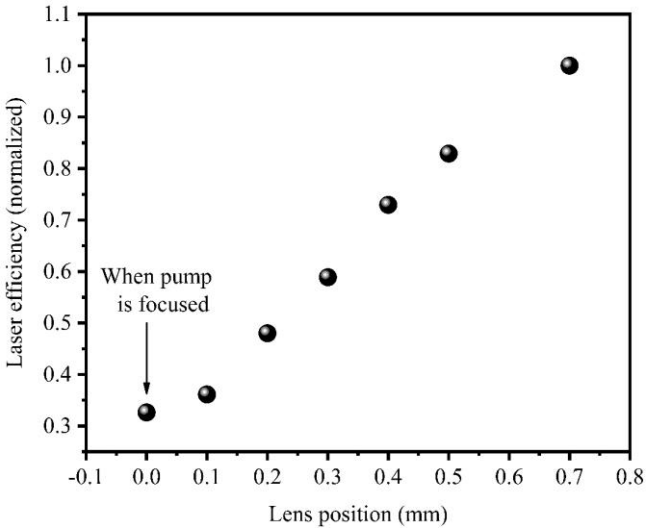

Figure 4.9: Laser efficiency (normalized) calculated from the laser pulse energy at FWHM.

Interestingly, laser efficiency increased when pump was defocused as shown in Figure 4.9. Here, laser

efficiency is calculated from the area of laser pulse at FWHM from Figure 4.6. The efficiency is the lowest when pump is focused onto the cuvette, since laser pulse duration is also the shortest in such pumping condition. Highest laser efficiency was extracted from maximum laser pulse duration (10 µs at FWHM) which happened when pump was defocused on the cuvette by moving the lens 0.7 mm away from its position to focus pump on cuvette. Before showing in detail what happens to laser efficiency and threshold as a result of pump focusing and defocusing on cuvette, we were interested to check whether the laser behavior obtained in Figure 4.6 is not unique to DCM. In this regard, we repeated the experiment of Figure 4.6 with Coumarin dye solution. Spectroscopic properties (Molar concentration, absorption at Pump wavelength) of Coumarin- 540 solution was similar to DCM and has already been given in chapter 2. Interestingly, we obtained similar behavior – increase in laser pulse duration when

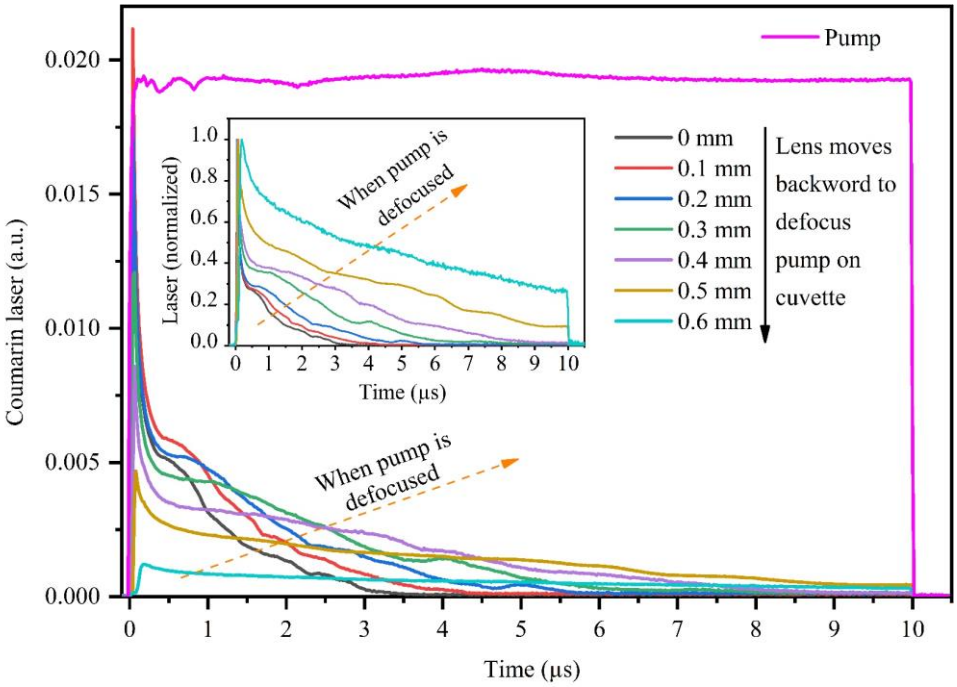

Figure 4.10: Coumarin laser pulse duration when 10 µs long pump is focused on the cuvette. The lens position in this case is defined as 0 mm. Then the lens is moved backward direction (e.g., away from cuvette) up to 0.6 mm with 0.1 mm step and laser pulse duration is plotted at each 0.1 mm lens displacement.

pump beam was defocused on cuvette with Coumarin also. The result is given in Figure 4.10. For a better view, normalized temporal profiles are also depicted at the inset of Figure 4.10. Note that, experiment with coumarin dye is shown here only for comparison and will not be investigated further.

4.2.1. Laser threshold and efficiency when pump is focused and defocused on cuvette

Here we will show in detail what happens to laser threshold and efficiency when we focus and defocus pump (10 µs) on the gain medium. Though Figure 4.9 provides information about laser efficiency when the pump was defocused by moving lens in one direction, here we will show laser efficiency and threshold by translating the lens in both +z and -z direction.

we designed a long cavity 19.8 cm using 200 mm output coupler as shown in Figure 4.11. Such long cavity was designed not to change cavity mode (on cuvette) significantly during cuvette translation

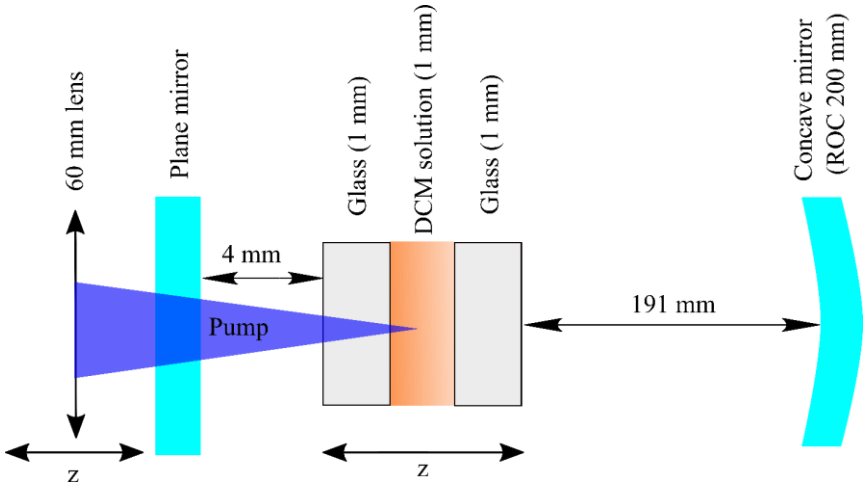

Figure 4.11: Plano-concave laser cavity to investigate laser efficiency and threshold when cuvette or lens moves away from focus.

while laser efficiency largely depends on mode matching between pump and cavity mode as already discussed. Another modification made in current experiment was that we used a 60 mm lens instead of 35 mm to focus the pump (Figure 4.5) to have an efficient mode matching between pump (86 ± 2 µm in radius as shown in Figure 2.3) and cavity (88 µm in radius) mode which is very necessary to compare laser efficiency and threshold between a mode matched and mismatched case. Laser efficiency and threshold as a function of lens position is shown Figure 4.12. It is seen here that laser threshold is the minimum when the lens focused pump at the middle of the cuvette. Similar threshold behavior was found when we moved the cuvette (not shown here) few mm before and after focus. This lowest threshold is just another meaning of the shortest laser build-up time observed in Figure 4.6 when pump was focused at the middle of cuvette. As soon as the lens was moved from 0 position, laser threshold started to increase because of low pump power resulting from increased pump area. However, to

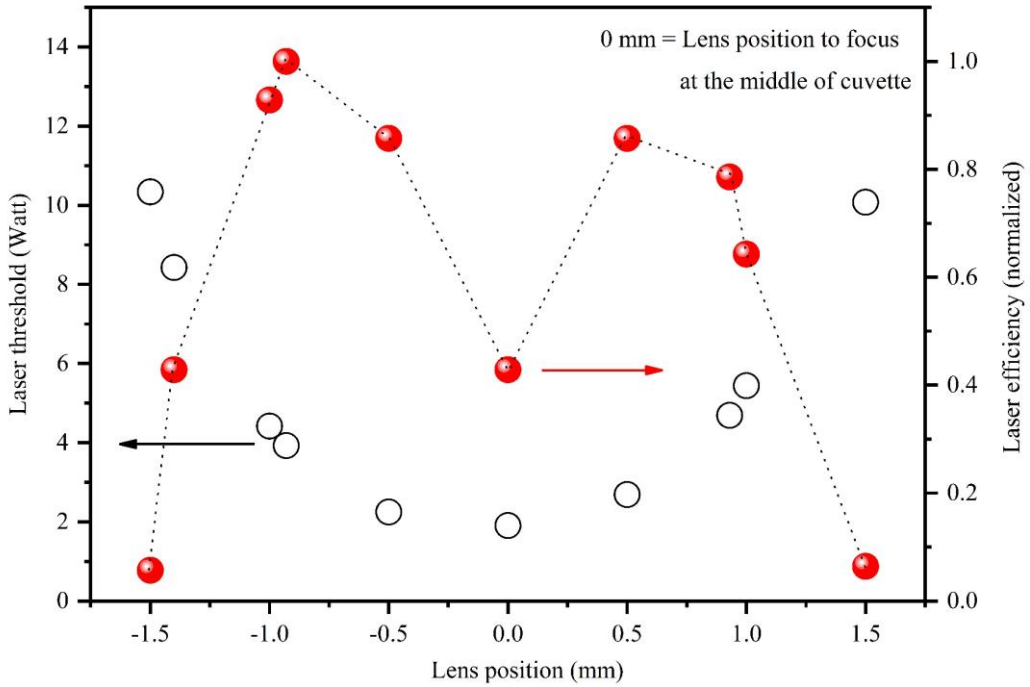

Figure 4.12: Laser threshold (left y axis) and efficiency (right y axis) as a function of lens position.

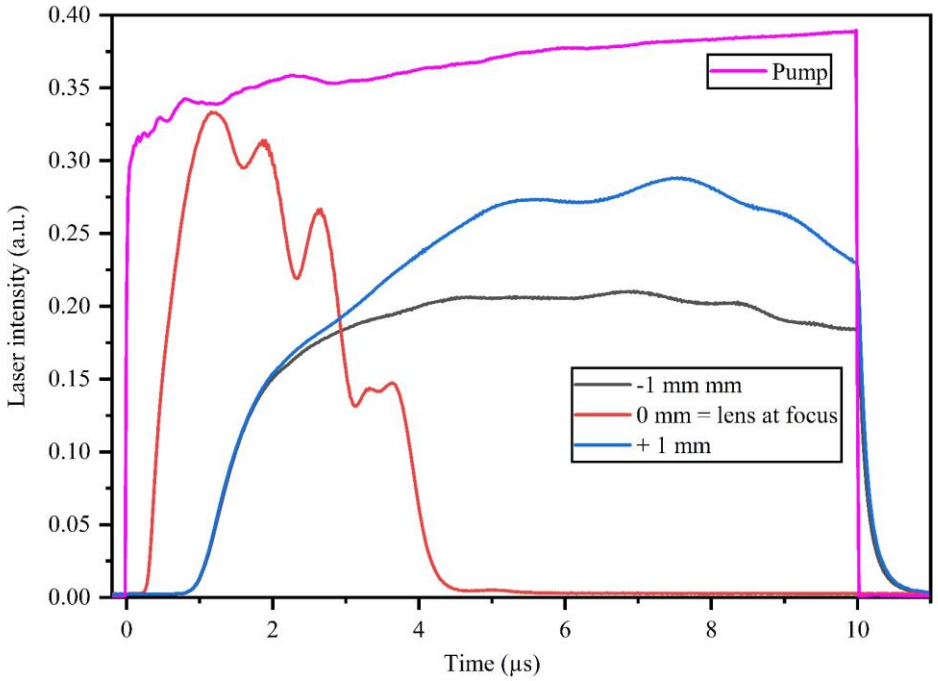

Figure 4.13 : Laser temporal profile when the lens was placed at focus and moved 1 mm forward or backward from lens focal plane.

understand laser efficiency observed in Figure 4.12 let's concentrate on Figure 4.14. It shows that two things happen in a mode matched laser cavity when pump is defocused on cuvette – a) spatial overlap

between pump and cavity mode gradually becomes less efficient and b) pulse duration or laser energy per pulse also increases as already shown before and here in Figure 4.13. Since laser efficiency depends

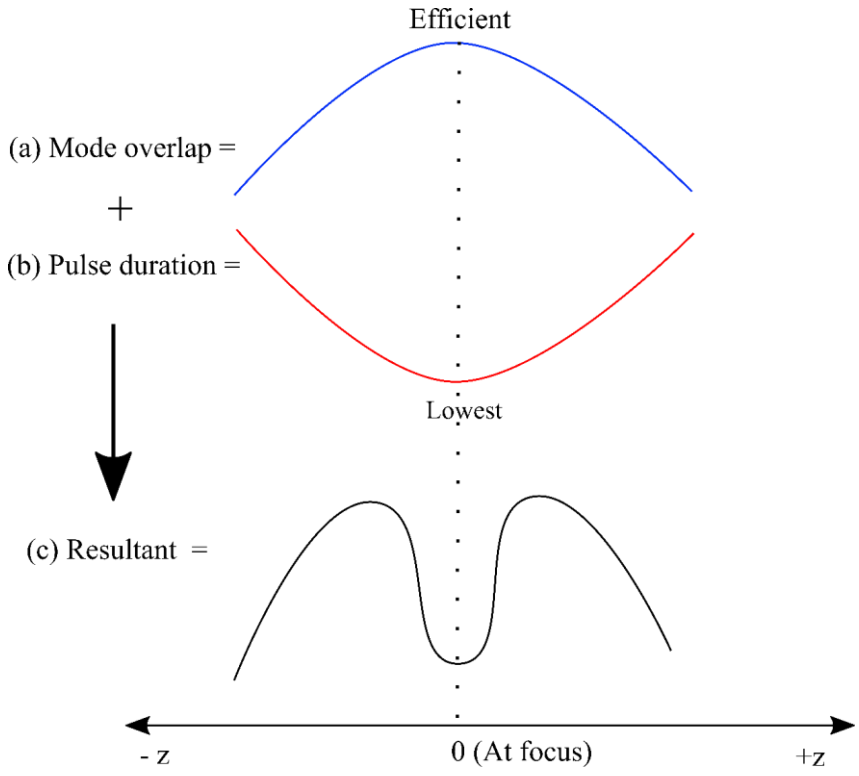

Figure 4.14: A schematic to show that in a mode matched laser cavity, mode overlap becomes less efficient when pump size is increased through defocusing the pump on cuvette. On the contrary, experiments showed that laser pulse duration increases when pump is defocused on cuvette. Since optical efficiency of laser depends on both mode overlap and pulse energy, laser efficiency as a function of pump focusing or defocusing may look like the resultant.

on both mode overlap and pulse energy, the resultant of those two effects may result such efficiency pattern in Figure 4.12. To clarify, when cuvette is at focus, the shortest laser pulse duration results the lowest efficiency even if the mode matching is perfect. As soon as the pump is defocused by moving the focusing lens up to around 0.5 - 1 mm, laser pulse duration becomes as long as the pump and hence laser efficiency becomes maximum. Probably, such amount of defocusing does not disturb mode-matching significantly. But, when the pump is defocused more, laser pulse duration does not have the room to increase more, and mode-matching becomes the key factor to decrease laser efficiency which is observed in Figure 4.12.

However, the efficiency plot also indicates that it might not be optimum to tightly focus at the middle of cuvette. Because laser pulse duration became as long as the pump (10 µs) when the pump was slightly defocused. 10 µs lasing is rare in organic laser without using any triplet quencher or solution flow

system. Therefore, it triggered the interest to understand why long pulse lasing became favorable when pump was just defocused on cuvette.

4.2.2. Investigation of dye laser pulse duration under different pumping strategy (focused and defocused)

As already stated before, we did not completely understand why dye laser pulse duration is longer when pump is defocused. But in this section, we will present our efforts and possible directions to understand that issue.

Indeed, few things happen when pump is defocused on gain medium-

a) thermal load is reduced on gain medium along with the reduction of unwanted excited state phenomena e.g., singlet excited state absorption which is detrimental for having long pulses in organic laser.

b) mode-matching between pump and cavity mode is disturbed which favors the multimode operation of a laser as already discussed at the beginning of this chapter.

To check if reducing thermal load on gain medium can increase laser pulse duration, we just reduced

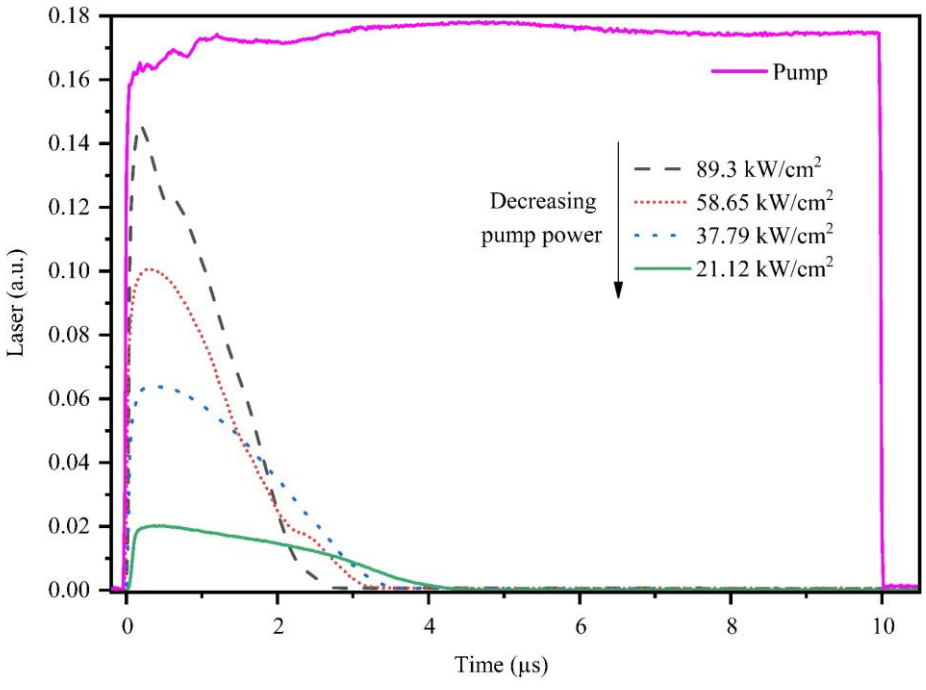

Figure 4.15: Laser temporal profile for different pump (10 μs) power densities (kW/cm^2).

pump power from 89.3 kW/cm^2 to 21 kW/cm^2 by fixing the lens at a specific position (0 mm: as shown in Figure 4.6). This resulted an increase in laser pulse duration from 1.3 µs to 2.7 µs respectively with a sacrifice of significant drop of laser peak power as shown in Figure 4.15.

In clear contrast, using similar pump power densities obtained through defocusing pump in Figure 4.6, we achieved around 10 µs lasing without significant drop in laser peak power. The difference in laser pulse duration when reducing pump power densities in two different ways mentioned above is shown in Figure 4.16. Here, it is seen that the tendency of increasing laser pulse duration is more significant when pump power densities are decreased by increasing pump size compared to just decreasing pump power by lowering diode current. For instance, at around 20 kW/cm^2 power density obtained through pump defocusing up to 0.5 mm (Figure 4.6) lens position resulting a pump radius around 125 µm (calculated from similar simulation shown in Figure 4.8), the laser pulse duration was just above 6 µs. As a clear contrast, laser pulse duration was only 2.7 µs at same pump power density obtained by reducing diode currents when the diode beam was focused to a 60 µm (in radius) spot on cuvette. To have a better insight of this issue, we used different pump sizes on cuvette but maintained similar pump power densities in other word same thermal load and excited state phenomena on gain medium. In this case, laser pulse duration was the longest and as well as the peak power was the highest for the largest pump size used. This is shown in Figure 4.17 but difference in the pulse duration (FWHM) is shown separately in Figure 4.18. This figure shows that despite using similar pump power density, laser pulse duration increased from 5.9 µs to 8.9 µs when pump radius was increased from 125 µm to 167 µm respectively. The results of Figure 4.15 - Figure 4.18 proved that only reduction of thermal load or ESA on gain medium cannot explain 10 µs operation of liquid dye laser but pump and cavity beam sizes should also be considered to explain it. Indeed, in above experiments the longest laser pulse was obtained when pump mode was significantly larger than cavity mode reaching a condition for multimode lasing.

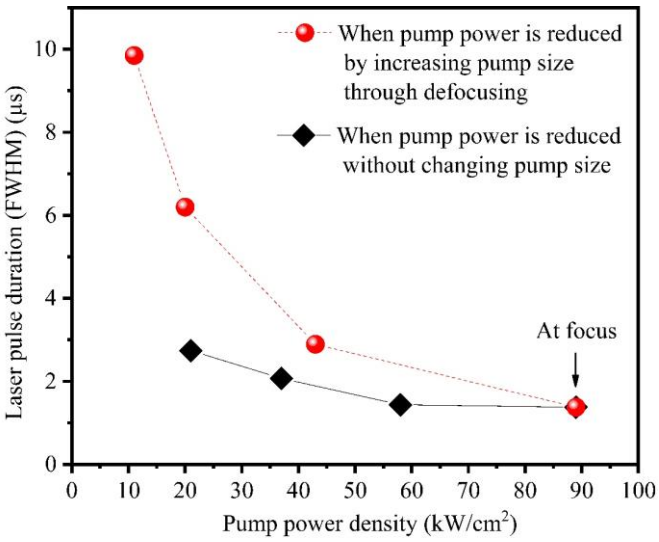

Figure 4.16 : Impact on laser pulse duration when pump power is reduced by increasing pump size and when pump power is reduced without changing pump size.

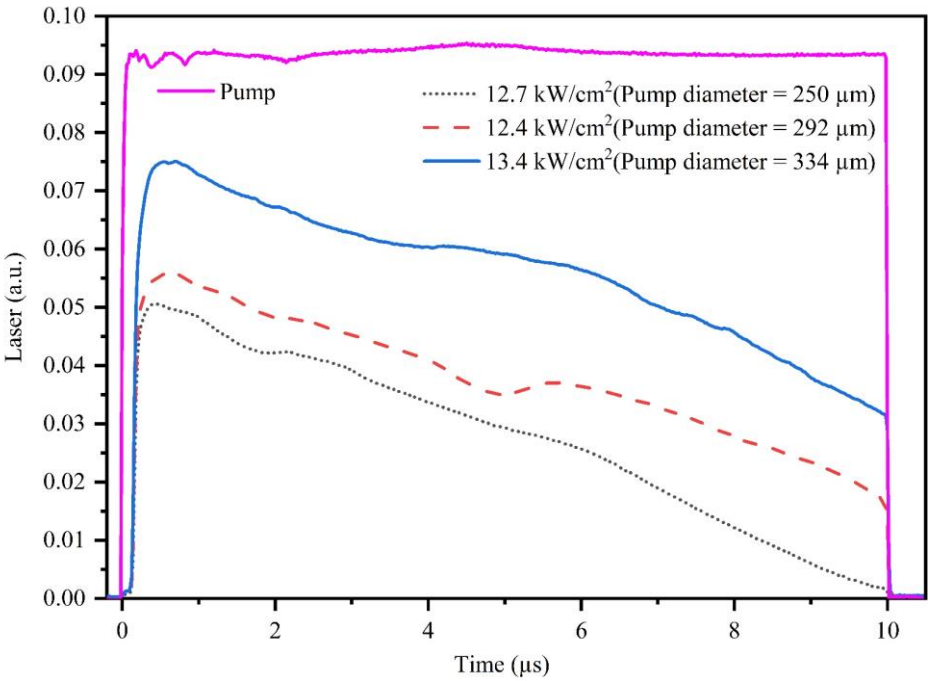

Figure 4.17 : Laser temporal profile for different pump (10 µs) radii but similar power density.

.

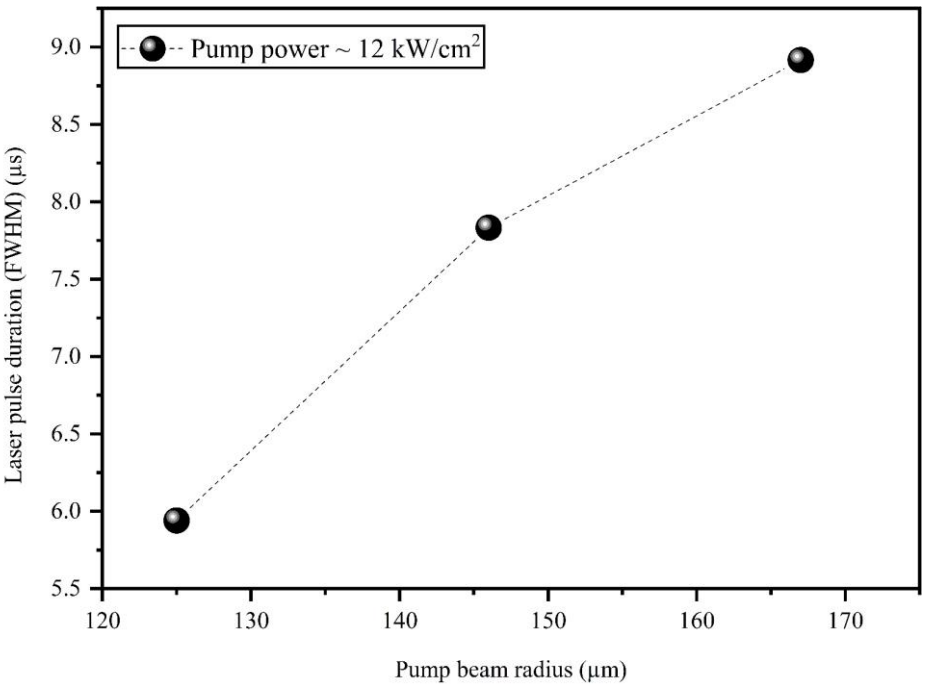

Figure 4.18: Laser pulse duration (FWHM) as a function of pump beam radius at similar pump power density ~ 12 kW/cm^2.

Therefore, there remains a high probability that 10 µs or longer pulse lasing is only favorable in a Plano-concave cavity liquid organic laser when minimum thermal load or ESA on gain medium and multimode laser operation can be achieved simultaneously. This possibility is investigated in the following where we kept the cuvette in the path of defocused pump as shown in Figure 4.19. In this way the thermal load

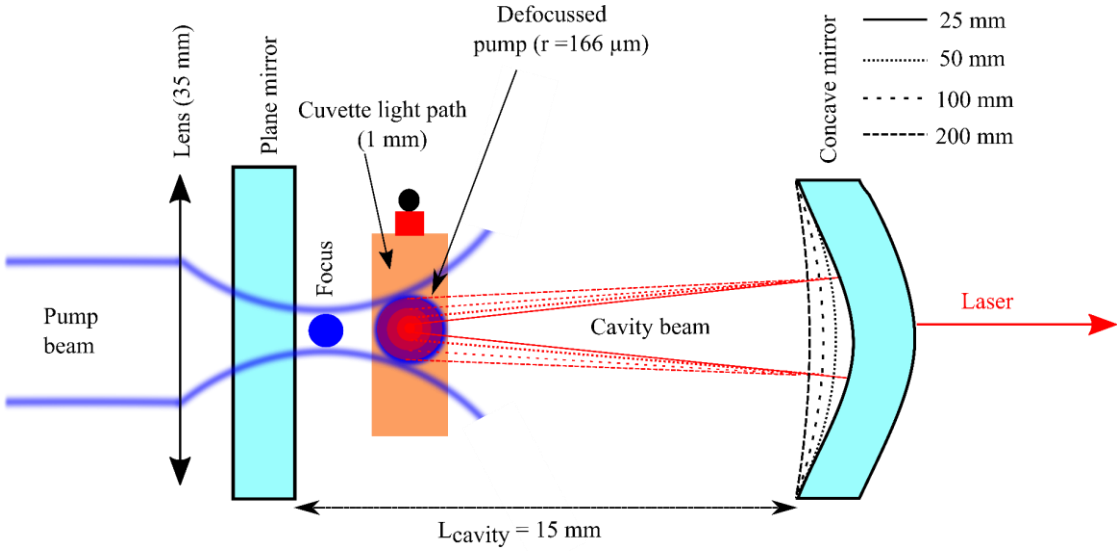

Figure 4.19: Schematic of experimental set up consisting of a Plano-concave laser cavity having L_{cavity}=15 mm. The cuvette is placed close to the plane mirror after the focus of 35 mm lens to make large pump area which is fixed (pump radius = 166 µm) in this experiment. Different radii of curvature output couplers (with same reflectivity) are used to vary cavity beam sizes to match or mismatch with the pump area.

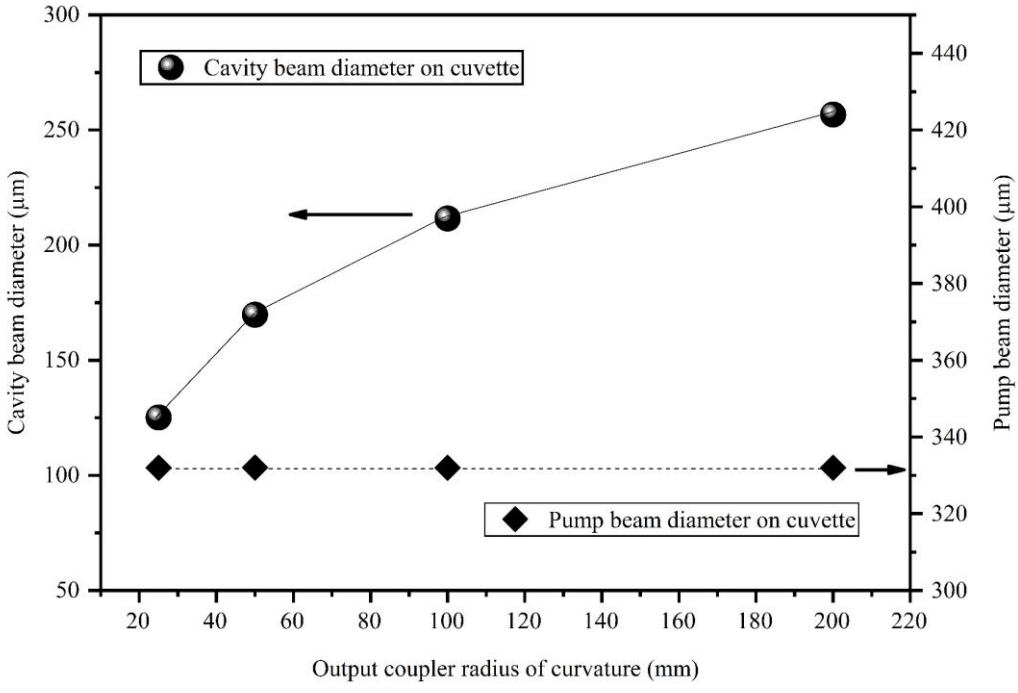

Figure 4.20: Cavity beam radii on cuvette (left y axis) and mode matching ratio between pump and cavity mode (right y axis) as a function of radius of curvature of output coupler (concave mirror).

load was kept low on the cuvette. This defocused pump diameter (332 µm) was chosen based on previous experiment of Figure 4.6 where the pump beam diameter was simulated to be 334 µm (Figure 4.8) when

the focusing lens was moved up to 0.7 mm. However, to fulfill the second condition of achieving multimode lasing, we choose 25 mm output coupler which created 125 µm (in diameter) (in a fixed length cavity) cavity mode radius on the cuvette resulting a mode matching ratio around 37% as shown in Figure 4.20. Using pump power (approximately 12 kW/cm^2) and this cavity configuration we obtained lasing as long as the pump (10 µs) as shown in Figure 4.21. M^2 of this laser was measured to be 1.95 verifying it to be a multimode laser. Then to compare the pulse duration of this multimode laser with pulse duration of single transverse laser using same pump power density (thermal load) and cavity configuration, we used several output couplers i.e. 50 mm, 100 mm and 200 mm (Figure 4.19). In this way, we increased fundamental (TEM_{00}) cavity mode sizes on cuvette (Figure 4.20) hence achieved better mode matching as shown in Figure 4.20 compared to the case when we used 25 mm output coupler. The result of changing output coupler ROC was straightforward as can be seen in Figure 4.21 – "10 µs operation from a multimode laser using 25 mm mirror was sacrificed in the process of obtaining a diffraction limited single transverse mode laser using 200 mm mirror." For a diffraction limited (M^2 = 1.08) laser using 200 mm output coupler, peak power was found to be the highest compared to others. However, as the pulse energy was also the lowest it does not render the maximum efficiency even if

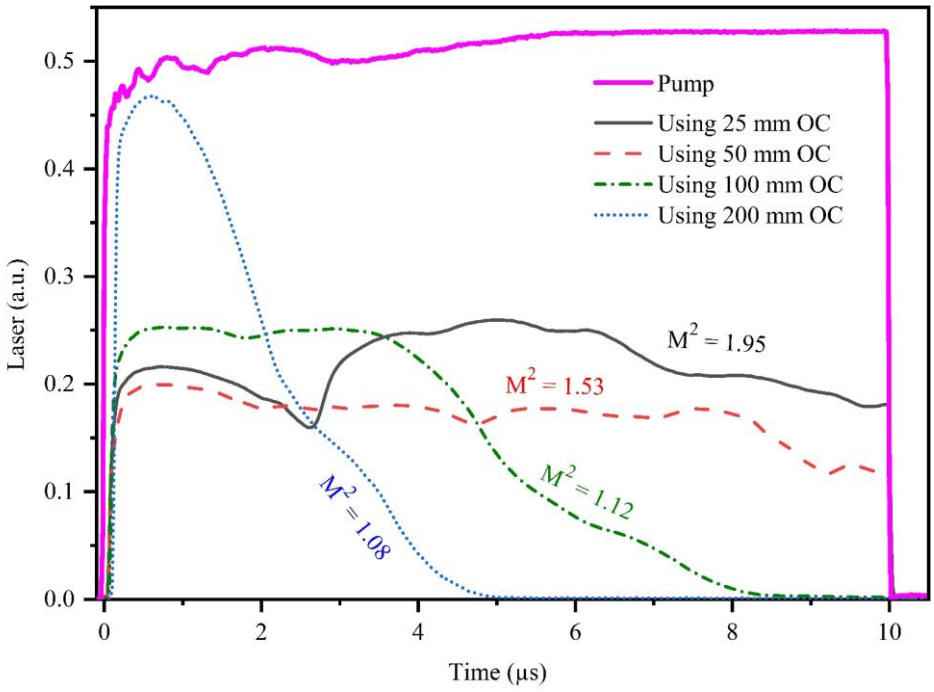

Figure 4.21: Laser temporal profile using different ROC output couplers in a 15 mm Plano-concave laser cavity. M^2 values of those lasers have been given to show the difference between pulse duration of a multimode and diffraction limited laser.

the beam originated from mode matched laser cavity. This phenomenon has already been discussed in Figure 4.12.

The plot of beam radius vs camera position after lens to extract the value of M^2 of those lasers using different ROC output couplers are shown in Figure 4.22 (a - d). Here the highest value of $M^2 \sim 1.95$ (for

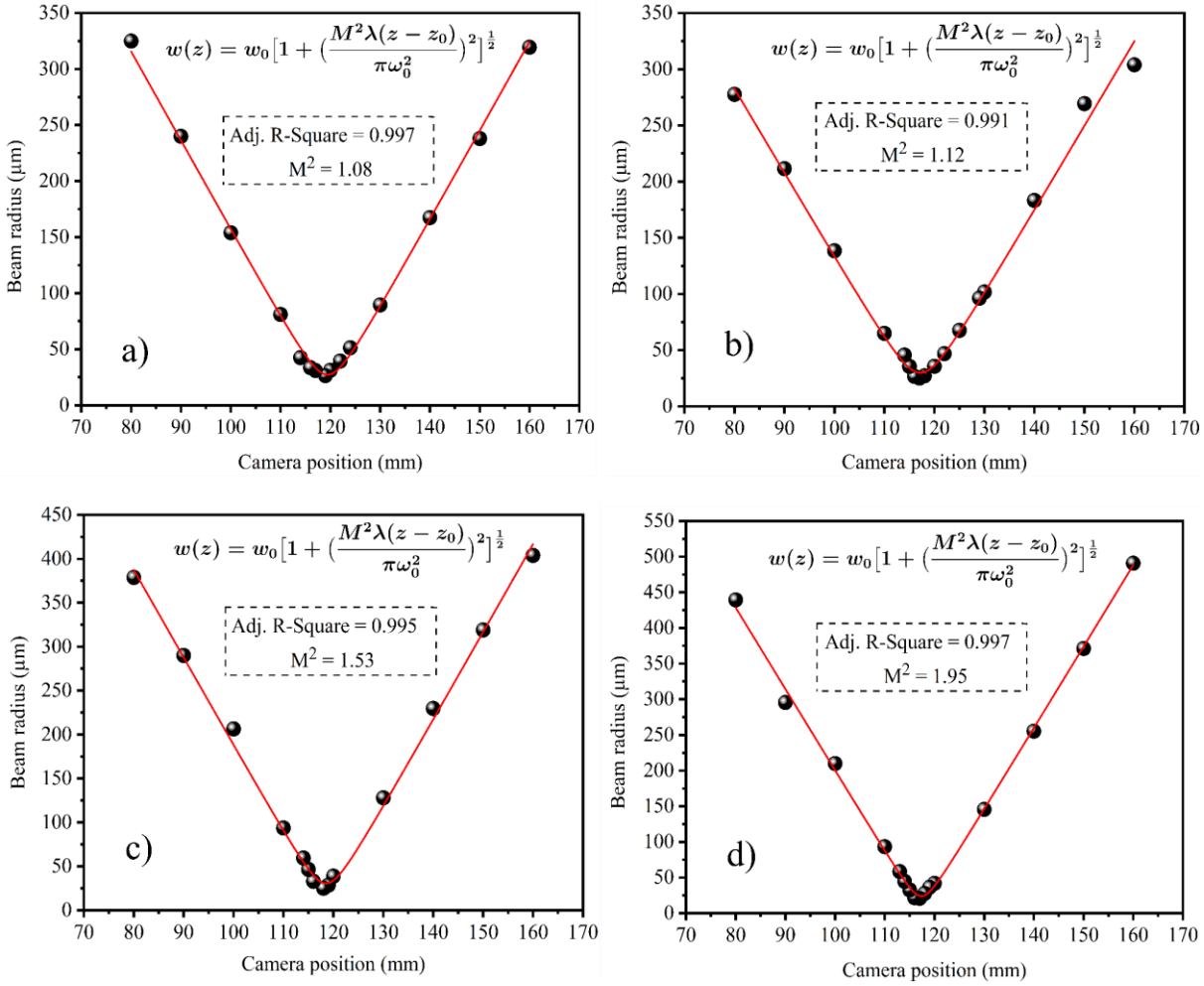

Figure 4.22 : M^2 of laser beam generated in a Plano-concave laser cavity (Figure 4.19) using different radius of curvature output coupler mirrors: a) 25 mm, b) 50 mm, c) 100 mm, d) 200 mm.

a mode mismatched cavity) approached to 1 when we increased cavity mode size by using different radius of curvature mirrors to match the size of pump beam. Interestingly, a related experiment with multimode laser having $M^2 > 3$ showed that when we blocked few transverse modes to further oscillate in the laser cavity, the laser M^2 decreased with a decrease in laser pulse duration. A Hemispherical laser cavity designed for this experiment is shown in Figure 4.23 where we see that a razor blade can be translated across the cavity axis. Such laser cavity can produce very small cavity mode when the gain medium is kept close to the plane mirror which is already discussed in chapter 2. Therefore, a multimode laser is expected since pump was defocused on cuvette to ensure a larger pump mode compared to the cavity mode.

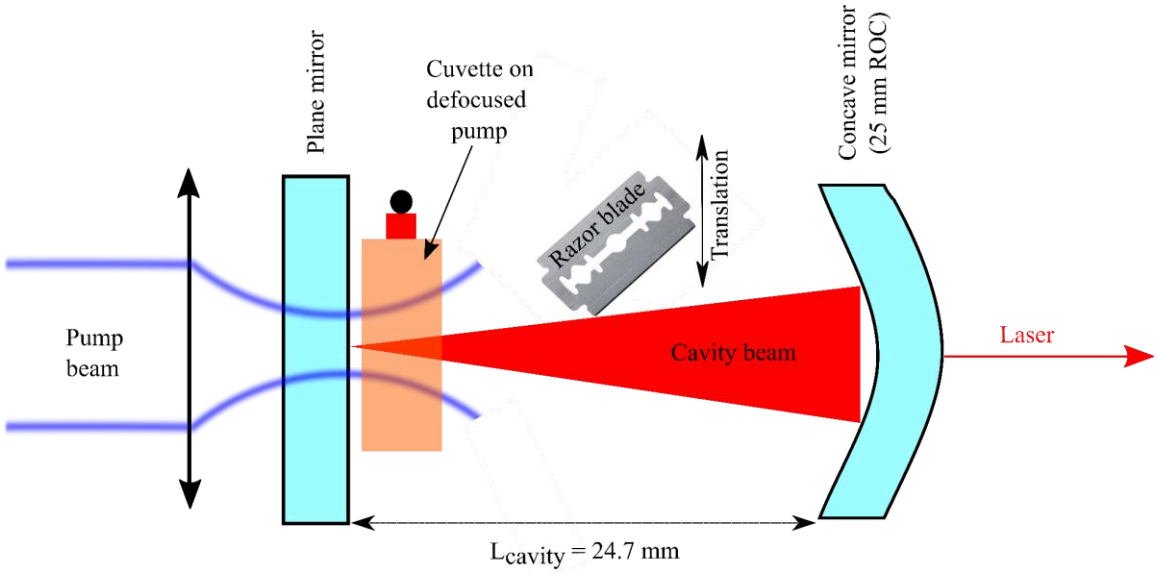

Figure 4.23: Experiment to block transverse laser modes by translation of razor blade across a near hemispherical laser cavity.

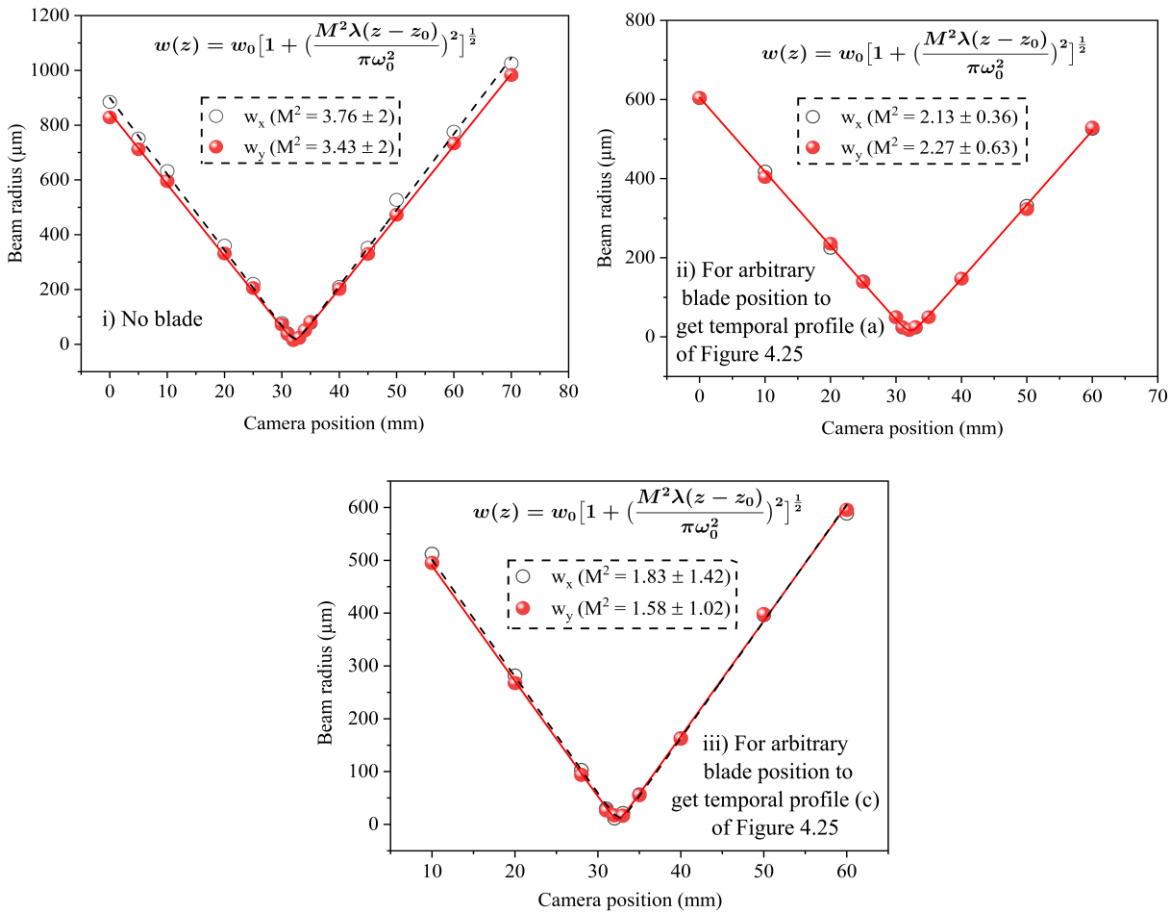

Figure 4.24: a) M^2 of a multimode laser, b) M^2 of laser when razor blade was in an arbitrary position to get temporal profile (a) of Figure 4.25 and c) M^2 of laser beam when razor blade was in another arbitrary position to get (c) of Figure 4.25.

$M^2 > 3$ of this laser is shown in Figure 4.24 (a) confirming it to be highly multimode. But when we start to translate the razor blade across the laser beam, laser M^2 was approaching towards unity (Figure 4.24 (b) – (c)) confirming that a portion of transverse modes were blocked. Interestingly, the laser pulse duration also started to decrease when the transverse modes were blocked. Laser temporal dynamics

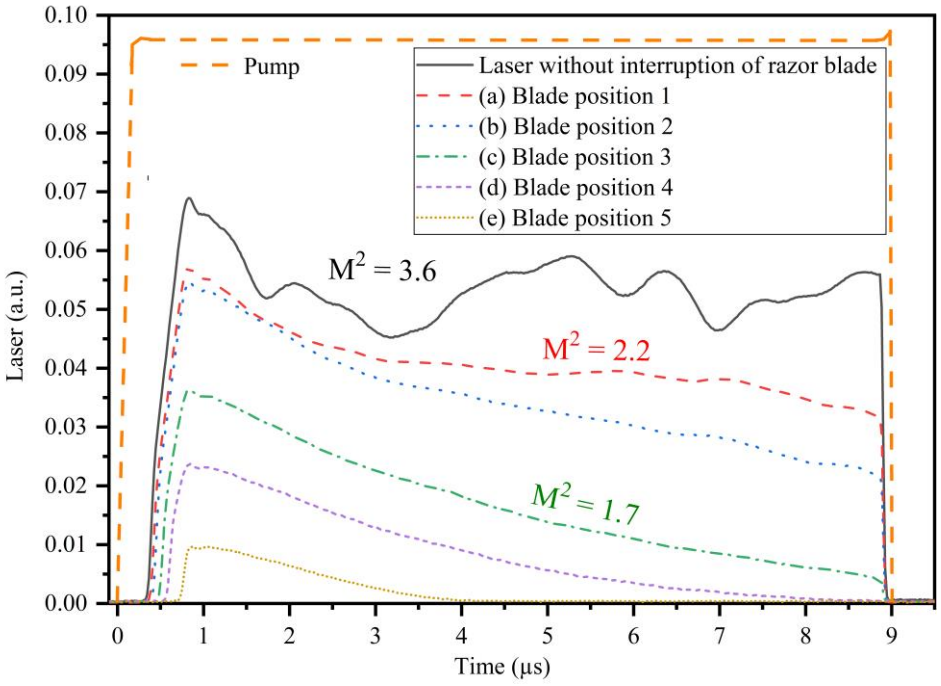

Figure 4.25: Pulse duration of a highly multimode laser (M^2>3) follows pump (9 μs) pulse. When transverse laser modes are blocked gradually by translating a razor blade across the laser beam, laser intensity and pulse duration also decreased with an improvement of M^2 value. The values of M^2 have been used from Figure 4.24.

is shown in Figure 4.25. Several things can be interpreted from this experiment. Introducing the razor blade across the cavity beam causes high losses for higher order laser modes but also creates moderate but still higher losses for low order modes. This explains why M^2 is decreases and at the same time build up time increases. At same extent, if we admit that pushing razor blade more starts to add losses for TEM_{00}, this can explain the pulse shortening according to the experiment shown in chapter 1. Still, no reason was found explain the long pulse operation of a multimode laser.

However, Figure 4.21 or Figure 4.25 does not indicate a lasing limit which interested us to investigate the longest pulse duration achievable in above discussed method. Unfortunately, our laser diode driver (PCO-7141, ENERGY INC.) was limited to produce longer than 10 μs pulse from laser diodes as already stated before. Therefore, we employed a new laser diode driver (Figure 4.26) to pump our cuvette with longer than 10 μs pulse. For this experiment, we used the same near hemispherical laser cavity with 25 mm output coupler (shown in Figure 4.23). In this case, we achieved up to 80 μs lasing as shown in Figure 4.27. In this experiment, pump pulse duration was increased from 20 μs – 80 μs keeping pump

power fixed still, we observed decrease in laser intensity but laser pulse duration was as long as pump duration in all the cases. As stated before, we could not go to the details of the experiment performed

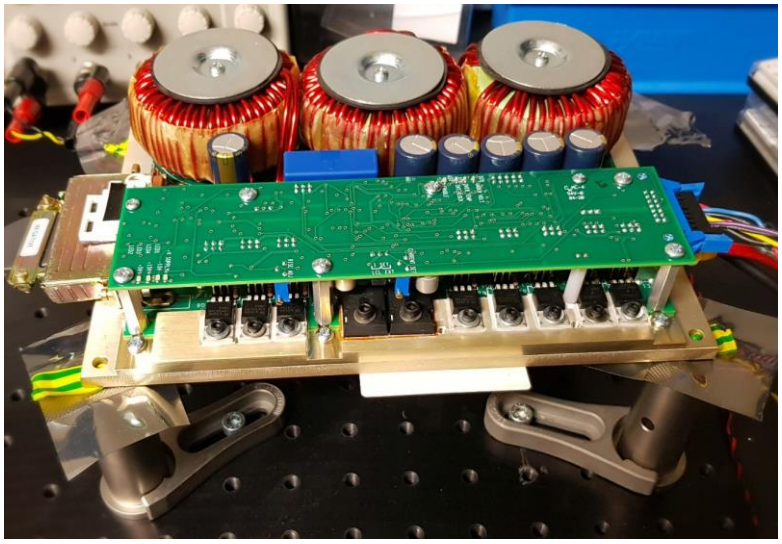

Figure 4.26 : Laser diode driver (PCO 6131, DIRECTED ENERGY INC) which can drive diode lasers <100 ns to CW.

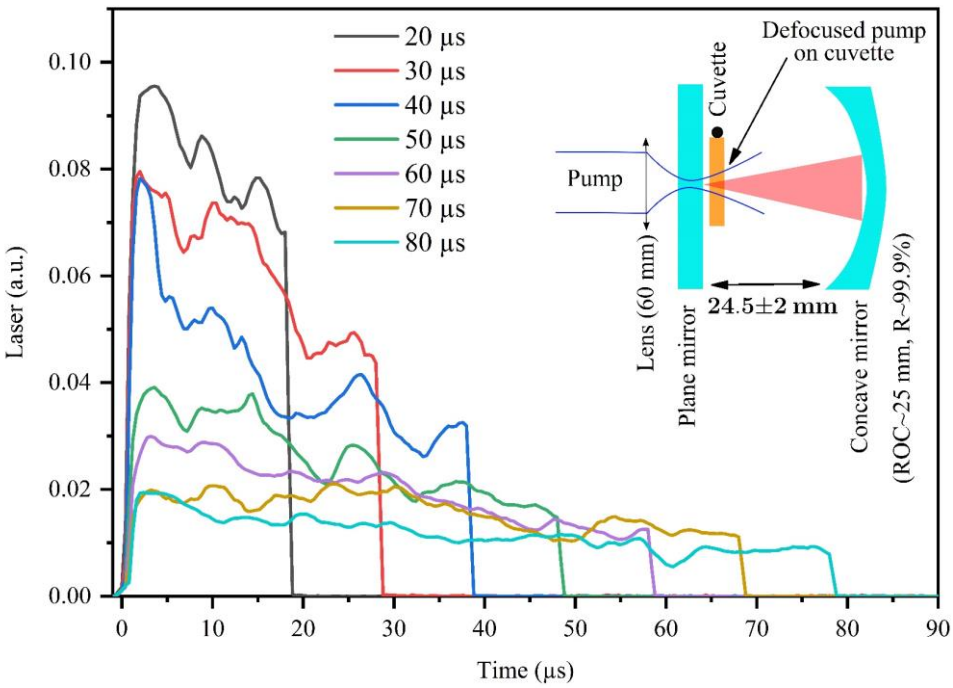

Figure 4.27 : Laser temporal behavior when pumped with long pulses (20 µs – 80 µs).

with this new driver due to time constraint. But it can be investigated in future when we will employ this driver for mode-locking experiments. However, a similarity visible in the laser temporal profiles of

Figure 4.27, Figure 4.25 and also in Figure 4.21 is wave like patterns especially when the laser was multimode. We are going to investigate this issue in the following.

4.2.3. An unusual observation in laser temporal profile

We observed wave like patterns in laser temporal profiles of Figure 4.27, Figure 4.13 and also in Figure 4.21. Although stochastic pulse instabilities of liquid dye laser have been reported in literatures [82–85], those wavy patterns in our case were not just instantaneous fluctuations which could occur due to e.g. thermal perturbation in the laser medium. In fact, they were persistent in laser profile since those profiles were recorded through averaging over 512 pulses at 10 Hz repetition rates. Therefore, we wanted to understand that phenomenon. However, current cavity configuration having the cuvette parallel to the cavity mirrors would complicate the situation due to Vernier Effects as already discussed before. Therefore, we redesigned our cavity placing the cuvette at Brewster angle. In this situation, the longitudinal mode distribution is more simple and does not contain sub cavity filtering effects as already discussed in chapter 1 (Figure 2.15 - Figure 2.18). Following that, we focused pump (5 µs) on the cuvette using 60 mm lens to create 88 µm (in radius) pump spot. We choose 25 mm output coupler mirror to create a cavity mode around 45 µm (in radius) on cuvette in a 24 mm long Plano-concave cavity. In this case we obtained lasing as long as the pump duration (Figure 4.29 (a)) with a multimode behavior of the laser beam (we measured its $M^2 = 4.2$). Similar result was also obtained in the experiment of Figure 4.23 using similar cavity geometry. The difference is, here we observe several dips in the laser temporal profile as can be seen in Figure 4.29 (a) which were probably smoothened in Figure 4.23 due to Vernier Effect.

We thought those dips in laser temporal profile might be related to transverse modes in a multimode laser. To investigate that we blocked few transverse modes by translating a razor blade across cavity beam as explained in Figure 4.23. By doing so, we let just one deep to exist in the laser temporal profile (Figure 4.29 (b)) which would simplify the situation for the following experiment we are going to discuss. However, this is already one indication that those dips in temporal profile are related to higher order transverse modes. It is also interesting to observe

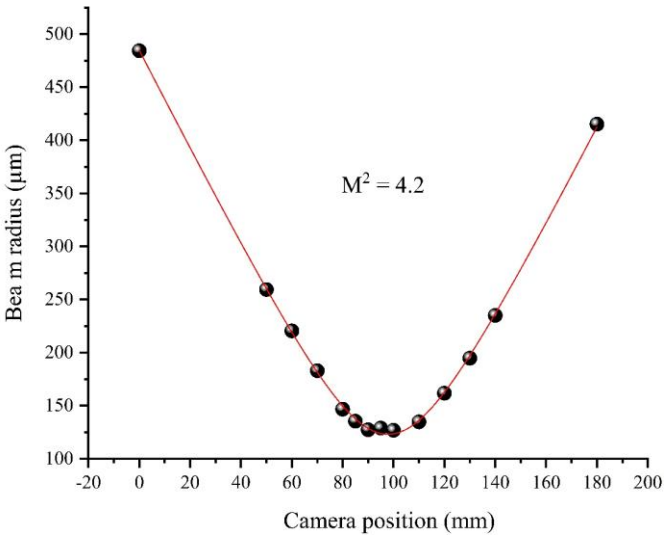

Figure 4.28: M^2 of laser beam generated in a near hemispherical cavity containing cuvette at Brewster angle and enclosed by 25 mm radius of curvature output coupler mirror.

the narrowing of laser spectrum (at FWHM) when we blocked few transverse modes (Figure 4.29 (b)) compared to the spectrum of a multimode laser (Figure 4.29 (a)).

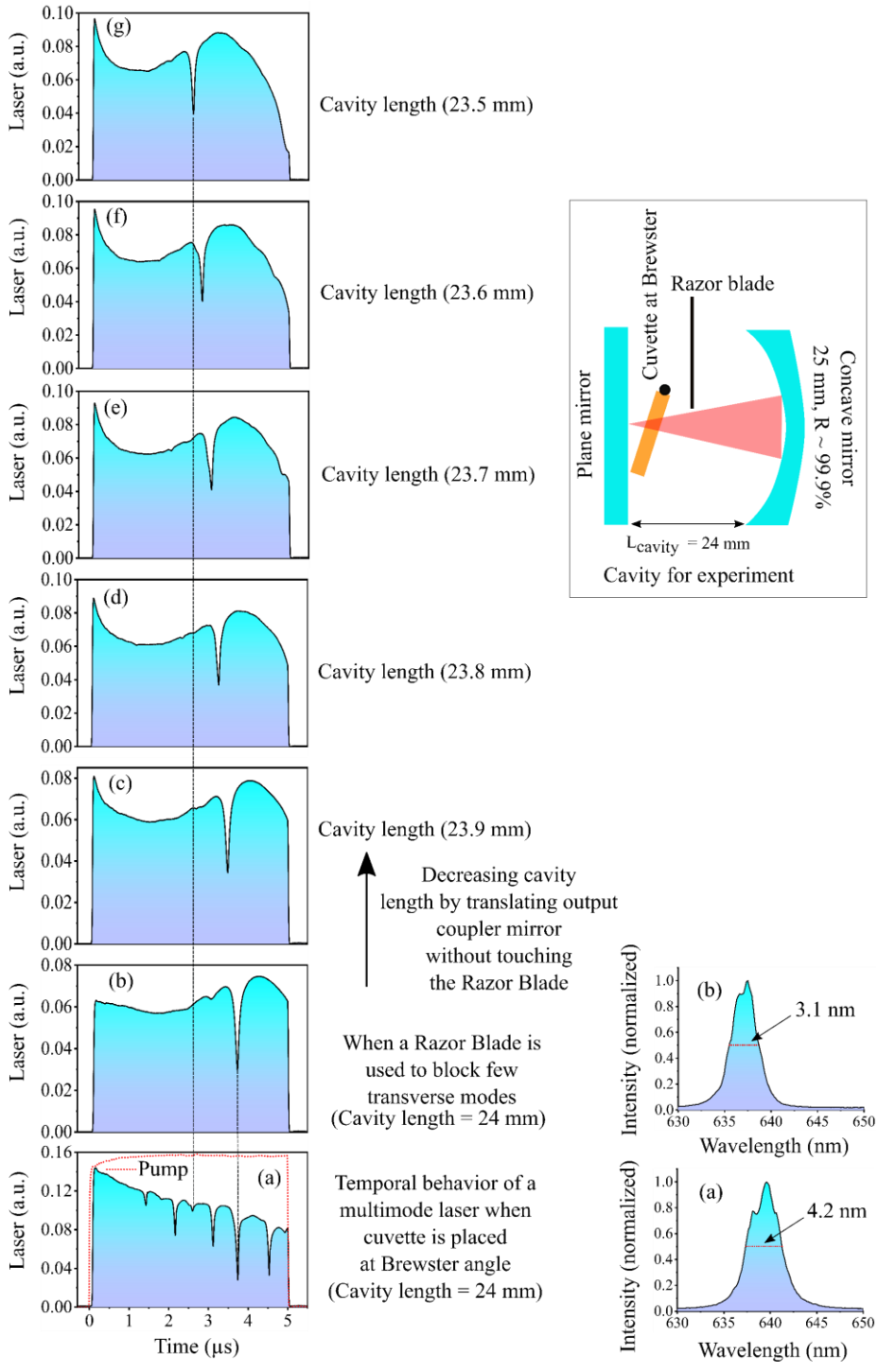

Figure 4.29 : (a) Temporal behavior along with spectrum of a multimode laser, (b) when a razor blade is used to block few transverse modes. (c) – (g): Laser temporal profiles when cavity length is decreased by translating the 25 mm concave mirror towards plane mirror without moving the razor blade. Pump duration used for this experiment was 5 μs.

Another interesting observation was that, when we reduced the cavity length by translating the output coupler mirror up to 0.5 mm with 0.1 mm step, a shift of the deep was also visible (after each step of translation) in Figure 4.29 (c - g). After a reduction of 0.5 mm in cavity length, the deep in the temporal profile was found at 2.6 µs which was originally at 3.7 µs before decreasing cavity length. Such decrease in cavity length (Figure 4.29 (c - g)) either indicates the usual characteristics of our laser cavity that decreasing cavity length would increase came with a shortening of its pulse duration which agrees with our previous findings (Figure 4.6). However, the shift of dip was also observed when we increased the cavity length by same amount. As expected, this time the deep shifted in opposite direction (Figure 4.30) compared to previous case in Figure 4.29 (c - g). In Figure 4.30, a clear increase in laser build-up time proves the effect of increasing cavity length. This time the laser pulse duration remained as long as the pump for each increased cavity length along with slightly low intensity due to same reason in opposite sense as discussed in case of decreasing cavity length.

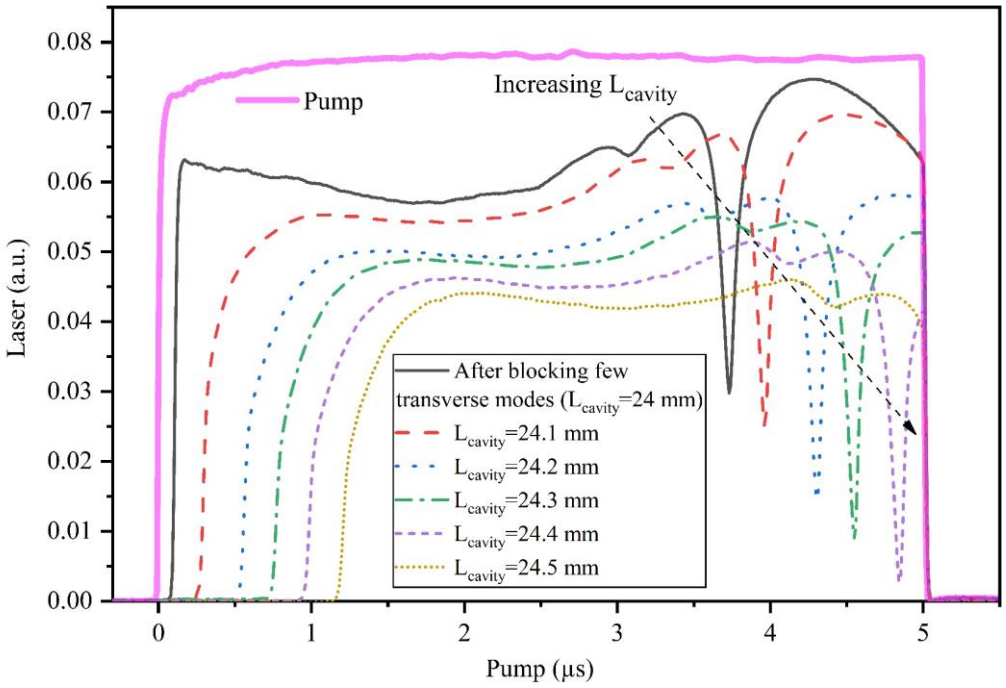

Figure 4.30: Temporal behavior of a multimode laser when increasing the cavity length by translating output coupler mirror.

One question still remains regarding the origin or formation process of those dips. In this regard we can say that those deeps may result from the beating of transverse and longitudinal modes in a multimode laser [86]. The frequency spacing of longitudinal modes (FSR $= \frac{C}{2L}$) of our 24 mm laser cavity is in the range of GHz whereas from Figure 4.29 (a), it can be estimated that the spacing between the dips is in MHz regime which eliminate the possibility of beating between only longitudinal modes to explain this

scenario. However, according to [86], the resonant frequency of a two mirror laser cavity can be written as,

$$\upsilon_{qmn} = \frac{C}{2L}[q + (m + n + 1)\, f(L)] \tag{4.1}$$

Where, q = longitudinal mode number, m and n are transverse mode numbers which can take the values of 0, 1, 2,.. as briefly discussed at the beginning of this chapter and f (L) is the Gouy phase shift for a stable laser cavity which can be written here as,

$$f(L) = \frac{1}{\pi}\cos^{-1}\sqrt{(1-\frac{L}{R_1})(1-\frac{L}{R_2})} \tag{4.2}$$

For a Plano-concave ideal hemispherical cavity where $R_1 = \infty$ and $R_2 = L$ that leads to f (L) = $\frac{1}{2}$. This value of f(L) creates equal possibility for a hemispherical cavity to show mode degeneracy like the case of a confocal laser cavity ($R_1 = R_2 = L$). To give more insight, let us calculate the transverse mode frequency for TEM_{00} and TEM_{01} mode in our near Hemispherical laser cavity (considering f (L) = $\frac{1}{2}$) according to (4.1) and (4.2).

$$\text{For } TEM_{q00}, \qquad \upsilon_{q00} = \frac{C}{2L}[q + (m + n + 1)f(L)] = \frac{c}{2L}[q + f(L)] \tag{4.3}$$

$$\text{For } TEM_{q01}, \qquad \upsilon_{q01} = \frac{C}{2L}[q + (m + n + 1)f(L)] = \frac{c}{2L}[q + 2f(L)] \tag{4.4}$$

Therefore, the separation between TEM_{00} and TEM_{01} becomes,

$$\Delta\upsilon = \upsilon_{01} - \upsilon_{00} = \frac{c}{4L} \tag{4.5}$$

Similarly, the separation between TEM_{00} and TEM_{10} modes is also $\frac{c}{4L}$, hence TEM_{10} and TEM_{01} modes are degenerate as shown in the schematic of Figure 4.31. In this figure, longitudinal modes are represented by q, q+1, q+2 and their separation are $\frac{c}{2L}$. The odd symmetry transverse modes (10, 01) (of qth longitudinal mode) are degenerate at $\frac{c}{4L}$ between q and q+1 longitudinal modes [87]. Interestingly, if we perform the same calculation to obtain equation (4.5) for q02 and q20 modes, we

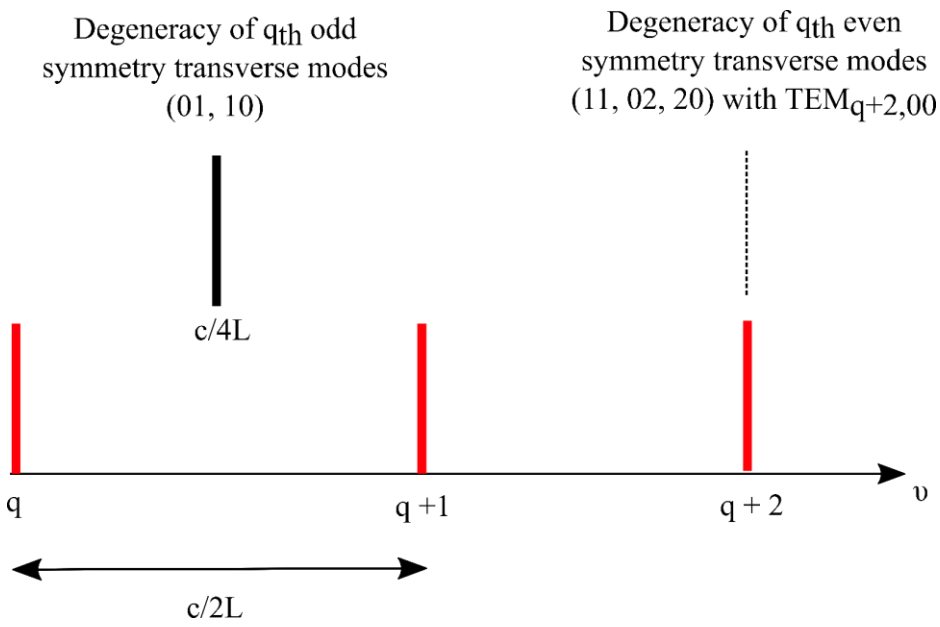

Figure 4.31: Degeneracy of modes in a hemispherical Plano-concave laser cavity.

will find that they are exactly degenerate at q+2,00 mode as also shown in the schematic of Figure 4.31 [87].

However, these calculations are based on the fact that cavity length is equal to the radius of curvature of output coupler in a Plano-concave laser cavity. In our experiment, as one can see in Figure 4.29, this condition is not exactly fulfilled. Therefore, longitudinal and transverse modes are not exactly degenerate but might maintain a close difference in frequency resulting beating with each other. Such explanation can be verified from experiment too. Firstly, We observed shift of deep position (Figure 4.29 and Figure 4.30) corresponding to the change in cavity length which is obvious from equation (4.1). Secondly, in Figure 4.30, when we increased the cavity length hence the cavity configuration was close to fulfill the condition (L_c = Radius of curvature of output coupler) of mode degeneracy, there could be a pure chance that deep was almost vanished from temporal profile. This means that there remains a high possibility that most of the deeps in temporal profile would be vanished when the cavity becomes pure hemispherical and hence the modes are all perfectly degenerate. However, in that case laser build up time is also higher with pulse duration as long as the pump which can be seen in Figure 4.30. This once again indicates that the multimode laser with inefficient mode matching can be a choice to design a long pulse dye laser with no circulation.

Now, to show that what happens to the deeps of laser temporal profile when mode matching becomes efficient, we just changed the radius of curvature of output coupler mirrors to 50 mm and 100 mm. The result can be found in Figure 4.32. Here, for 100 mm output coupler the mode matching was efficient

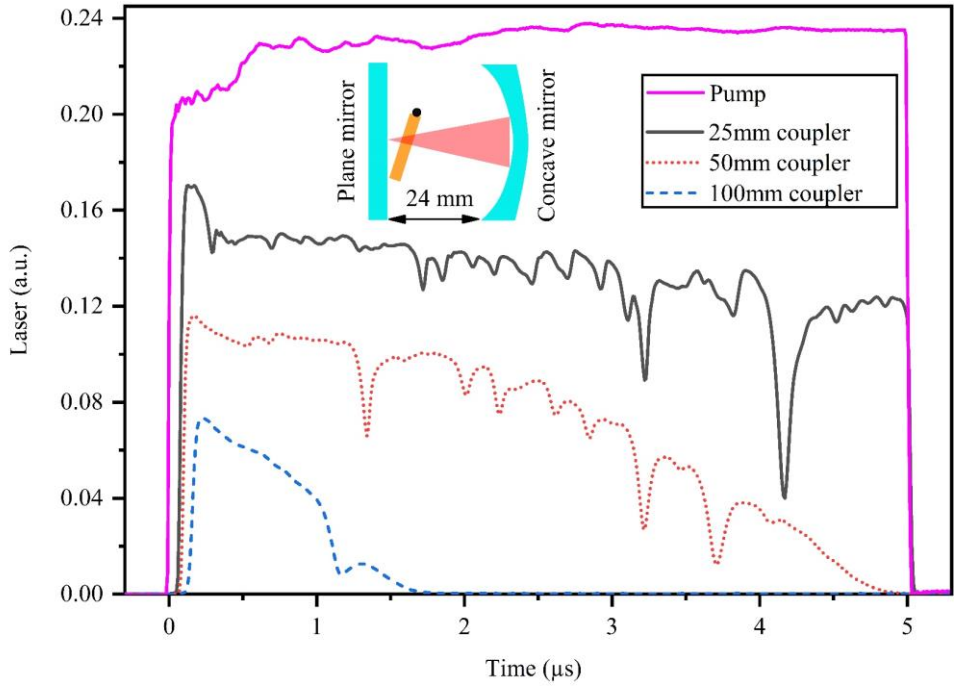

Figure 4.32: Laser temporal behavior when the cuvette is placed at Brewster angle inside a Plano-concave laser cavity. Three different ROC output coupler has been used to vary the spatial mode overlap between pump and cavity beam. The mode overlap is overlap is inefficient when using 25 mm coupler which becomes partially good and efficient for 50 and 100 mm output coupler respectively.

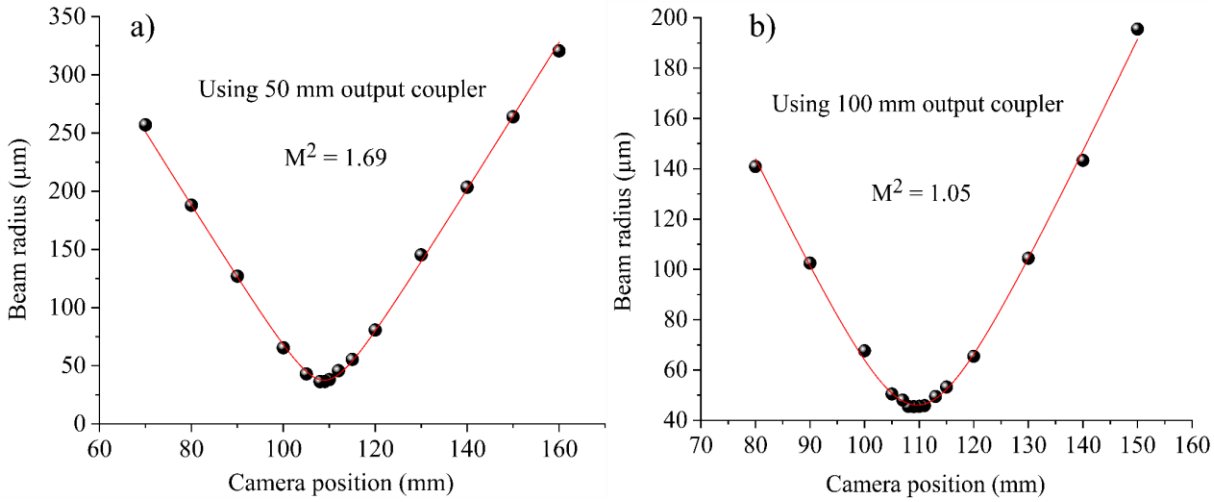

Figure 4.33: Laser beam M^2 using (a) 50 mm and (b) 100 mm output coupler mirror in a 24 mm laser cavity where cuvette was placed at Brewster angle between the two-mirror cavity.

(pump mode 88 μm in radius, cavity mode 95 μm in radius), and the deeps were almost vanished and also the laser pulse was the shortest. Due to efficient mode matching, the laser beam was also diffraction limited TEM_{00} as given in Figure 4.33 (b). In contrary, for 50 mm coupler the mode matching (pump

mode 88 µm in radius, cavity mode 70 µm in radius) was partially good which resulted lasing for slightly longer duration compared to the lasing duration using 100 mm coupler. For this output coupler, the laser beam was also slightly multimode as can be seen said from its $M^2 = 1.69$ (Figure 4.33 (a)). Finally, as expected the longest laser pulse was obtained using 25 mm output coupler for which the mode matching was the most inefficient in a way that favors multimode operation of the laser.

4.3. Conclusion

In conclusion of this chapter, we can say that the longest pulse lasing up to 80 µs is achieved in circulation free liquid dye (DCM) laser. In the process to achieve such long pulse lasing, an interesting physics has been found that circulation free liquid dye laser can produce long pulse when they are highly multimode provided the effects of triplets and thermal are neglected at low pump repetition rate (10 Hz in this case). In this study, we obtained multimode lasing by increasing the pump size on gain medium compared to the cavity beam size by defocusing pump on cuvette. However, during long pulse operation their multimode behavior was confirmed by measuring beam M^2 which was found to be higher than 1. Interestingly, under same pump and cavity configuration when we changed output coupler ROC to match the large pump size in order to improve mode matching or blocked few transverse modes, laser pulse duration started to decrease. In both cases, improved value of M^2 confirmed that the laser was turning towards a single mode operation sacrificing its longer pulse duration. A prefect blocking of higher order laser modes would be possible if we could use a circular aperture able to block all higher order modes except TEM_{00}. That can be a perspective for cleaner demonstration but is not expected to change our findings. Interesting structures were found in the temporal profile of multimode long pulse laser when we placed the cuvette at Brewster angle. From experimental ivestigation, we related those structures to the beating of different transverse modes in a highly multimode laser. However, this might not be enough and hence further study is required to investigate this issue in detail. For instance, in a confocal laser cavity longitudinal and transverse modes become degenerate hence by designing a confocal resonator for similar experiments may rule out or significantly reduce those patterns in temporal profile. Indeed, our work also lacks (due to time constraint) answer to the question “why an organic laser provides long pulse operation only when they are multimode.” In this regard, in addition to theoretical understanding experimental demonstration is also required by studying the temporal dynamics of their transverse modes. Such understanding might be useful for the future perspective of this work towards demonstrating a mode-locked circulation free liquid dye laser.

5. Conclusion of thesis and Future perspectives

5.1. Conclusion

While organic laser community keeps on developing novel lasing materials or improving their ongoing research to fight against photostability issue as well as to unveil long pulse (CW/q-CW) operation of state-of-art organic laser, we have walked slightly off the track to reach the same goal. We investigated a liquid dye (DCM) laser without any circulation tubing under low-cost diode pumping. This kind of laser set-up is comparable to a low cost, compact and user-friendly solid-state dye laser but even simpler to implement skipping all types of fabrication step. Interestingly, such simple laser showed very high photostability up to almost billion (10^9) of pulses at 1 kHz repetition rates. Such stability is almost comparable to older generation liquid dye lasers. Whereas in the same experimental environment (same laser cavity, pump power etc.) a solid-state dye laser using same gain medium showed photostability up to only ~10^4 no. of pulses which is 5 order or magnitude lower than the stability of the circulation-free liquid dye laser. Their high photostability reflects the fact that diffusion or slow convection of dye molecules due to localized heating in the dye solution helps to efficiently replenish them between consecutive pump pulses. This statement can be experimentally verified by measuring their photo-stability at different repetition rates to increase/decrease localized heating inside dye solution which can be a future extension of this work. However, such high photostability of the laser system triggered our interest to also investigate their maximum rate operation since solid-state dye lasers are rarely found to operate at high repetition rate e.g., several kHz mainly due to avoid fast photo degradation. In that regard, we found that, despite showing high photostability, their lasing repetition rate was limited to only 2.4 kHz which could not be explained from their triplet state lifetime. Therefore, we related that limitation to the creation of a thermal lens in the laser medium which tended to destabilize the laser cavity at certain repetition rates. Though thermal lens is aberrative in nature, quadratic part of thermal lens can be corrected by knowing its focal length. To materialize that, we designed a pump probe experiment and measured thermal lens focal lengths for different pump repetition rates. Knowing the static value of thermal lens focal length for 15 kHz pump, we employed a suitable focal length (opposite to the focal length of thermal lens) correction lens inside our Plano-concave laser cavity and obtained up to 14 kHz lasing. To verify if this finding is not unique to DCM laser only, we tested Coumarin-540 laser in the same experimental setup and obtained similar results. In addition, we realized that designing a thermal lens insensitive laser resonator could also result similar performance (in repetition rate) from circulation free liquid dye lasers. In this work, though we proved this principle by designing a near hemispherical laser cavity, a concentric cavity would be the most suitable candidate for that purpose which can also be a future perspective of this work. It would be really interesting to hit the lifetime of triplet state by obtaining higher repetition rate lasing adopting either of above methods to investigate organic laser behavior in that regime. Anyway, these results suggest that thermal lensing of laser medium is the primary barrier for circulation free liquid dye lasers to be operated at high repetition rates.

The final part of this thesis turned to be more interesting when we started to investigate long pulse operation in circulation free liquid dye laser but could not understood the observations completely. We found that the liquid dye laser can produce long pulses up to several tens of µs when it is highly multimode (mixing of TEM_{00}, $TEM_{01,}$ TEM_{10} and so on in laser mode). Usually, our longitudinal pumping scheme results diffraction limited TEM_{00} beam quality, but we switched from this single mode to multimode lasing by making the pump size larger through defocusing pump on the cuvette which lets the possibility open for higher order modes along with fundamental cavity mode to oscillate in the cavity. At first, we thought that such behavior might be resulting from thermal effect and also excited state phenomena (e.g. T-T absorption) when long pump pulse is focused on cvette. Therefore, we reduced thermal load significantly by reducing pump size on gain medium and found that long pulse lasing (10 µs) could only be observed when there was a huge mismatch between pump and cavity mode , a condition achieved using 25 mm ROC output coupler. As soon as the mode matching was improved by using 50 mm, 100 mm and 200 mm output couplers without changing cavity length, the laser pulse duration clearly shortened for same thermal load, hence same excited state phenomena (e.g. T-T absorption). Similar behavior was obtained when we blocked few higher order modes (in not a very quantitative way) by razor blade and observed that the laser pulse duration decreased with an improvement of M^2 the laser beam. In both cases, the pump size was unchanged hence thermal load and excited state phenomena were similar which verifies that the long and short pulse operation was related to the multimode and single transverse mode behavior of the laser, respectively. When the laser was multimode, we observed wavy patterns in a laser temporal profile which turned into fine dips when the cuvette was placed at Brewster angle. It suggested that those patterns did not come out as a result of Vernier effect when cuvette was placed parallel to the cavity mirrors, but they were resulting from the two-mirror cavity. We explained those dips in temporal profile as an outcome of mode beating between transverse and longitudinal modes as the cavity was near hemispherical. In that case, longitudinal and transverse modes should be degenerate but can be slightly shifted in frequency if the cavity is not perfectly hemispherical like the one we had. This was experimentally verified by observing shifts (in position) of those dips in temporal profile during any change in cavity length, hence beat frequency. Although, mode beating could explain the dips in laser temporal profile, we could not understand why a multimode laser can produce lasing in long pulse regime which was up to 80 µs in our case. It will be interesting to investigate the temporal behavior of the transverse modes to understand if their joint contribution can favor long pulse operation in organic lasers.

However, their long pulse operation certainly opens the possibility to investigate their mode-locking regime to demonstrate diode pumped compact, low-cost, user-friendly mode-locked dye lasers. Pathways toward that goal will be given in the following.

5.2. Future perspectives

5.2.1. Introduction

Diode pumped organic lasers have never been mode-locked at the time when this PhD started. Probably, the main reason behind that is the unavailability of long pulse organic lasers at that time while mode-locking is the technique to generate ultrashort pulses (< 1 ns) from an ideally CW or q-CW laser. Since in this thesis we obtained several tens of microsecond operation from them, we want to push our research forward to build a mode-locked ultra-fast organic laser as already mentioned before. Meanwhile we want to clarify that mode-locking has not been obtained during this thesis. But this chapter will give some general guidelines to lighten the path for future mode-locking studies.

Ultra-short pulse (USP) lasers have wide applications in different fields of science and technology. They can produce very high peak power in the order of MW/GW without generating excessive heat on the target. At the beginning, liquid dye lasers were the popular choice to generate USP due to their wide emission spectrum and highly multimode (longitudinal) characteristics. However, gradually they lost popularity owing to their complex design with solution flow system and also for their expensive pump sources. Therefore, soon after the invention of Ti:S crystal which has wider emission spectrum compared to liquid dye laser became state-of-art for generating ultra-short pulses. Recently, more solid-state materials are found to routinely generate ultra-short pulses [88–92] with comparable performance to Ti:S lasers. Being solid-state, these materials eliminate the solution handling issues related to the liquid dye laser. With the advent of high power diode lasers, diode pumped USP lasers have successfully reduced the cost of mode-locked laser system [93–98]. A step further in compactness of laser system has been achieved through the demonstration of mode-locked VECSELS [99].

Despite above achievements in solid-state mode locked lasers, they cannot completely replace liquid dye lasers. Because all solid-state mode locked lasers are found to lase in the near infrared and hence unable to cover the spectral range between 400 nm – 700 nm [100]. Though their second or third harmonic can reach few specific wavelengths in visible, still cannot cover the full visible wavelengths. However, above spectral range is demanding in the field of spectroscopy, medicine, isotope separation and so on. Historically dye lasers have been the key player to fulfill those demands. Moreover, they also show wide tunability over visible spectrum. Another problem associated with solid-state mode locked laser especially with Ti:S crystal is its high cost as well as the complex mode locking technique based on Kerr lens which is very sensitive to mechanical perturbations [100]. For above reasons, a diode pumped circulation free liquid dye laser can be very attractive to build future low cost, compact, simple, user friendly and tunable mode-locked sources.

5.3. Mode-locking

We have already briefed about longitudinal modes of a laser cavity. Indeed, a laser may have millions of those modes dancing in the cavity at different frequencies with no specific phase relation among them. If by some external means one can establish a fixed phase relationship between the longitudinal modes, a train of ultrashort pulses separated by cavity round trip time ($\frac{2L}{c}$) will come out of the laser Cavity as shown in Figure [101].

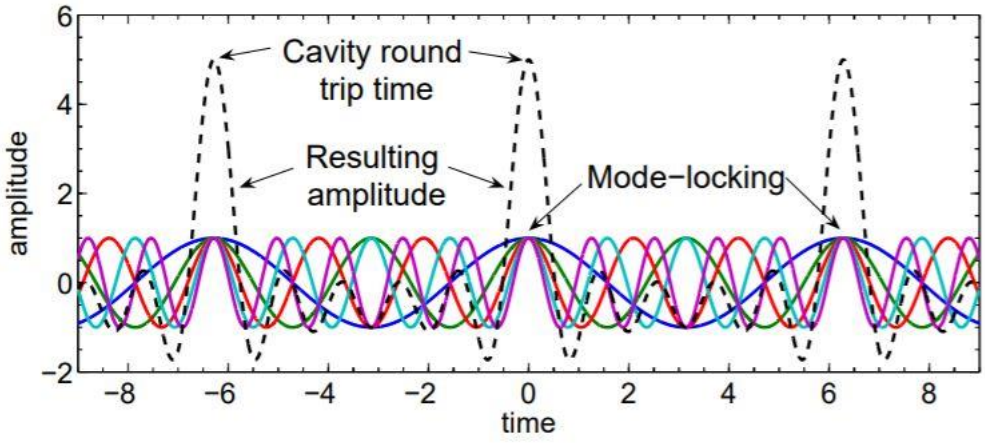

Figure 5.1: Mode-locking technique to produce ultrashort pulses by establishing a fixed phase relationship among the modes in the cavity. All waves of different frequencies interfere at time an interval equal to the cavity round trip time and produce a short burst of intense light.

There exist active and passive techniques to establish a fixed phase relationship between longitudinal modes. In active mode locking technique, acousto optics or electro optics modulators are used to periodically modulate the cavity losses at a repetition rate (c/2L) equal to the cavity round trip time. In that case, one needs to insert an acousto optic or electro optic modulator inside laser cavity which cannot be a considered as a suitable technique for mode locking in our case. Because we are obliged to keep our cavity short (several mm - cm) since the cavity length imposes adverse effects on laser efficiency in a pulsed laser as already discussed in the first chapter. In fact, this mode locking technique is used in true CW solid-state laser (e.g., Nd:Yag). Therefore, we want to adopt passive mode locking technique where a saturable absorber is used inside laser cavity which acts as a high loss for lower intensity light but becomes transparent for high intensity pulses that able to saturate the absorber. In the following, we will discuss the limited progress made during this thesis to build a future mode locked organic laser.

5.3.1. Advancement towards future mode-locking

Demonstration of few tens of microsecond long pulses from organic laser in previous chapter can be considered a step forward towards the goal to obtain mode-locking. Because the buildup of mode-

locking requires time to complete several round trips in a laser cavity. For a passively mode locked Ti:S laser with 1.75 m long laser cavity, mode locking build-up time was calculated to be 60 µs [102]. Therefore, it can be expected to be much shorter when a cm sized cavity would be involved. For example, in a 15 cm VECSEL, the mode-locking (ps pulses) was observed after 1000 round trips indicating the mode locking build up time was around 1 µs (since 1 ns is required to complete 1 round trip ($\frac{2L}{c}$) in a 15 cm cavity). It clearly verifies the fact that why organic laser with several hundreds of ns pulse duration had never been investigated for mode-locking and at the same time suggests that it cannot not be a wild dream anymore to hope for a mode locked organic laser provided that their lasing duration is found to be longer than 1 µs and we can easily make more than 15 cm cavity (Figure 4.11). Although, several issues need to be understood regarding their long pulse operation which will be dealt prior to future mode-locking experiment. However, here we want to mention our preference regarding the SA we want to use for passive mode-locking.

5.3.1.1. Selection of appropriate saturable absorber and further characterization

- **Issues considered prior to choose saturable absorber**

Early era of femtosecond pulse generation in a liquid dye laser routinely used a dye saturable absorber called DODCI [103]. The performance of that saturable absorber despite having a slow recovery time in the order of ns was quite good to mode-lock CW liquid dye lasers having quite long cavity length (meters). However, to mode-lock a pulsed dye laser like the one we have with cavity length in the range between mm to cm, those saturable absorbers are not suitable anymore. Because in short cavities the round trip time is shorter than the recovery time of those saturable absorbers. Therefore, a saturable absorber having recovery time in the range of ps would be suitable for our work.

Semiconductor Saturable Absorber Mirror (SESAM) with fast recovery time developed during the 90's by U. Keller [104,105] would be a perfect candidate for this. Apart from fast recovery time, other optical characteristics of SESAM for instance a low saturation fluence and weak non-saturable losses, high modulation depth, have made them state-of-art to mode-lock laser sources [99,106–108] for example vertical external cavity lasers (VECSELs). However, their operation bandwidth or absorption band in other word is found to cover the infrared part of the spectrum due lattice-matching issues (except few examples of deep red-operating SESAM using GaInP/AlGaInP [109–111], but currently the rest of the visible spectrum cannot be covered).

- **Proposed SA to be used for building our mode-locking laser**

Not a long time back from now, high quality monolayer (single atomic layer) graphene [112] has flourished the market hence opened the door for many research applications [113]. Well established companies e.g.,

Graphenea (in spain) have mastered the technology to produce monolayer high quality graphene films which can be transferred on any desired surface without the need of any special skill. Interestingly 1cm×1cm monolayer film of graphene can be found in ~100$. Apart from their low cost, this material possesses interesting optical properties such as ultrafast recovery time (ps or less) which makes them suitable for mode-locking [114–117] or q-switching [118] laser sources, easy integration with solution-process techniques (graphene flakes can be inserted into polymer layers for example). More importantly, graphene shows absorption properties from visible to infrared band of the spectrum [113]. All those properties of graphene fulfill the requirement of the SA we are looking for.

- **Graphene characterization**

We bought monolayer (easily transferrable) graphene from Graphenea (https://www.graphenea.com/) and transferred it on a cavity mirror (HT at 445 nm and HR at 590 nm – 632 nm) to use it directly in mode-locking laser cavity. The procedure is presented in Figure taken from Graphenea website. The graphene was supplied to us on top of a polymer and the film was covered by a sacrificial layer as shown

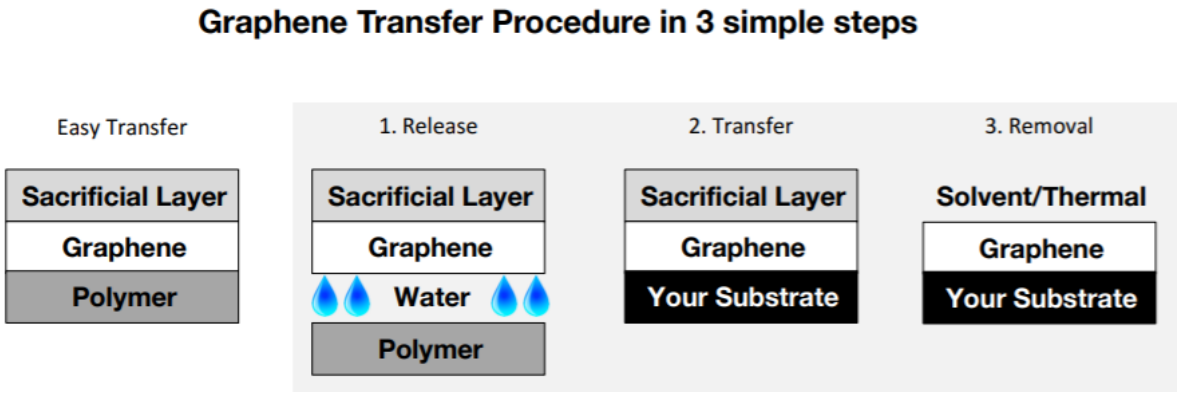

Figure 5.2: Graphene transfer procedure from polymer to a desired substrate (https://www.graphenea.com/).

in the most left picture. To transfer it on a desired surface (cavity mirror in our case), we followed the first step by putting the graphene in de-ionized. Within seconds, the graphene with sacrificial layer was detached from the polymer and we placed our mirror inside water to fish the floating graphene film from below. After that the mirror containing graphene (and sacrificial layer) was kept in open air for 30 minutes which was followed by 1h of annealing in an oven under 150°C temperature. Before removing the sacrificial layer, which was still present, the graphene coated mirror was kept 24h in a vacuum chamber for better attachment to the surface. Finally, the sacrificial layer was removed by an acetone bath for 1 hour followed by another bath in isopropanol for another 1h. This procedure removes the sacrificial layer. It is recommended to use a blow of N_2 gas to make it dry before using. Following graphene transfer on mirror it was necessary to verify if the graphene was monolayer since saturation

intensity would be higher if the number of layer increases. We verified that using Raman Spectroscopy facility of another lab named 'Laboratoire des Sciences des Procédés des Matériaux' (LSPM) of our university - thanks to LSPM for its kind co-operation. Indeed, Raman spectroscopy provides information on the vibrational modes of molecules, and is frequently used to obtain the structural fingerprints of molecules, but it has also been used to determine graphene layer numbers in flakes [119].

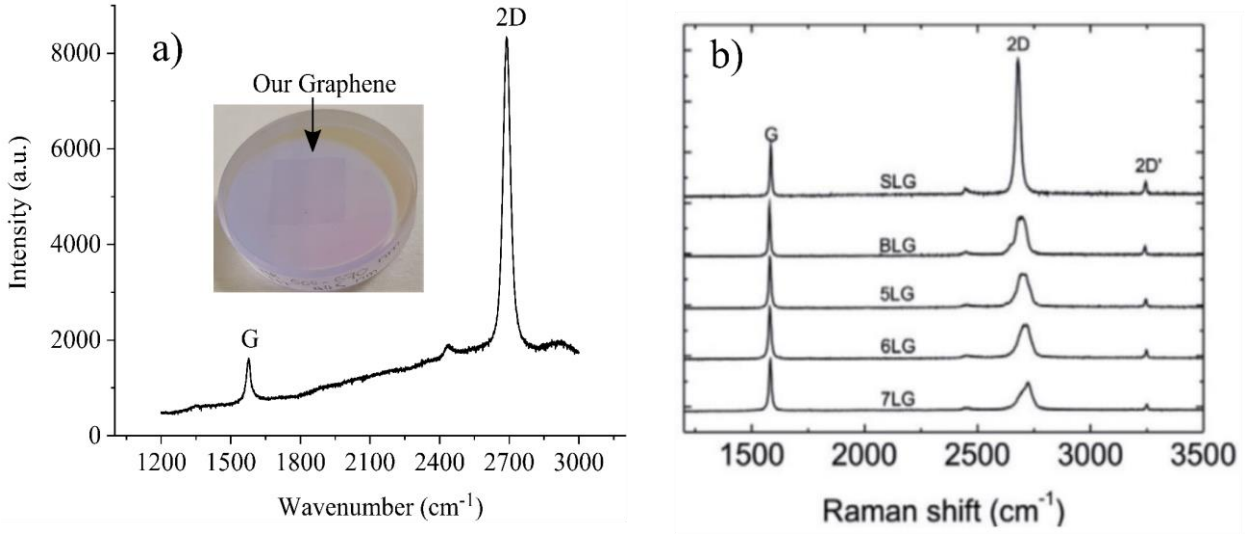

Figure 5.3: (a) Trace of Raman signal of our monolayer graphene, (b) an example of Raman signal found when graphene layer increases. (SLG: Single layer graphene, BLG: Bi-layer graphene and so on).

The result of Raman spectrum of our graphene (on top of mirror) is shown in Figure (a) along with a similar plot adopted from [119] for comparison. The most prominent spectral feature of carbon-based materials is the appearance of G-band and a 2D band [120] which are clearly seen in our sample Figure (a). G band (1587 cm^{-1}) corresponds to an in-plane vibrational mode of SP^2 carbon atoms which exist both in monolayer and multi-layer graphene (Figure (b)). The 2D band corresponds to a vibrational mode that is very strong having quite sharp peak in monolayer graphene compared to the graphene having more layers [119,121]. Therefore, $\frac{I_{2D}}{I_G}$ is a good indicator of graphene's quality (monolayer or multilayer). However, from here we confirmed that our graphene on the mirror was a monolayer one.

- **Saturation intensity of monolayer graphene SA**

It is better to have an idea regarding the laser intensity required to saturate graphene which might give a good direction towards cavity design for mode-locking. Perhaps we need to design a cavity to have different cavity beam spot sizes on gain medium and graphene in order to saturate graphene SA which will be discussed later. Currently we do not have any credible experimental value of the laser intensity

to saturate our monolayer graphene. However, there are huge discrepancies in literature regarding the value of saturation intensity of monolayer/ multi-layer graphene. In fact, it depends on the quality of graphene (fabrication process), laser used for the experiment (fs, ps or ns), laser spot size used on graphene during experiment and wavelength of the laser. Interestingly, depending on the laser pulse duration used (fs/ps), the saturation intensity of monolayer graphene can go up to 100 MW/cm^2 or more whereas their saturation intensity has been reported to be as low as in the range of few tens of MW/cm^2 or even lower when a ns laser was used [122]. For instance, using 100fs laser N. H. Park et al. [123] measured saturation intensity of monolayer graphene as ~75 MW/cm^2. However, a detail of above discussion can be found in [122].

5.3.1.2. A proposition of laser cavity for mode-locking

We propose following cavity configuration for future mode-locking experiment. In such cavity configuration, we can play with cavity mode sizes on gain medium and graphene as well.

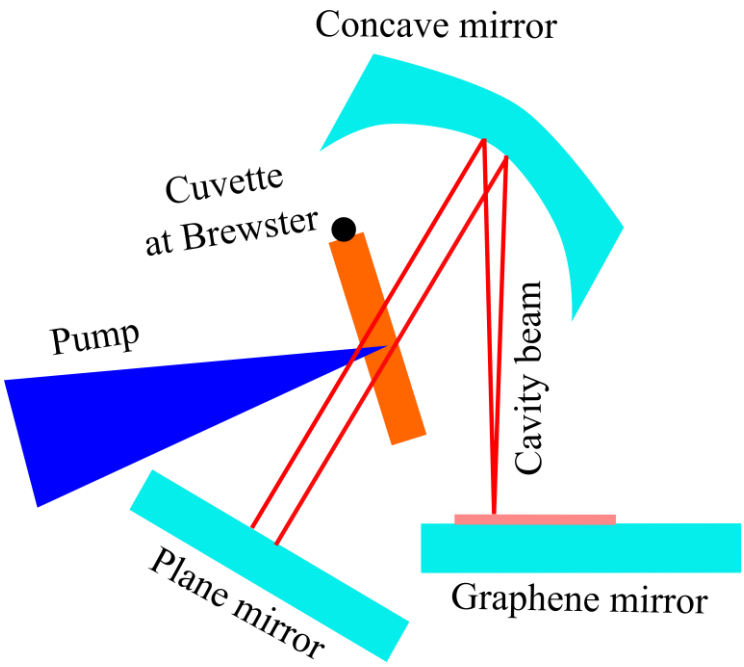

Figure 5.4: A proposition for mode-locked cavity.

At the same time we should also think about the design aspects of saturable absorber deposited on commercially bought DBR mirror. It has been demonstrated that using a spacer layer between SA and mirror helps to control saturable and non-saturable losses of SA [124]. In thesis, we are not going to the details of that issue but both parameters are crucial needs to be investigated before mode-locking

experiment. Very encouraging results have been shown that mode locking with graphene SA is possible by just using a monolayer graphene on the top of a commercially bought broadband DBR mirror [125]. Still, more work is needed to understand the physics and make an efficient device compatible with applications.

Bibliography

[1] T.H. Maiman, R.H. Hoskins, I.J. D'Haenens, C.K. Asawa, and V. Evtuhov, Phys. Rev. **123**, 1151 (1961).

[2] Y. Cui, D.E. Withers, C.F. Rae, C.J. Norrie, Y. Tang, B.D. Sinclair, W. Sibbett, and M.H. Dunn, Opt. Lett. **18**, 122 (1993).

[3] T. Woggon, S. Klinkhammer, and U. Lemmer, Appl. Phys. B Lasers Opt. **99**, 47 (2010).

[4] R. Bogue, Sens. Rev. **31**, 13 (2011).

[5] A. Salehi, X. Fu, D.H. Shin, and F. So, Adv. Funct. Mater. **29**, 1 (2019).

[6] Y. Yang, G.A. Turnbull, and I.D.W. Samuel, Appl. Phys. Lett. **92**, 92 (2008).

[7] Z. Zhao, O. Mhibik, M. Nafa, S. Chénais, and S. Forget, Appl. Phys. Lett. **106**, 051112 (2015).

[8] S. Forget and S. Chénais, *Organic Solid-State Lasers* (Springer Berlin Heidelberg, Berlin, Heidelberg, 2013).

[9] B. Wardle, *Principles and Applications of Photochemistry* (John Wiley \& Sons, 2009).

[10] M.N. Valeur, Bernard and Berberan-Santos, *"Molecular Fluorescence: Principles and Application,Sohn Wiley & Sons.* (John Wiley \& Sons, 2012).

[11] A.E. Siegman, *Lasers_Book* (1986).

[12] M. Guymont, *Structure de La Matière Atomes, Liaisons Chimiques et Cristallographie* (2010).

[13] B. Valeur, *Molecular Fluorescence - Principles and Applications* (2001).

[14] M. Klessinger and J. Michl, 537 (1995).

[15] M. Lehnhardt, T. Riedl, T. Weimann, and W. Kowalsky, Phys. Rev. B - Condens. Matter Mater. Phys. **81**, 1 (2010).

[16] F.P. Schäfer, W. Schmidt, and J. Volze, Appl. Phys. Lett. **9**, 306 (1966).

[17] O.G. Peterson, S.A. Tuccio, and B.B. Snavely, Appl. Phys. Lett. **17**, 245 (1970).

[18] C. Eggeling, J. Widengren, R. Rigler, and C.A.M. Seidel, Anal. Chem. **70**, 2651 (1998).

[19] R.L. Fork, C.H. Brito Cruz, P.C. Becker, and C. V. Shank, Opt. Lett. **12**, 483 (1987).

[20] B.H. Soffer and B.B. McFarland, Appl. Phys. Lett. **10**, 266 (1967).

[21] O.G. Peterson and B.B. Snavely, Appl. Phys. Lett. **12**, 238 (1968).

[22] F. Amat-Guerri, A. Costela, J.M. Figuera, F. Florido, I. Garcia-Moreno, and R. Sastre, Opt. Commun. **114**, 442 (1995).

[23] A. Costela, I. Garcia-Moreno, J.M. Figuera, F. Amat-Guerri, J. Barroso, and R. Sastre, Opt. Commun. **130**, 44 (1996).

[24] A. Costela, I. Garcia-Moreno, J.M. Figuera, F. Amat-Guerri, R. Mallavia, M.D. Santa-Maria, and R. Sastre, J. Appl. Phys. **80**, 3167 (1996).

[25] A. Costela, I. García-Moreno, C. Gómez, O. Garcia, and R. Sastre, J. Appl. Phys. **90**, 3159 (2001).

[26] A. Costela, I. García-Moreno, M.L. Carrascoso, and R. Sastre, Opt. Commun. **201**, 437 (2002).

[27] K.M. Abedin, M. Álvarez, A. Costela, I. García-Moreno, O. García, R. Sastre, D.W. Coutts, and C.E. Webb, Opt. Commun. **218**, 359 (2003).

[28] M. Canva, P. Georges, J.-F. Perelgritz, A. Brum, F. Chaput, and J.-P. Boilot, Appl. Opt. **34**, 428 (1995).

[29] T.H. Nhung, M. Canva, T.T.A. Dao, F. Chaput, A. Brun, N.D. Hung, and J.-P. Boilot, Appl. Opt. **42**, 2213 (2003).

[30] R.E. Hermes, T.H. Allik, S. Chandra, and J.A. Hutchinson, Appl. Phys. Lett. **63**, 877 (1993).

[31] M. Koschorreck, R. Gehlhaar, V.G. Lyssenko, M. Swoboda, M. Hoffmann, and K. Leo, Appl. Phys. Lett. **87**, 1 (2005).

[32] M.A. Díaz-García, F. Hide, B.J. Schwartz, M.D. McGehee, M.R. Andersson, and A.J. Heeger, Appl. Phys. Lett. **70**, 3191 (1997).

[33] L. Persano, P. Del Carro, E. Mele, R. Cingolani, D. Pisignano, M. Zavelani-Rossi, S. Longhi, and G. Lanzani, Appl. Phys. Lett. **88**, 121110 (2006).

[34] S. Stagira, M. Zavelani-Rossi, M. Nisoli, S. DeSilvestri, G. Lanzani, C. Zenz, P. Mataloni, and G. Leising, Appl. Phys. Lett. **73**, 2860 (1998).

[35] M. Zavelani-Rossi, G. Lanzani, S. De Silvestri, M. Anni, G. Gigli, R. Cingolani, G. Barbarella, and L. Favaretto, Appl. Phys. Lett. **79**, 4082 (2001).

[36] L. Persano, A. Camposeo, P. Del Carro, E. Mele, R. Cingolani, and D. Pisignano, Appl. Phys. Lett. **89**, 87 (2006).

[37] M. Taguchi, Y. Higase, and K. Yamashita, Opt. Express **27**, 35548 (2019).

[38] N. Tsutsumi, K. Kaida, K. Kinashi, and W. Sakai, Sci. Rep. **9**, 1 (2019).

[39] S. Klinkhammer, X. Liu, K. Huska, Y. Shen, S. Vanderheiden, S. Valouch, C. Vannahme, S. Bräse, T. Mappes, and U. Lemmer, Opt. Express **20**, 6357 (2012).

[40] X. Liu, P. Stefanou, B. Wang, T. Woggon, T. Mappes, and U. Lemmer, Opt. Express **21**, 28941 (2013).

[41] A.S.D. Sandanayaka, T. Matsushima, F. Bencheikh, K. Yoshida, M. Inoue, T. Fujihara, K. Goushi, J.C. Ribierre, and C. Adachi, Sci. Adv. **3**, 1 (2017).

[42] Y. Yang, Y. Zhou, Z. Liao, J. Yu, Y. Cui, I. Garcia-Moreno, Z. Wang, A. Costela, and G. Qian, Opt. Express **23**, 4385 (2015).

[43] Z. Yu, Y. Wu, Q. Liao, H. Zhang, S. Bai, H. Li, Z. Xu, C. Sun, X. Wang, J. Yao, and H. Fu, J. Am. Chem. Soc. **137**, 15105 (2015).

[44] H. Huang, Z. Yu, D. Zhou, S. Li, L. Fu, Y. Wu, C. Gu, Q. Liao, and H. Fu, ACS Photonics **6**, 3208 (2019).

[45] C. Wei, Y. Du, Y. Liu, X. Lin, C. Zhang, J. Yao, and Y.S. Zhao, J. Am. Chem. Soc. **141**, 5116 (2019).

[46] H. Rabbani-Haghighi, S. Forget, S. Chénais, and A. Siove, Opt. Lett. **35**, 1968 (2010).

[47] O. Mhibik, T. Leang, A. Siove, S. Forget, and S. Chénais, Appl. Phys. Lett. **102**, 041112 (2013).

[48] H. Rabbani-Haghighi, S. Forget, A. Siove, and S. Chénais, EPJ Appl. Phys. **56**, 34108 (2011).

[49] T. Matsushima, S. Yoshida, K. Inada, Y. Esaki, T. Fukunaga, H. Mieno, N. Nakamura, F. Bencheikh, M.R. Leyden, R. Komatsu, C. Qin, A.S.D. Sandanayaka, and C. Adachi, Adv. Funct. Mater. **29**, 1 (2019).

[50] H. Sakata and H. Takeuchi, Appl. Phys. Lett. **92**, (2008).

[51] C. Foucher, B. Guilhabert, A.L. Kanibolotsky, P.J. Skabara, N. Laurand, and M.D. Dawson, Opt. Mater. Express **3**, 584 (2013).

[52] M. Rodriguez, A. Costela, I. Garcia-Moreno, F. Florido, J.M. Figuera, and R. Sastre, Meas. Sci. Technol. **6**, 971 (1995).

[53] R. Bornemann, E. Thiel, and P.H. Bolívar, Opt. Express **19**, 26382 (2011).

[54] V.M. Katarkevich, A.N. Rubinov, T.S. Efendiev, S.S. Anufrik, and M.F. Koldunov, Appl. Opt. **54**, 7962 (2015).

[55] A. Costela, I. García Moreno, C. Gómez, O. García, R. Sastre, A. Roig, and E. Molins, J. Phys. Chem. B **109**, 4475 (2005).

[56] A. Costela, I. García-Moreno, R. Sastre, D.W. Coutts, and C.E. Webb, Appl. Phys. Lett. **79**, 452 (2001).

[57] O.A. Burdukova, M. V. Gorbunkov, V.A. Petukhov, and M.A. Semenov, Laser Phys. Lett. **13**, (2016).

[58] O. Burdukova, M. Gorbunkov, V. Petukhov, and M. Semenov, Appl. Phys. B Lasers Opt. **123**, 0 (2017).

[59] O. Burdukova, V. Petukhov, and M. Semenov, Appl. Phys. B Lasers Opt. **124**, 1 (2018).

[60] M. Behringer and H. König, PhotonicsViews **17**, 60 (2020).

[61] S. Wang, X. Wang, F. Kallmeyer, J. Chen, and H.J. Eichler, Appl. Phys. B Lasers Opt. **92**, 43 (2008).

[62] T.Y. Fan and R.L. Byer, IEEE J. Quantum Electron. **23**, 605 (1987).

[63] A. Hamja, S. Chénais, and S. Forget, J. Appl. Phys. **128**, (2020).

[64] S. Chenais, S. Forget, S. Chenais, S. Forget, S. Organic, and L. Polymer, 390 (2011).

[65] H. Kogelnik and T. Li, Proc. IEEE **54**, 1312 (1966).

[66] Y. Oyama, M. Mamada, A. Shukla, E.G. Moore, S.C. Lo, E.B. Namdas, and C. Adachi, ACS Mater. Lett. **2**, 161 (2020).

[67] A.D. Gomes, H. Bartelt, and O. Frazão, Laser Photonics Rev. **15**, 1 (2021).

[68] M. Meyer, J.C. Mialocq, and B. Perly, J. Phys. Chem. **94**, 98 (1990).

[69] E. McKenna, J. Xue, A. Verdoni, M. Yetzbacher, R. Fan, and A. Mickelson, J. Opt. Soc. Am. B **21**, 1294 (2004).

[70] K. Yagi, S. Shibata, T. Yano, A. Yasumori, M. Yamane, and B. Dunn, J. Sol-Gel Sci. Technol. **4**, 67 (1995).

[71] W. Hu, H. Ye, C. Li, Z. Jiang, and F. Zhou, Appl. Opt. **36**, 579 (1997).

[72] D.M. Coles, A.A.P. Trichet, P.R. Dolan, R.A. Taylor, C. Vallance, and J.M. Smith, Laser Photonics

Rev. **9**, 538 (2015).

[73] S.L. Chua, B. Zhen, J. Lee, J. Bravo-Abad, O. Shapira, and M. Soljačić, J. Mater. Chem. C **2**, 1463 (2014).

[74] F. Song, C. Zhang, X. Ding, J. Xu, G. Zhang, M. Leigh, and N. Peyghambarian, Appl. Phys. Lett. **81**, 2145 (2002).

[75] Z. Zhao, O. Mhibik, T. Leang, S. Forget, and S. Chénais, Opt. Express **22**, 30092 (2014).

[76] W. Xie, S.C. Tam, Y.L. Lam, and Y. Kwon, Opt. Commun. **189**, 337 (2001).

[77] S. Chénais, F. Druon, S. Forget, F. Balembois, and P. Georges, Prog. Quantum Electron. **30**, 89 (2006).

[78] H. Su, Y. Zhang, Y. Zhao, K. Ma, and J. Wang, Opt. Fiber Technol. **51**, 1 (2019).

[79] S. Dey, S. Rallabandi, S. Singh, and P.B. Bisht, Opt. Laser Technol. **134**, 106652 (2021).

[80] A. Marcano O and J. Castillo, Pure Appl. Opt. J. Eur. Opt. Soc. Part A **3**, 339 (1994).

[81] K. Dobek, M. Baranowski, J. Karolczak, D. Komar, K. Kreczmer, and J. Szuniewicz, Appl. Phys. B Lasers Opt. **122**, 2 (2016).

[82] H. Atmanspacher and H. Scheingraber, Phys. Rev. A **34**, 253 (1986).

[83] P.G. Weber, IEEE J. Quantum Electron. **19**, 1200 (1983).

[84] T.T. Kajava, H.M. Lauranto, and R.R.E. Salomaa, Appl. Opt. **31**, 6987 (1992).

[85] V.M. Baev, J. Eschner, J. Sierks, A. Weiler, and P.E. Toschek, Opt. Commun. **94**, 436 (1992).

[86] J.P. Goldsborough, Appl. Opt. **3**, 267 (1964).

[87] A.E. Siegman, *Lasers_Book* (1986).

[88] S. Uemura and K. Torizuka, IEEE J. Quantum Electron. **39**, 68 (2003).

[89] S. Ghanbari, R. Akbari, and A. Major, Opt. Express **24**, 14836 (2016).

[90] A. Seas, V. Petričević, and R.R. Alfano, Opt. Lett. **17**, 937 (1992).

[91] C. Chudoba, J.G. Fujimoto, E.P. Ippen, and H.A. Haus, **26**, 292 (2001).

[92] P.C. Wagenblast, U. Morgner, F. Grawert, T.R. Schibli, F.X. Kärtner, V. Scheuer, G. Angelow, and M.J. Lederer, Opt. Lett. **27**, 1726 (2002).

[93] C.G. Durfee, T. Storz, J. Garlick, S. Hill, J.A. Squier, M. Kirchner, G. Taft, K. Shea, H. Kapteyn, M. Murnane, and S. Backus, CLEO Sci. Innov. CLEO_SI 2012 **20**, 1223 (2012).

[94] U. Demirbas, I. Baali, D.A.E. Acar, and A. Leitenstorfer, Opt. Express **23**, 8901 (2015).

[95] K. Gürel, V.J. Wittwer, M. Hoffmann, C.J. Saraceno, S. Hakobyan, B. Resan, A. Rohrbacher, K. Weingarten, S. Schilt, and T. Südmeyer, Opt. Express **23**, 30043 (2015).

[96] J.A. der Au, F.H. Loesel, F. Morier-Genoud, M. Moser, and U. Keller, Conf. Lasers Electro-Optics Eur. - Tech. Dig. **23**, 433 (1998).

[97] P.W. Roth, A.J. Maclean, D. Burns, and A.J. Kemp, Opt. Lett. **36**, 304 (2011).

[98] F. Canbaz, E. Beyatli, L.-J. Chen, A. Sennaroglu, F.X. Kärtner, and U. Demirbas, Opt. Lett. **39**, 327 (2014).

[99] B.W. Tilma, M. Mangold, C.A. Zaugg, S.M. Link, D. Waldburger, A. Klenner, A.S. Mayer, E. Gini, M. Golling, and U. Keller, Light Sci. Appl. **4**, e310 (2015).

[100] O.A. Burdukova, V.A. Petukhov, and M.A. Semenov, J. Russ. Laser Res. **42**, 100 (2021).

[101] W. Koechner, Solid-State Laser Eng. 534 (2006).

[102] D.H. Sutter, I.D. Jung, F.X. Kärtner, N. Matuschek, F. Morier-Genoud, V. Scheuer, M. Tilsch, T. Tschudi, and U. Keller, IEEE J. Sel. Top. Quantum Electron. **4**, 169 (1998).

[103] J.A.R. Williams, H. Goldsmith, P.M.W. French, and J.R. Taylor, Opt. Lett. **13**, 811 (1988).

[104] U . Keller, Nature **424**, 831 (2003).

[105] U. Keller and A.C. Tropper, Phys. Rep. **429**, 67 (2006).

[106] D.N. Papadopoulos, S. Forget, M. Delaigue, F. Druon, F. Balembois, and P. Georges, Opt. Lett. **28**, 1838 (2003).

[107] A. Laurain, D. Marah, R. Rockmore, J. McInerney, J. Hader, A.R. Perez, W. Stolz, and J. V. Moloney, Optica **3**, 781 (2016).

[108] A.C. Tropper, H.D. Foreman, A. Garnache, K.G. Wilcox, and S.H. Hoogland, J. Phys. D. Appl. Phys. **37**, R75 (2004).

[109] M. Gaponenko, P.W. Metz, A. Härkönen, A. Heuer, T. Leinonen, M. Guina, T. Südmeyer, G. Huber, and C. Kränkel, Adv. Solid State Lasers, ASSL 2014 **39**, 6939 (2014).

[110] S. Ranta, A. Härkönen, T. Leinonen, L. Orsila, J. Lyytikäinen, G. Steinmeyer, and M. Guina, **38**, 2289 (2013).

[111] R. Bek, H. Kahle, T. Schwarzbäck, M. Jetter, and P. Michler, Appl. Phys. Lett. **103**, 1 (2013).

[112] K.S. Novoselov, V.I. Fal'Ko, L. Colombo, P.R. Gellert, M.G. Schwab, and K. Kim, Nature **490**, 192 (2012).

[113] F. Bonaccorso, Z. Sun, T. Hasan, and A.C. Ferrari, Nat. Photonics **4**, 611 (2010).

[114] J.-L. Xu, X.-L. Li, Y.-Z. Wu, X.-P. Hao, J.-L. He, and K.-J. Yang, Opt. Lett. **36**, 1948 (2011).

[115] C.C. Lee, T.R. Schibli, G. Acosta, and J.S. Bunch, J. Nonlinear Opt. Phys. Mater. **19**, 767 (2010).

[116] I.H. Baek, H.W. Lee, S. Bae, B.H. Hong, Y.H. Ahn, D. Il Yeom, and F. Rotermund, Appl. Phys. Express **5**, 3 (2012).

[117] Z. Sun, T. Hasan, F. Torrisi, D. Popa, G. Privitera, F. Wang, F. Bonaccorso, D.M. Basko, and A.C. Ferrari, ACS Nano **4**, 803 (2010).

[118] H. Yu, X. Chen, H. Zhang, X. Xu, X. Hu, Z. Wang, J. Wang, S. Zhuang, and M. Jiang, ACS Nano **4**, 7582 (2010).

[119] V. Kumar, A. Kumar, D.J. Lee, and S.S. Park, Materials (Basel). **14**, (2021).

[120] A.C. Ferrari, J.C. Meyer, V. Scardaci, C. Casiraghi, M. Lazzeri, F. Mauri, S. Piscanec, D. Jiang, K.S. Novoselov, S. Roth, and A.K. Geim, Phys. Rev. Lett. **97**, 1 (2006).

[121] Y. Hwangbo, C.K. Lee, A.E. Mag-Isa, J.W. Jang, H.J. Lee, S.B. Lee, S.S. Kim, and J.H. Kim, Carbon N. Y. **77**, 454 (2014).

[122] F. Zhang, S. Han, Y. Liu, Z. Wang, and X. Xu, Appl. Phys. Lett. **106**, 1 (2015).

[123] N.H. Park, H. Jeong, S.Y. Choi, M.H. Kim, F. Rotermund, and D.-I. Yeom, Opt. Express **23**, 19806 (2015).

[124] C.A. Zaugg, Z. Sun, V.J. Wittwer, D. Popa, S. Milana, T.S. Kulmala, R.S. Sundaram, M. Mangold, O.D. Sieber, M. Golling, Y. Lee, J.H. Ahn, A.C. Ferrari, and U. Keller, Opt. Express **21**, 31548 (2013).

[125] J. Ma, H. Huang, K. Ning, X. Xu, G. Xie, L. Qian, K.P. Loh, and D. Tang, Opt. Lett. **41**, 890 (2016).